Understanding the Ediacaran Assemblages of Avalonia:

A Palaeoenvironmental, Taphonomic and Ontogenetic Study

Supplementary Volume

Appendices

Alexander G. S. C. Liu

Exeter College

Submitted for consideration for the degree of Doctor of Philosophy, Trinity Term 2011

Department of Earth Sciences, University of Oxford

Appendices Table of Contents

Appendix A

Small Fronds and Filaments from the Drook Formation, Pigeon Cove, Newfoundland

The following pages catalogue and figure a selection of specimens of juvenile rangeomorph fronds and associated filamentous fossils from the Pigeon Cove surface (locality DRK2PC; Appendix D2), as documented in Chapter 2. Tentative taxonomic identifications are made to genus level, but for the reasons outlined in Chapter 2, it has not been possible to identify species in most cases.

Selected images of small fronds (Appendix A1) and filaments (Appendix A2) from the Pigeon Cove surface are presented, followed by length, width and orientation data for each of the specimens (Appendix A3). A complete digitised map of the Pigeon Cove small frond horizon is provided (Appendix A4). Finally, Appendix A5 documents fossils from other Avalonian horizons that were not detailed in the stratigraphic range discussion of Chapter 2.

Scales are not included in individual images of fronds and filaments, since accurate measurements (to the nearest millimetre) relating to each specimen are presented in Appendix A3. All images of fossils and casts in this appendix show the top surface of bedding planes, with fossils preserved in positive epirelief.

APPENDIX A1

FIGURED SPECIMENS OF JUVENILE FRONDS

The following images document the variation within the Pigeon Cove frondose community. Images are arranged by taxon where possible. Figure labels, rather than following the usual A,B,C, or 1,2,3 system, reflect the original field labels assigned to the specimens. These correspond to their location on the maps of the surface (Fig. 2.3; Appendix A4), and also to the dataset presented in Appendix A3.

Charniodiscus

Several of the small fronds on the surface appear to possess a positive epirelief rim around their outer edge, and occasionally a structure similar to a basal holdfast (Fig. A1.1). These features are similar to those seen in *Charniodiscus* specimens from other Avalonian beds, and therefore hint at a possible affinity with this taxon (see also Appendix B1). Some specimens show similarities with *Charniodiscus spinosus* Laflamme et al. 2004 (Fig. A1.1 [C16, C117]), with a short stem, and a broad frond which tapers distally to a point. Definite *C. spinosus* specimens are not currently known from the Drook Formation (Fig. 2.17), and therefore it is not possible to confidently classify these examples without further occurrences of larger, more mature specimens. All possible *Charniodiscus* juveniles possess alternating primary branching along a distally tapering frond. Holdfast structures are either circular (e.g. Fig. A1.1 [C16]), or angular (e.g. Fig. A1.1 [C6, C81]), though this latter morphology could result from a combination of tectonic deformation acting upon the disc, and preservation only of the side not covered by the frond. If these specimens really are *Charniodiscus* juveniles, they would considerably extend the range of that taxon in Newfoundland (Fig. 2.17).

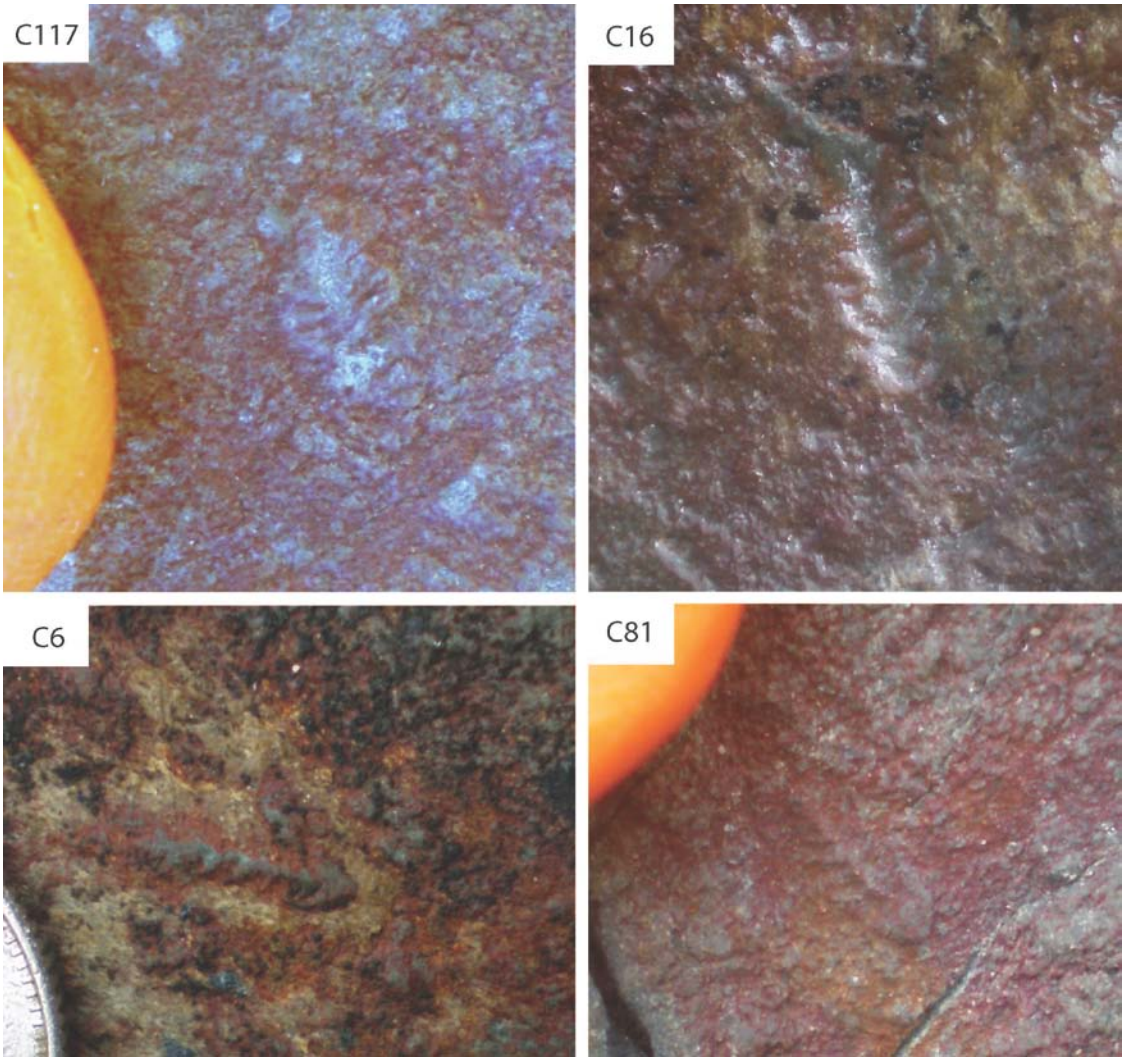

Fig. A1.1. Potential *Charniodiscus* specimens from the Drook Formation, Pigeon Cove. For exact dimensions of specimens, see Appendix A3.

Multiple specimens akin to *Charnia* are preserved at Pigeon Cove (Fig. A1.2). These exhibit furled, undisplayed rangeomorph branching, alternating along an elongate frond, with no stem extending up the central axis (Fig. A1.2). In some specimens, these primary branches are arranged parallel to one another, in a manner typical of *Charnia masoni* (e.g. Fig. A1.2 [C1, C63]), while in other specimens, the primary branches appear to radiate and change their angles in a similar style to *Charnia antecedens* (Fig. A1.2 [C8]). Other specimens show rather more complex rangeomorph branching, with variable branching angles and a broader frond morphology (e.g. Fig. A1.2 [C13]). Such specimens resemble rangeomorph taxa such as

Beothukis Brasier and Antcliffe 2009, but the lack of resolvable higher-order branching precludes classification of these individuals.

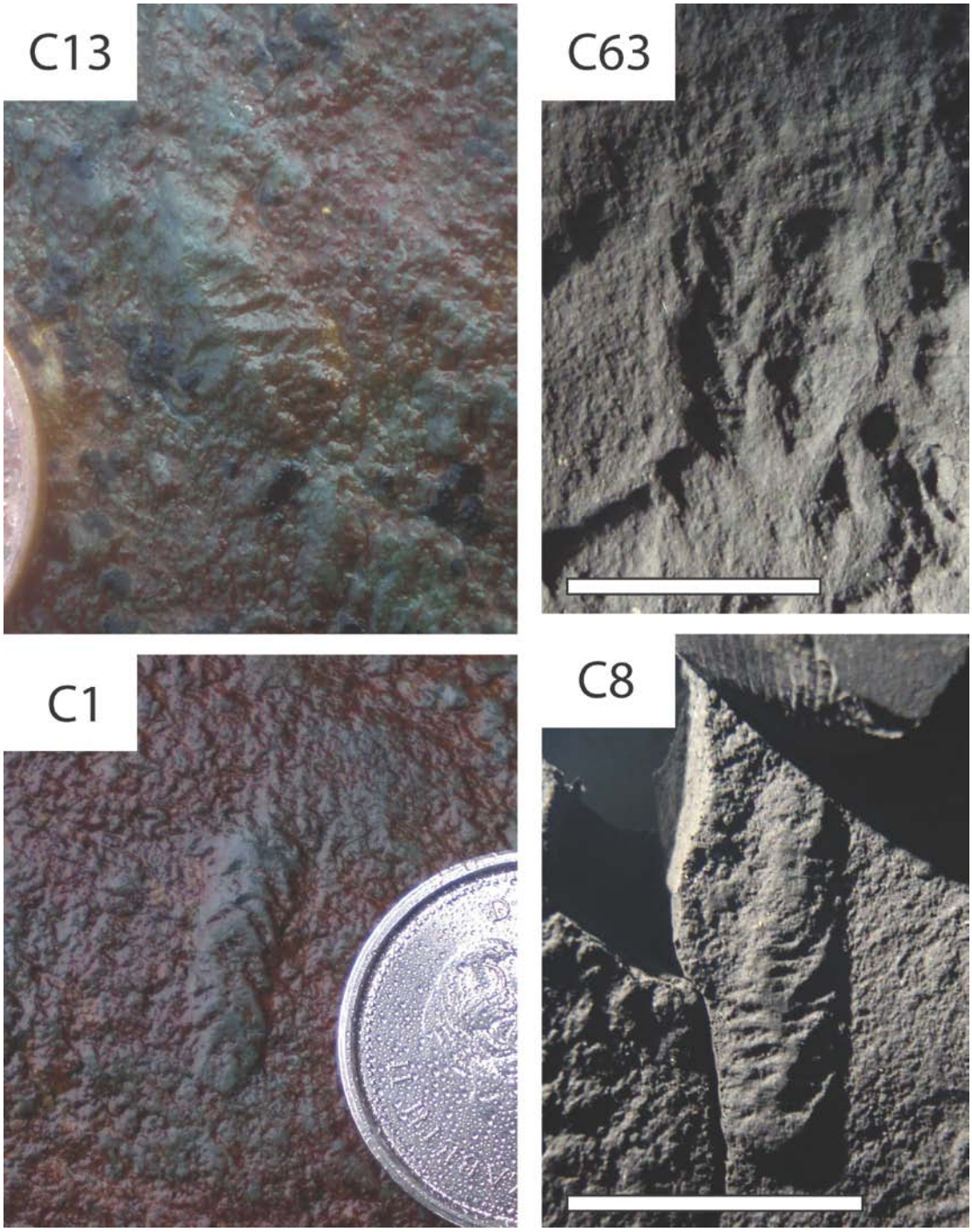

Fig. A1.2. *Charnia masoni* [C1, C63] and spatulate aff. *Charnia* [C8, C13] fronds from the Drook Formation, Pigeon Cove, Newfoundland. Scale bar = 10 mm. Images of specimens [C8] and [C63] are taken from casts housed in the collections of the Palaeobiology Group, Department of Earth Sciences, University of Oxford.

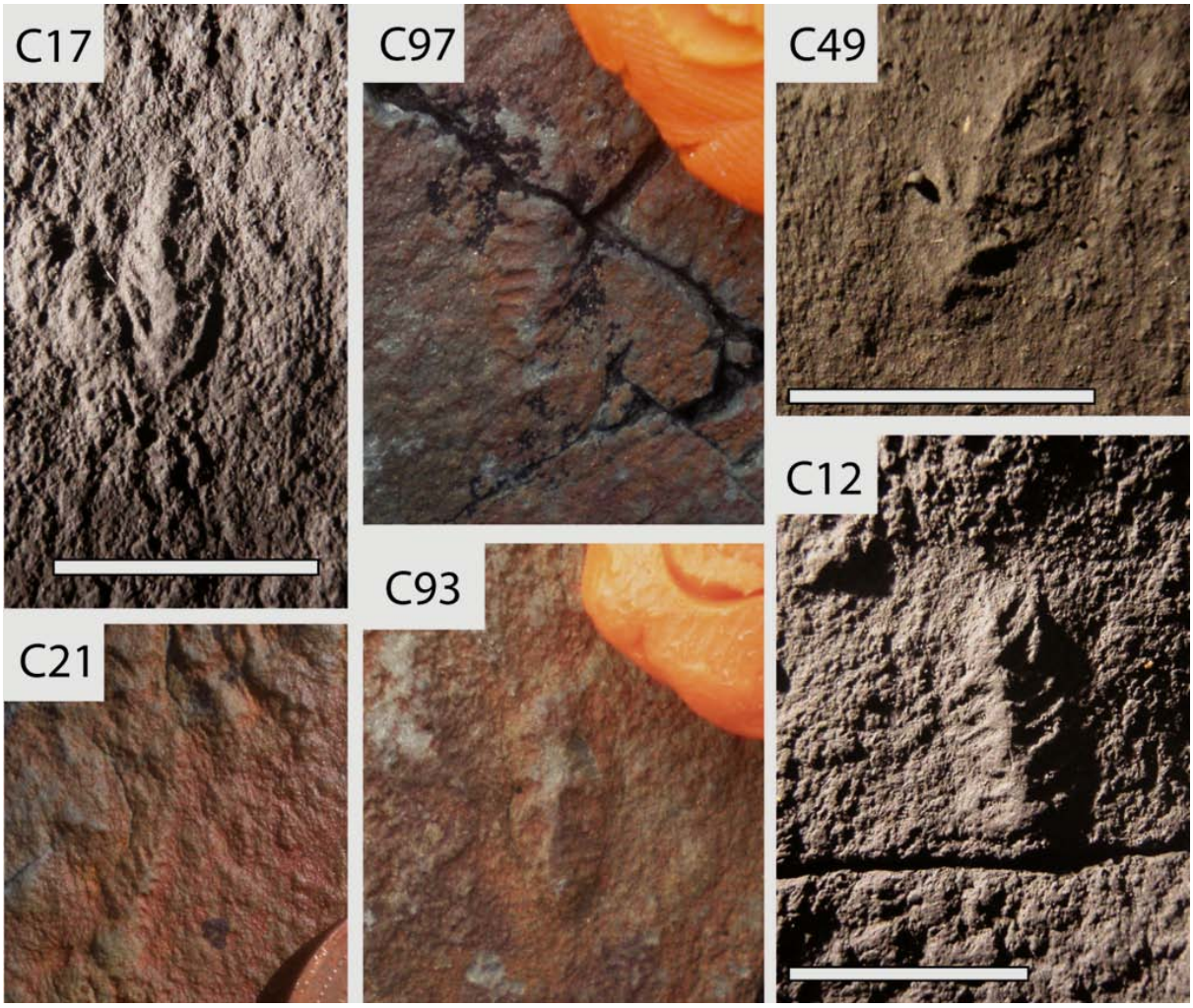

Fig. A1.3. Short fronds from the Drook Formation, Pigeon Cove, Newfoundland. Some possess 'lanceolate' fronds [C17, C49, C93], while others taper gradually (e.g. [C21]). Several specimens may be incomplete, since they do not possess either basal holdfast structures, or tapering points [C12, C97]. The small rounded lumps in [C49] are bubbles formed during the casting process. Scale bars where present = 10 mm.

A large number of fronds on the Pigeon Cove surface are short and do not possess sufficient features to be classified within a specific rangeomorph genus. Some of these appear to be complete, with fronds distally tapering to a point, and possible evidence for a holdfast disc, while others appear to be incomplete, showing no convincing evidence of tapering at either end (Fig. A1.3). All such specimens possess a central stem running up the length of the frond, while primary branching angle varies substantially through the population, and often even within individual specimens (e.g. Fig. A1.3 [C12]).

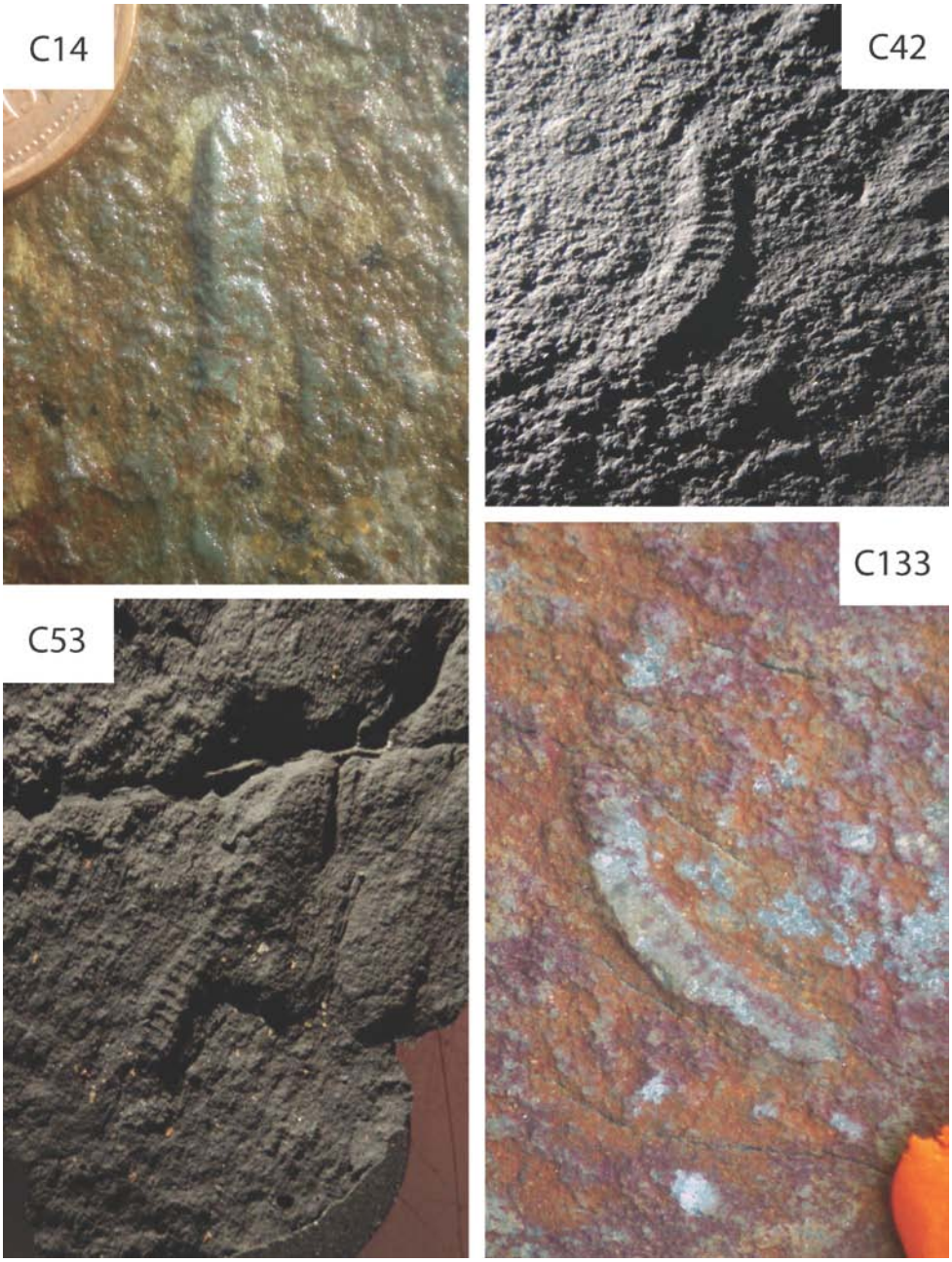

Fig. A1.4. 'Furled' small fronds from the Drook Formation, Pigeon Cove, Newfoundland. These specimens appear to show only one row of rangeomorph primary branches, but faint evidence in some specimens (e.g. [C14, C42]) of a second row demonstrates that they are actually long fronds (similar to *Trepassia*) which are folded along their midline. Images [C42 and C53] are taken from casts.

Some of the small fronds at first glance only show one set of transverse ridges, with no central midline (e.g. Fig. A1.4 [C53, C133]). These initially show some resemblance to Ediacaran tubular body fossils, but on closer inspection, it is clear that they are likely to be

unipolar rangeomorph fronds where only one row is visible. Crucially, some of these specimens do show evidence for a second row, but this often possesses much shorter primary branches than its neighbour, oriented at different angles (e.g. Fig. A1.4 [C14, C42]). This suggests that rather than preserving a different member of the Ediacara biota, these specimens represent rangeomorph specimens where the second row lies outside the plane of preservation. Possible mechanisms that could explain this include one row being folded beneath the rest of the frond, embedded within the sediment, or even raised above the sediment-water interface. These specimens hint at what may be happening laterally in rangeomorph construction, and demonstrate the flexibility of the organic matter. It does not appear that the fronds were particularly 3-dimensional, since these specimens, which presumably fell to one side of their central axis, collapsed upon themselves and folded back such that part of the frond 'front' or 'back' is always preserved.

Finally, the most common small fronds on the surface are long, narrow specimens exhibiting first order branching patterns. These individuals are likely to possess an affinity with the *Trepassia* genus (Fig. A1.5). Such specimens are long and thin, and often clearly taper to a finely-branched tip (Fig. A1.5 [C31, C55, C136]). The vast majority exhibit a central stem running down the length of the frond, with primary branches propagating alternately ([C136] is the anomaly, as discussed in Chapter 2). It appears that the smallest, youngest branches are added distally ([C31, C136]), and a variety of branching angles exist within the assemblage (Fig. A1.5).

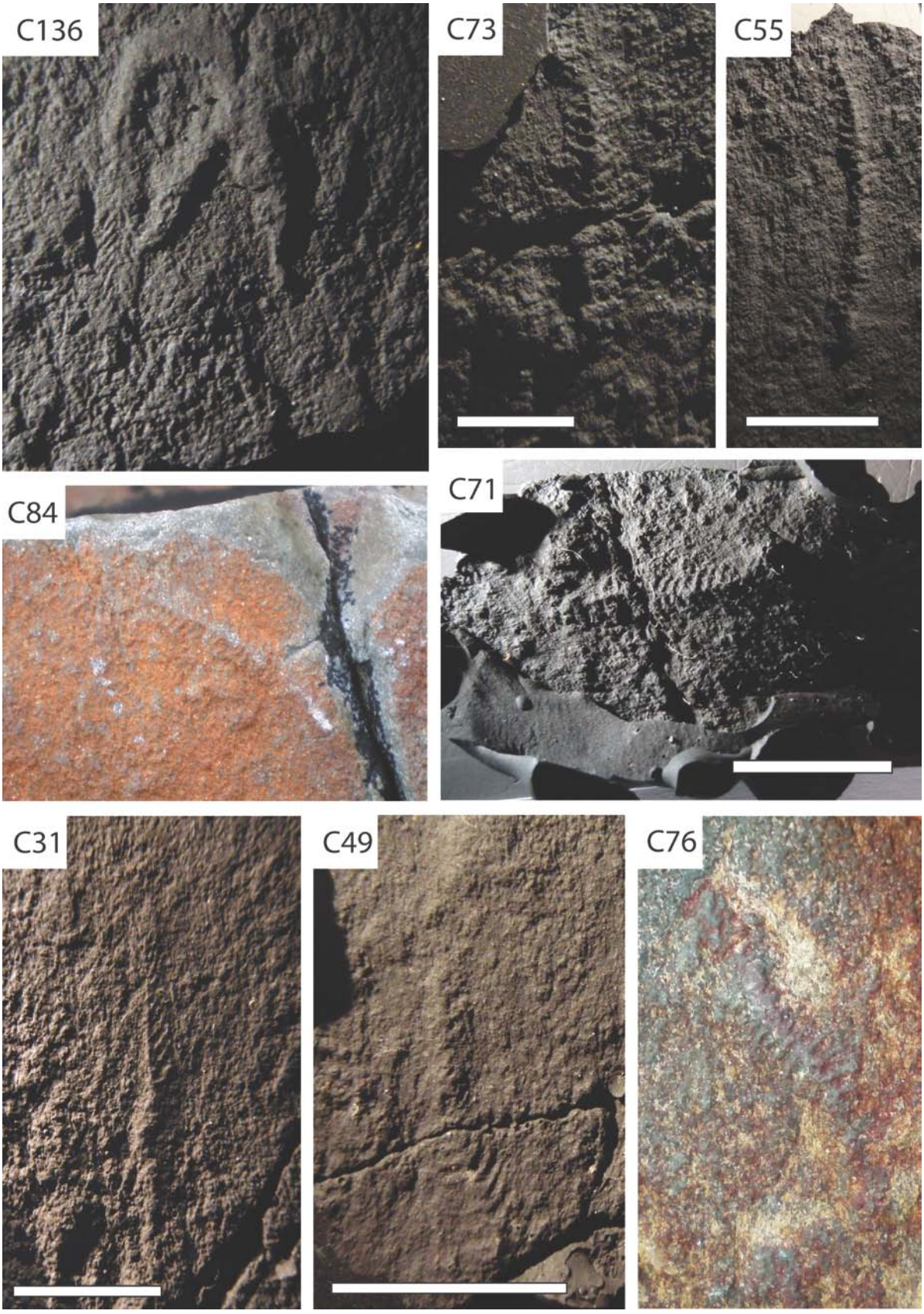

Fig. A1.5. aff. *Trepassia* specimens from Pigeon Cove, Newfoundland. Scale bars (where present) = 10 mm. All images except [C76] and [C84] are taken from casts.

Appendix A2

Specimens of the filamentous fossils from Pigeon Cove

The following figures present examples of the filamentous fossils from the Drook Formation of Pigeon Cove, documenting a representative selection of morphologies, and the variation within the assemblage. Again, rather than conventional labelling of component images, each figure is labelled with the field codes for the specimens, which correlate with the data presented in Appendix A3, and the position of the specimen on the overall map of the surface (Appendix A4; Fig. A4.3).

The filamentous fossils are all ~1 mm in width, several centimetres in length (see Appendix A3), and preserved on the Pigeon Cove surface in positive epirelief, rising up to 1 mm above the surface of the preserved bedding plane (e.g. Figs. A2.1–A2.4). All filaments, like their neighbouring fronds, are preserved beneath a 300 mm thickness of tuff. Filaments mostly lie broadly straight on the bedding plane, but some specimens are seen to loop back on themselves (e.g. Fig. A2.1 [F1]), demonstrating the flexible nature of the original organic material. They all exhibit a long, thin morphology, with little in the way of additional morphological features (Figs. A2.1–A2.3). Rare specimens are observed to branch (e.g. Fig. A2.1 [F7]; Fig. A2.2 [F112]), and it is apparent that the filaments lie on top of ivesheadiomorph impressions found on the same bed (for example, the specimen in Fig. A2.1 [F58] is draped over the lobe of a pizza disc ivesheadiomorph). Their spatial relationship with rangeomorphs is unknown, since no examples of contact between the two types of fossil were observed on the Pigeon Cove bedding plane.

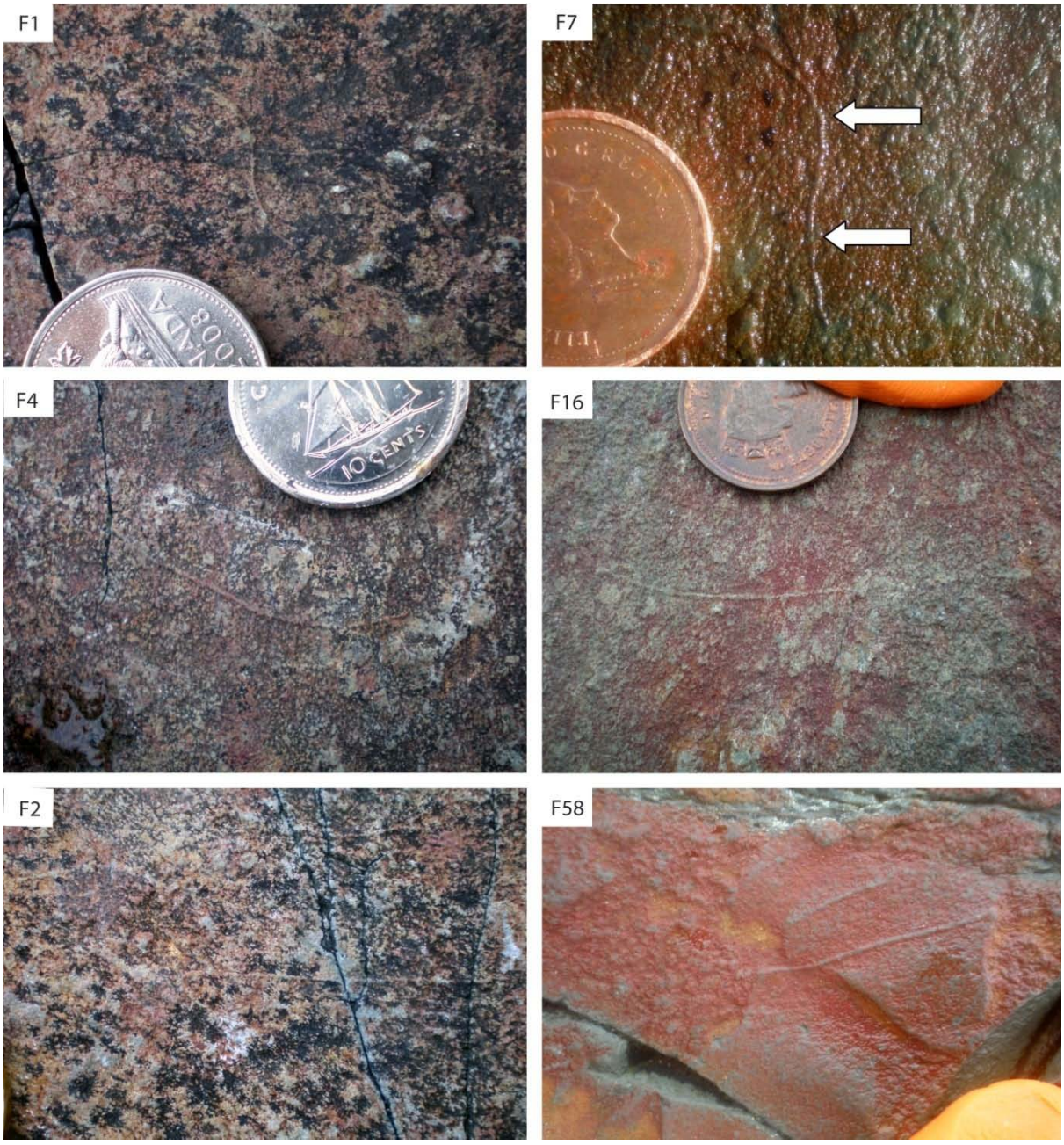

Fig. A2.1. A selection of filamentous fossils from the Pigeon Cove surface, Drook Formation, MPER, Newfoundland. Locality DRK2PC in Appendix D2. Note the positive epirelief preservation, evidence for branching in [F7] (arrowed), the looping morphology of [F1], and the superimposition of a filament over an ivesheadiomorph on [F58]. Coins for scale are either Canadian or British. For accurate dimensions for each specimen, refer to Appendix A3.

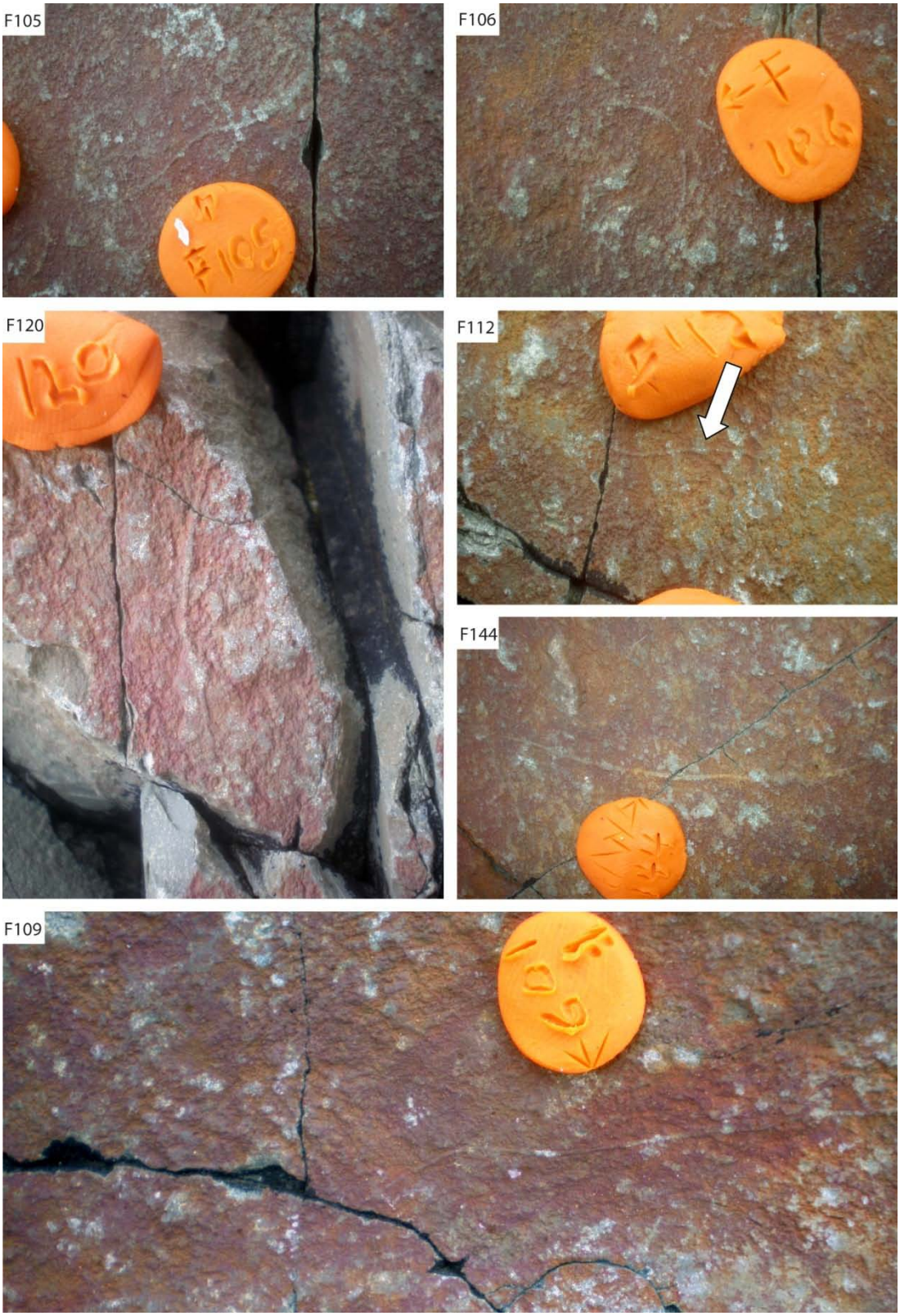

Fig. A2.2. A selection of filamentous fossils from the Pigeon Cove surface, Drook Formation, MPER, Newfoundland. Locality DRK2PC in Appendix D2. Note the consistency in filament thickness, and branching in the filament in [F112] (arrowed). Letters carved into the plastercine have a width of 1 mm.

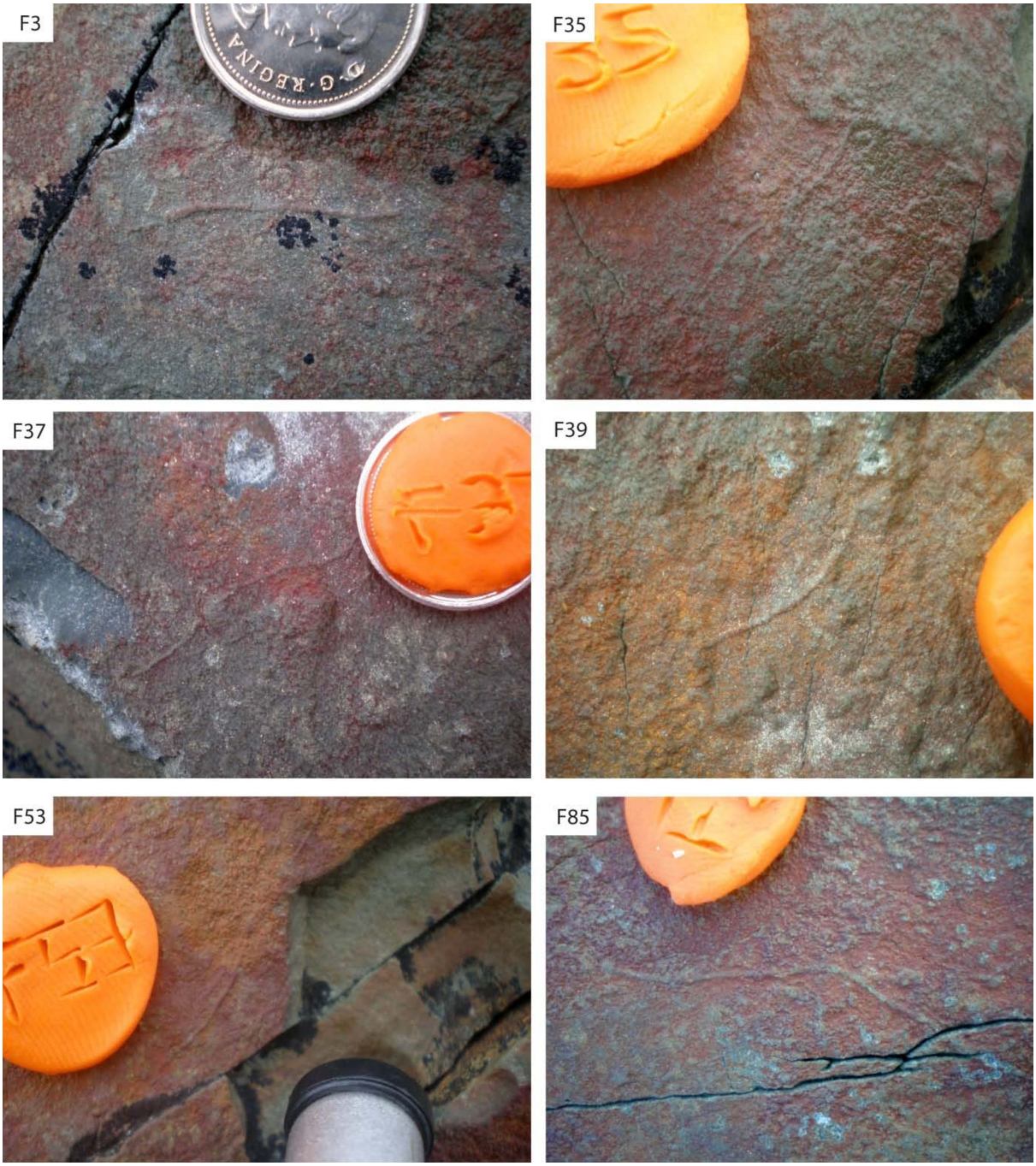

Fig. A2.3. A selection of filamentous fossils from the Pigeon Cove surface, Drook Formation, MPER, Newfoundland. Locality DRK2PC in Appendix D2. Note the lack of distinctive morphological features, the long, thin morphology of the specimens, and their apparently flexible nature.

The specimens figured in Figures A2.1–A2.3 are somewhat typical of the assemblage as a whole. Some specimens appear to be slightly more interesting (Fig. A2.4), exhibiting complex branching patterns (Fig. A2.4 [F80]), or potential evidence for discs or fronds (Fig. A2.4

[F75]). Such specimens may bear some resemblance to frondose individuals found within the same assemblage (e.g. aff. *Trepassia* species). They are rare components of the assemblage, but worthy of mention due to their additional characteristics.

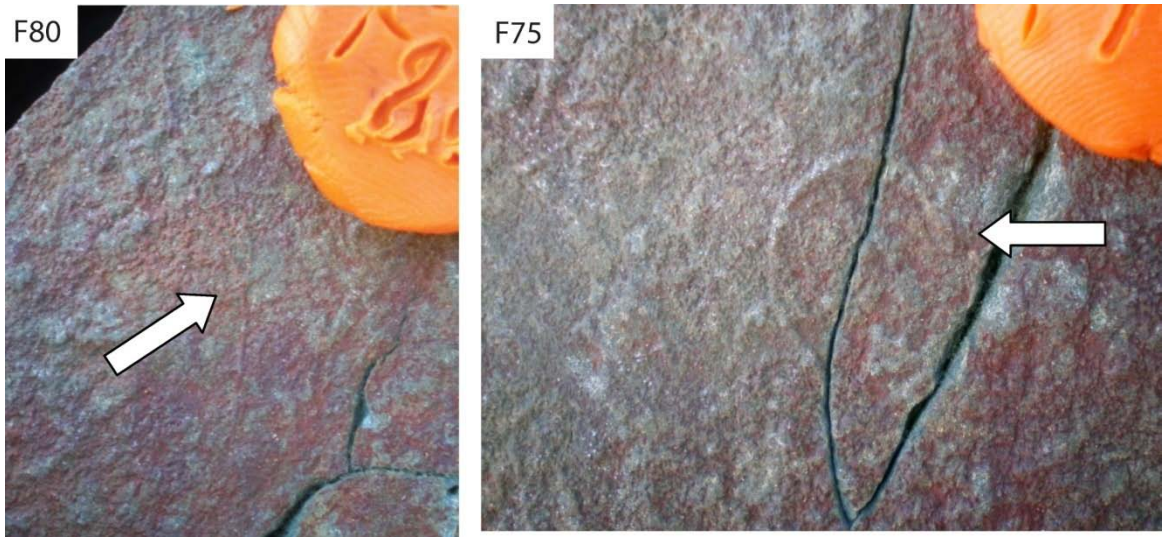

Fig. A2.4. A selection of the more interesting filamentous fossils from the Pigeon Cove surface, MPER, Avalon Peninsula, Newfoundland. [F80]: A filament which splits into several branches at its top (initial point of branching is arrowed), though what the branches then progress into is unclear. [F75]: A filament which appears to possess a bulbous termination at its right-hand end (arrowed). This could potentially be a holdfast structure, or a frond, or an artefact of the surface topography. Unfortunately, neither image was taken in good lighting, and fresh study of the specimens, which remain *in situ* on the bedding plane, is required to determine exactly what each one truly represents.

Appendix A3

Pigeon Cove Fossil Dataset

The following table presents the raw data collected in the field for each Pigeon Cove specimen, documenting length, width, and orientation information. A series of graphs show the general patterns observed in the data from this assemblage.

Map Zone	Field Code	Length (mm)	Width (mm)	Orientation (°)	Additional Notes
Alpha	A1	27	6	-	Positive bump
Alpha	C1	13	4	315	
Alpha	C2	12	1	253	At edge of Pizza
Alpha	C3	10	1	178	At edge of Pizza
Alpha	C4	5	3	332	
Alpha	D1	25	20	266	
Alpha	F1	-	-	-	Wavy
Alpha	F2	-	-	228	Wavy
Beta	C5	15	2	353	Just one side
Beta	C6	8	1	45	Xmas tree like frond
Gamma	A2	30	10	143	
Gamma	C10	8	3	341	
Gamma	C11	10	2	248	
Gamma	C12	14	4	275	
Gamma	C13	14	2	38	
Gamma	C14	15	2	20	
Gamma	C15	19	3	80	
Gamma	C16	9	3	47	
Gamma	C17	7	3	232	
Gamma	C21	9	2	45	Dubious
Gamma	C22	5	4	355	
Gamma	C23	10	2	79	
Gamma	C24	30	2	N/A	Bends
Gamma	C25	No Fossil			
Gamma	C26	3	2	311	
Gamma	C27	22	2	73	
Gamma	C28	10	3	256	
Gamma	C29	10	4	228	
Gamma	C30	19	4	6	
Gamma	C7	20	2	99	
Gamma	C8	17	5	233	
Gamma	C9	20	2	201	
Gamma	D2	25	12	258	
Gamma	F10	50	1	65	
Gamma	F3	23	1	9	
Gamma	F4	27	1	181	

Map Zone	Field Code	Length (mm)	Width (mm)	Orientation (°)	Additional Notes
Gamma	F5	65	2	52	
Gamma	F6	30	1	53	Curves
Gamma	F7	23	1	50	Curves
Gamma	T1	30	12	95	
Gamma	C32	15	2	220	Bent
Gamma	C31	15	2	340	
Delta	T2	72	24	216	
Delta	D3	35	22	128	One concentric ring
Delta	A2	30	5	8	
Delta	F11	25	1	35	
Delta	F12	17	1	48	
Delta	C33	10	2	57	Curved
Delta	D4	14	1	-	
Delta	C47	10	2	59	
Delta	F25	20	1	10	
Delta	F24	15	1	24	Slightly curved
Delta	C48	9	4	267	Around pizza disc
Delta	C49	12	3	224	Around pizza disc
Delta	C50	10	3	284	Around pizza disc
Delta	F26	30	1	31	Within pizza disc
Delta	C51	16	2	23	
Delta	F27	40	2	45	Dubious
Delta	C52	11	2	45	
Delta	C53	15	3	125	Possible kink
Delta	C55	6	2	43	
Delta	C54	16	4	88	
Delta	C56	7	4	50	
Delta	C57	10	4	124	
Phi	F17	15	1	264	
Phi	F18	8	1	150	
Phi	F19	22	1	59	Curved
Phi	F20	20	1	161	
Phi	F16	65	1	150	
Phi	F14	15	1	57	Curved
Phi	C38	13	3	78	
Phi	A3	6	5	-	
Phi	F13	27	1	6	Curved
Phi	C36	6	2	79	
Phi	C35	11	2	72	
Phi	C34	3	1	67	
Phi	C39	20	1	127	Curved, dubious
Phi	C40	9	3	333	
Phi	F21	16	1	317	
Phi	C42	10	3	356	
Phi	C43	10	2	92	
Phi	C44	5	1	66	Within pizza disc
Phi	C45	10	2	43	
Phi	F22	45	1	54	
Phi	F23	27	1	50	Within pizza disc, branches
Phi	C61	11	2	57	

Map Zone	Field Code	Length (mm)	Width (mm)	Orientation (°)	Additional Notes
Phi	F29	30	1	-	Curved
Phi	F28	26	1	-	Loops
Theta	C58	14	2	199	
Theta	A4	30	5	-	
Theta	C60	10	5	179	
Theta	C59	9	3	80	
Theta	A5	7	2	78	
Theta	C62	8	3	86	In pizza disc
Theta	C63	10	2	74	Very nice, in pizza disc
Theta	C64	4	2	140	
Theta	C65	14	4	179	Messy
Theta	F30	25	1	165	
Theta	F31	30	1	163	
Theta	C66	5	3	18	
Theta	F32	35	1	237	Curves
Theta	C69	8	2	37	
Theta	C68	23	2	70	
Theta	C67	5	2	79	
Theta	C76	17	3	53	
Theta	F33	25	1	25	
Theta	C71	15	3	49	
Theta	C70	4	2	130	
Theta	C73	15	4	32	
Theta	C74	9	4	82	
Theta	C75	7	2	100	
Theta	C72	10	5	197	Looks like a spindle
Theta	A6	7	2	25	
Theta	A7	7	2	80	
Pi	A9	30	9	65	
Pi	F36	25	1	102	Bends
Pi	F37	18/23	1	144	Bends
Pi	C80	7	2	56	Weak
Pi	F38	13	1	110	
Pi	F39	20	1	134	Bends
Pi	F40	18	1	8	Branches, wavy
Pi	PF1	80	25	79	zone with small pizza disc
Pi	A10	12	3	61	Finger
Pi	C81	6	2	1	
Pi	F41	50	1	87	Within Pizza disc
Pi	C82	6	2	72	Scruffy
Pi	PF2	160	15	77	Zone within pizza disc
Pi	C83	10	3	76	
Pi	C84	20	3	27	Very nice
Pi	F42	23	1	63	Very nice
Pi	T3	70	30	124	
Pi	C85	12	3	28	
Pi	PF3	100	50	55	Fans out
Pi	A11	14	6	79	
Pi	C86	9	2	106	
Pi	A12	40	12	42	Scratch marks?

Map Zone	Field Code	Length (mm)	Width (mm)	Orientation (°)	Additional Notes
Tau	B1	250	22	N/A	Bubble mat
Tau	F43	24	1	65	
Tau	PF4	280	50	48	Zone - filaments up to 4m wide
Tau	F44	38	1	0	
Tau	C87	7	3	22	
Tau	F45	20	1	42	Branches
Tau	F46	20	1	31	
Tau	F47	10	1	91	Curves
Tau	F48	17	1	78	
Tau	C88	19	2	80	Bent - poor preservation
Tau	F49	20	1	31	
Tau	C89	21	2	209	
Tau	C90	6	2	259	
Tau	C91	10	4	207	
Tau	F50	10	1	84	Possible branching
Tau	C92	13	2	256	
Tau	F51	25	1	N/A	L. Bend
Tau	A13	6	1	3	
Tau	A14	40	25	N/A	Frond-like on a pizza disc
Tau	PF5	35	20	58	Zone, within pizza disc
Tau	F52	40	3	357	
Tau	C93	9	3	241	Nice, possible external walls
Tau	C94	28	2	246	
Tau	A15	7	2	224	Possibly two filaments
Tau	F53	30	1	272	
Tau	C95	20	3	21	Horseshoe shape
Tau	F54	23	1	191	
Tau	C96	7	3	154	Spindle?
Tau	F55	10	1	168	
Tau	C97	9	4	223	
Tau	F56	33/25	1	39/55	2 Branches
Tau	F57	6	1	316	
Tau	C98	7	2	74	
Tau	C99	9	2	90	Poor preservation
Sigma	F34	35	1	165	
Sigma	C77	8	3	249	
Sigma	F35	28	1	268	Wavy
Sigma	A8	4	0.5	183	Possible small fiament
Sigma	F58	41	1	62	
Sigma	F59	14	1	114	curved
Sigma	C78	8	2	60	dubious, poor preservation
Sigma	F60	40	1	232	Positive, on a pizza
Sigma	C79	10	3	75	curved
Mu	F61	11	1	14	Faint
Mu	F62	13	1	48	
Mu	C100	10	2	102	Poor preservation
Mu	C101	8	2	292	
Mu	C102	8	2	265	
Mu	C103	7	2	299	
Mu	A16	24	5	343	Branching structure

Map Zone	Field Code	Length (mm)	Width (mm)	Orientation (°)	Additional Notes
Mu	C104	21	3	80	May be two fronds
Mu	C105	7	2	233	
Mu	F63	6	1	200	
Mu	F64	12	1	241	Straight
Mu	C106	11	2	232	
Mu	F65	7	1	165	
Mu	C107	13	5	87	Possibly incomplete
Mu	F66	50	4	95	Thick strand
Mu	F67	80	1	233	
Mu	F68	33	1	40	
Mu	F69	16	1	278	
Mu	F70	45	1	52	
Mu	F71	33	1	21	Kink
Mu	C108	7	3	61	
Mu	F72	14	1	35	Poor preservation
Mu	C109	6	2	270	Poor preservation
Lamda	C110	4	2	160	
Lamda	F73	9	1	153	
Lamda	C112F	12	1	210	Branches - actually a filament
Lamda	C113	9	3	68	Dubious
Lamda	C111	24	6	104	One of 3 possible large fronds
Lamda	F75	10	1	-	Curves
Lamda	F74	11	1	15	
Lamda	F76	14	1	52	
Lamda	F77	33	1	35	
Lamda	C114	10	2	48	In a small pizza
Lamda	F79	14	1	323	
Lamda	F78	7	1	344	Branches
Lamda	F80	32	1	191	wavy
Lamda	F81	32	1	172	wavy
Lamda	F82	10	1	258	Very curvy
Lamda	C115	9	2	69	
Lamda	C116	13	2	357	
Lamda	F83	12	1	358	
Lamda	F84	10	1	305	
Lamda	F85	41	1	80	Kink
Lamda	C117	4	4	161	Incomplete - nice
Lamda	C118	18	3	358	
Lamda	F86	18	1	-	Branches
Lamda	C119	8	2	340	Poor preservation
Lamda	A17	18	13	14	Odd
Lamda	F87	13	1	142	
Lamda	C121	5	3	6	Poor preservation
Lamda	F88	13	1	112	
Lamda	F89	15	1	81	
Lamda	C120	8	3	75	
Omega	A18	6	7	n/a	Incomplete
Omega	F90	5	1	40	Curves
Omega	F91	4	1	5	
Omega	F92	16	1	308	Edge of pizza

Map Zone	Field Code	Length (mm)	Width (mm)	Orientation (°)	Additional Notes
Omega	F93	15	1	108	
Omega	F94	14	1	344	Faint
Omega	F95	9	1	103	Small bend
Omega	A20	7	3	83	Pit
Omega	F96	12	1	116	
Omega	A21	24	4	324	
Omega	F97	23	1	292	
Omega	F98	12	1	51	
Omega	F99	130	1	12	
Omega	TF1	23	1	75	
Omega	F101	50	1	62	
Omega	F102	28	1	111	
Omega	F103	12	1	145	
Omega	F104	6	1	85	
Omega	F105	25	1	128	Wavy
Omega	F106	14	1	63	Curves
Omega	F107	11	1	80	
Omega	F108	7	1	27	Strange shape
Omega	C122	8	2	62	
Omega	A23	4	2	47	Positive lump
Omega	C123	9	2	0	Dubious
Omega	F109	103	1	65	Very clear
Omega	F110	8	1	102	Bends
Omega	A24	60	11	16	
Omega	PF6	190	25	80	
Omega	D5	15	14	-	
Omega	F111	22	1	124	
Omega	F112	21	1	164	
Omega	C124	10	2	25	Broken
Omega	D6	30	21	64	
Omega	PS1	130	1	16	
Omega	C125	16	3	18	Bends
Omega	F113	15	1	56	
Omega	F114	10	1	330	
Omega	F115	59	1	320	
Omega	F116	27	1	70	One of 3
Omega	A25	52	24	67	
Omega	F117	70	3	54	Probable association with pizza
Omega	C126	12	3	17	
Omega	F118	10	2	247	
Omega	A26	32	25	N/A	
Omega	F119	19	1	45	
Omega	F120	34	1	76	
Omega	F121	43	1	48	
Omega	C128	8	3	71	
Omega	F122	32	1	75	Bends
Omega	A27	18	2	58	
Omega	F123	44	1	44	
Omega	F124	10	1	50	
Omega	F125	19	1	82	
Omega	F126	21	1	55	Wavy
Omega	A28	63	5	178	Tapers

Map Zone	Field Code	Length (mm)	Width (mm)	Orientation (°)	Additional Notes
Omega	C129	5	3	30	Poor preservation
Omega	F127	11	1	67	Curves
Omega	PF7	60	10	202	Zone
Omega	F128	27	1	56	Curves
Omega	C130	20	3	0	
Omega	F127	14+	1	40	
Omega	A29	17	4	188	Strongly positive
Omega	C131	14	2	27	Gentle curve
Omega	F130	9	1	55	
Omega	C132	11	3	76	
Omega	C133	18	3	79	Curves, possible pectinate
Omega	F131	33	1	27	Possible disc
Omega	F132	14	1	122	
Omega	F133	22	1	55	
Omega	F134	30	1	164	Runs on to small pizza disc
Omega	C134	7	2	6	
Omega	C135	7	1	24	
Omega	C136	11	3	230	Cast. Total length 33mm
Omega	PS2	790	1	18	Incomplete, 2 pic's
Omega	A30	72	17	132	
Omega	F135	40	1	42	2 filaments, very curved
Omega	C137	10	2	46	
Omega	F136	15	1	96	
Omega	F137	10	1	24	
Omega	F138	17	2	58	Possible frond + disc, very interesting
Omega	F139	17	1	11	
Omega	F140	24	1	84	
Omega	F141	14	1	95	
Omega	C138	6	3	347	Possible 2nd frond
Omega	F142	6	1	65	
Omega	F143	6	0.2	85	V.V. Thin
Omega	A31	11	7	62	
Omega	F144	65	1	12	Small wardii???

Table A3.1. Dimension, location and orientation data for the small fronds and filaments observed on the Pigeon Cove bed DRK2PC. For field codes, C = frond, F = filament, B = bubble mat, A = anomalous impression, T = *Thectardis*, D = discoidal fossil. Map zones in the first column correspond to Fig. A4.1.

Bed Section	Bearing for 'North'
Alpha	117
Beta	80
Gamma	100
Delta	70-74
Sigma	72
Pi	66
Tau	51
Mu	54
Omega	53
Lamda	53
Phi	72
Theta	72

Table A3.2. Bearings for the direction of North (up dip) as measured during the Pigeon Cove small frond survey.

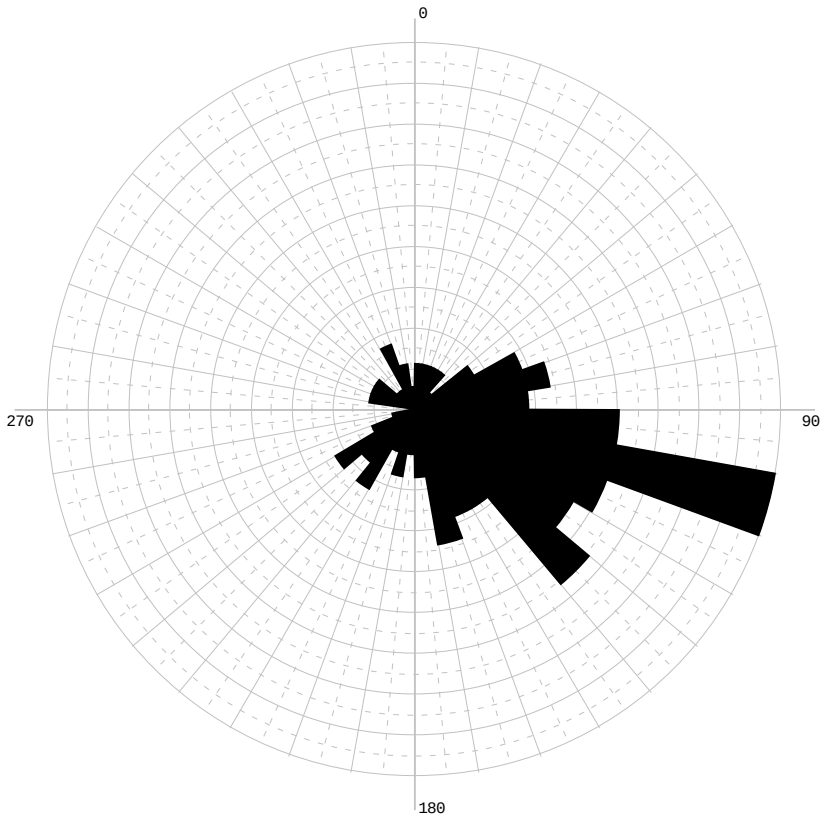

Fig. A3.1. Small filament orientations: n = 134, max. = 16. Values corrected to magnetic North.

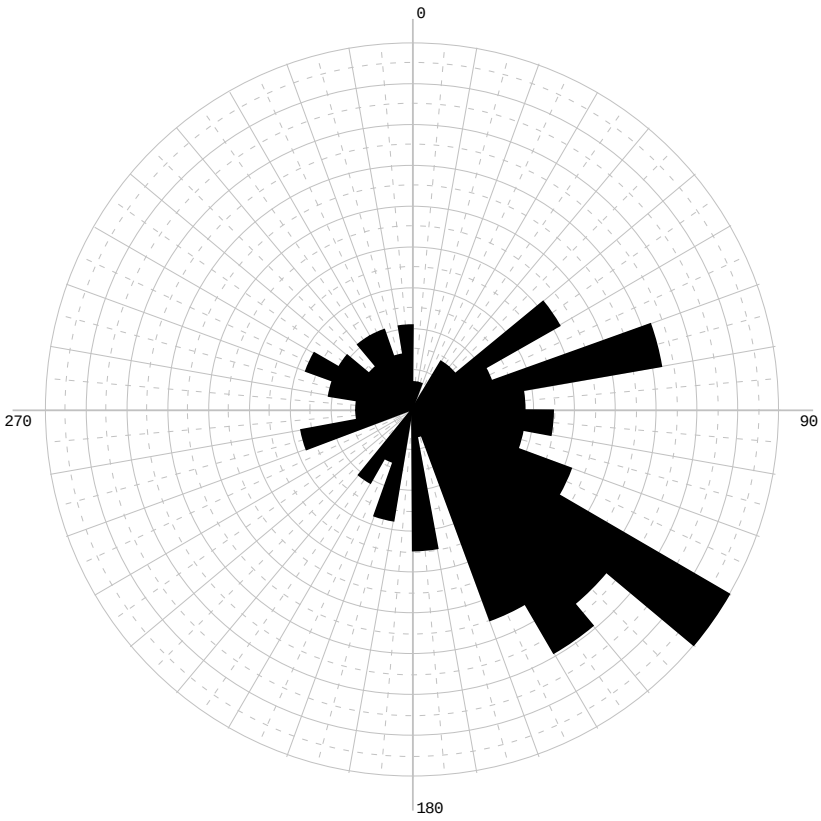

Fig. A3.2. Small frond orientations from Pigeon Cove. n = 129, max. = 19. Corrected to magnetic North.

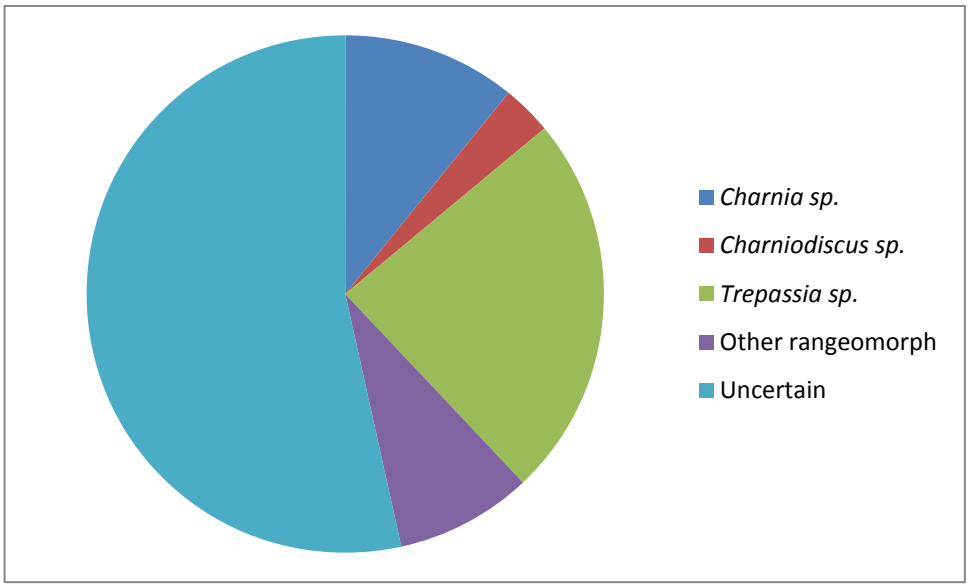

Fig. A3.3. Pie chart showing the relative proportions of identifiable frondose genera in the Pigeon Cove small-frond assemblage. n = 129. The difficulty involved in identifying these small fronds accounts for the large proportion of 'uncertain' taxa. Specimens were assigned as 'uncertain' rather than as 'other rangeomorphs' since it was not always possible to determine whether true rangeomorph branching was present.

Appendix A4

Map of the Pigeon Cove Surface

The Pigeon Cove surface was mapped in detail to document all specimens of small fronds and filaments. To achieve this, the surface was divided into sections, which were assigned Greek letters, as detailed in Fig. A4.1. These sections correspond to the 'Map Zones' detailed in the table in Appendix A3.

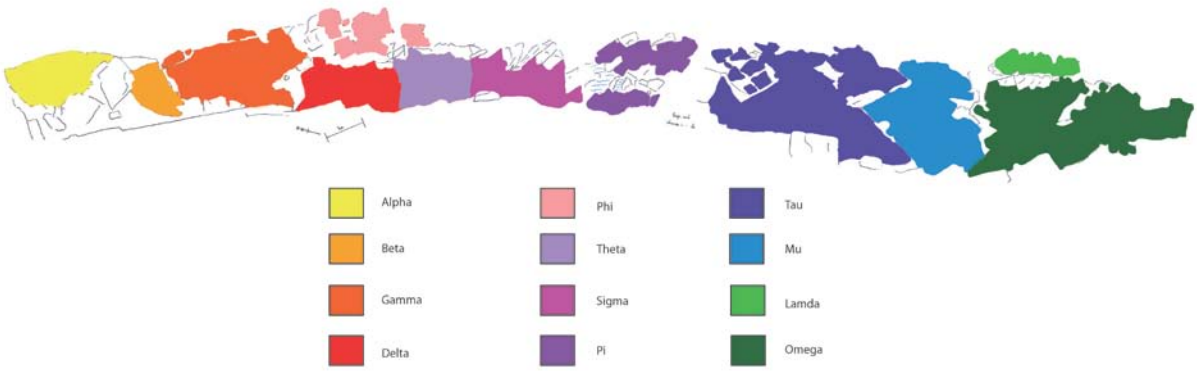

Fig. A4.1. A digitised map of the Pigeon Cove surface, showing the zones, delineated in the field, which constitute the surface.

Each section was then scrutinised, and all fronds and filaments, along with other interesting features of possible biological origin, were measured and their positions documented. The base maps were then stitched together, and the entire surface was digitised using Adobe Photoshop CS4, to produce the maps in Fig. A4.2.

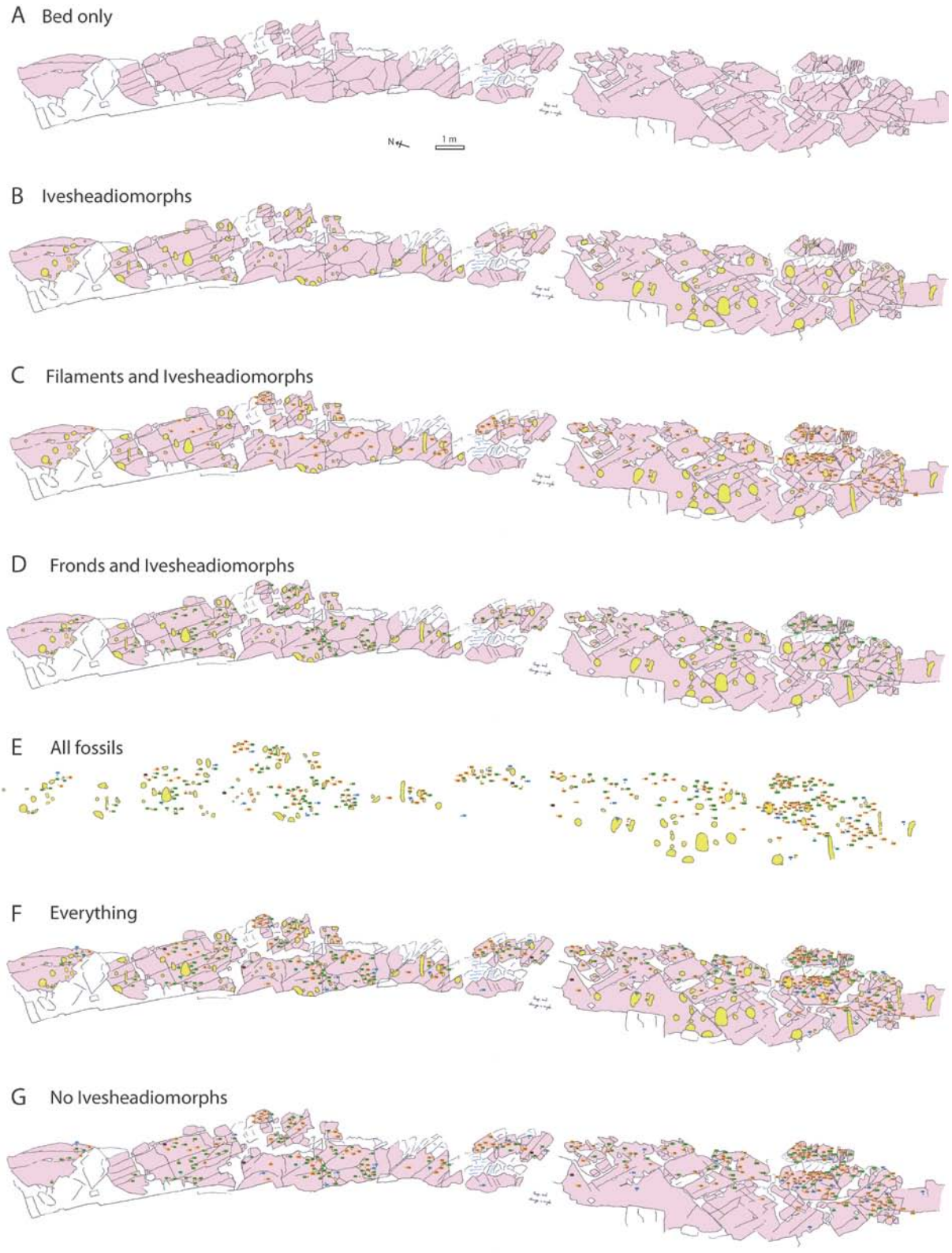

Fig. A4.2. The digitised map of the Pigeon Cove surface, with various images showing different combinations of fossils switched ‘on’ or ‘off’. For a key to the fossil labels, see the larger map in Fig. A4.3.

Fold out map

Appendix A5
Fossils from other Avalonian sites

This sub-appendix is simply included as a place to deposit images of specimens discovered during the course of the doctoral project that are relevant to the discussions within this thesis, but which cannot be reviewed in full in the general text.

The rocks of the St John's and Signal Hill Groups of Newfoundland provide a good comparative study with which to compare the successions of the Longmynd in Shropshire. The shallow water settings of the Gibbett Hill and Ferryland Head Formations on the Avalon Peninsula are analogous in lithology to those of the Burway to Lightspout Formations of the Longmyndian Supergroup. What is more, these shallow Newfoundland settings have been observed by the writer to possess discoidal fossil impressions, previously unreported, resembling *Intrites punctatus* and *Beltanelliformis minutae* (Fig. A5.1C–E). Their occurrence alongside other typical Longmyndian impressions such as *Arumberia* (Fig. 5.1A), and within red-beds, suggests that the preserved stratigraphic ranges of these taxa are controlled by the depositional environment rather than by true evolutionary trajectories. These specimens will be described in further detail in the Master's Thesis of Jack Matthews, University of Oxford, 2011.

Fig. A5.1. Longmyndian fossils from the Signal Hill and St John's Groups of Newfoundland. **A**: *Arumberia*, from near FRY 11, Gibbett Hill Fmn. **B**: *Palaeopascichnus* or *Neonereites*, FRY 12, Gibbett Hill Fmn. Although this taxon is not found in the Longmynd, it is known from the shallow-water levels of the Fermeuse Formation in Newfoundland. **C**: *Intrites punctatus*, locality FRY 11, Gibbett Hill Fmn. **D**: *Beltanelliformis* aff. *minutae*, Ferryland Head Fmn. **E**: *Intrites* sp., Ferryland Head Fmn. Scale bars = 10 mm.

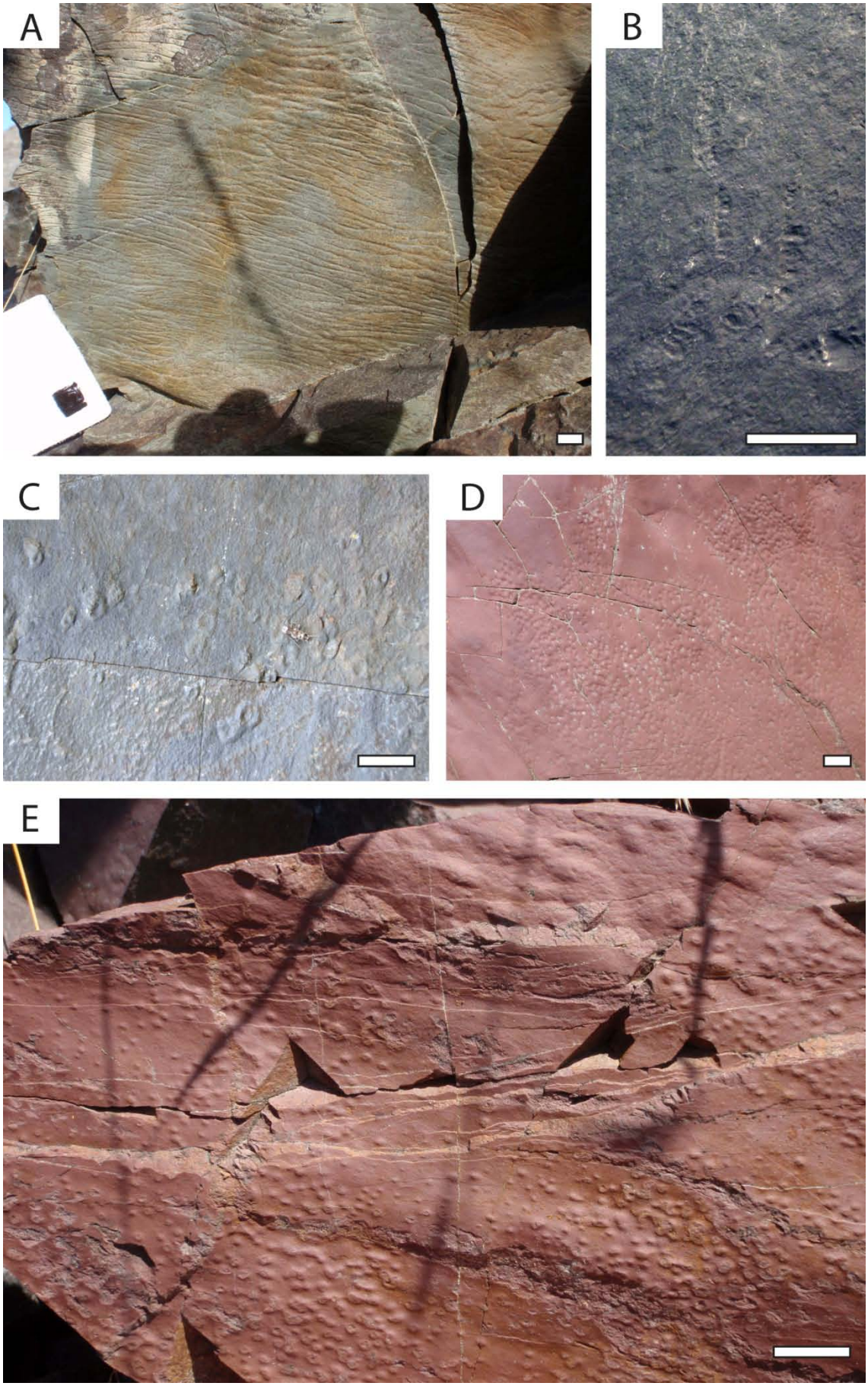
A
B
C
D
E

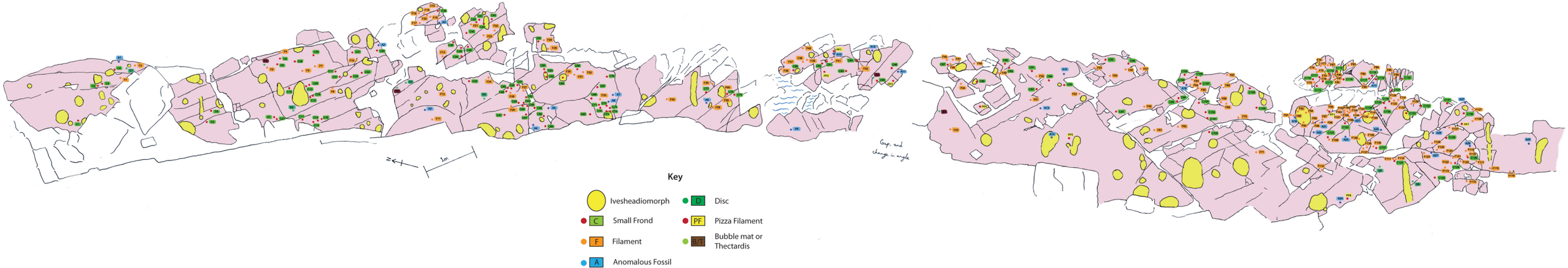
1m
Gap and change in angle
Key
Ivesheadiomorph
D Disc
C Small Frond
PF Pizza Filament
F Filament
B/T Bubble mat or Thectardis
A Anomalous Fossil

Appendix B

Charniodiscus specimens from the E Surface, Mistaken Point Formation, Mistaken Point, Newfoundland

In this Appendix, multiple *Charniodiscus* specimens are documented from the E Surface of Mistaken Point, Newfoundland. They demonstrate the range of preservation quality observed on a single bedding plane, and all remain *in situ* in the field, locality MP2 (Figs. 3.1–3.2; Appendix D2). The E Surface is divided by a ~5m wide gully, with the resulting surfaces distinguished here as E Surface East, and E Surface West. Due to its closer proximity to the sea, and subsequent erosion, the specimens from the eastern surface are substantially more weathered. Therefore, specimens from the two sides are presented separately. Appendix B1 contains images of all specimens, and outlines the spectrum of preservation observed within *Charniodiscus* taxa on the E Surface. Appendix B2 provides orientation data from the assemblage, broken down by species. All bedding plane images document the top surface of the bedding plane, with fossils being preserved largely in positive epirelief.

APPENDIX B1

IMAGES OF *CHARNIODISCUS* SPP.

The figured specimens correspond to the orientation data presented in Fig. 3.7, which can be seen in full in Appendix B2. All images were obtained during the 2009 field season. Rather than using standard labelling nomenclature for the following figures, I have labelled the specimens within each figure with their number in my dataset, assigned while imaging the specimens in 2009. These numbers correspond to the accompanying orientation data (Appendix B2).

The Western side of the E Surface

The western outcrop of the E Surface on Mistaken Point possesses the best quality preservation of the entire surface, since it is raised about 5–8 m above sea level, and therefore is not affected by significant wave erosion. Preservation quality decreases down-dip (closer to the sea), and also towards the central midline of the bed (where a small stream continually runs down the surface). The spectacular detail seen in fossils on this surface attracts tourists from around the world, and their daily presence each summer has caused a significant amount of erosion due to the constant trampling of feet. In recent years, wardens from the MPER Portugal Cove South Visitor Center have acted to mitigate this effect by enforcing a 'no footwear' policy on the surface, with soft slippers being distributed to visitors. Despite decades of human activity, the level of detail preserved in the fossils on this surface remains unrivalled within the MPER.

Specimens of *Charniodiscus procerus* Laflamme et al. 2004 (Fig. B1.1) and *Charniodiscus spinosus* Laflamme et al. 2004 (Fig. B1.2) can be exceptionally preserved on this surface, exhibiting all of the diagnostic morphological features of their taxa.

The taxonomy of the *Charniodiscus* genus requires significant revision. The genus was originally defined (as *Charniodiscus concentricus* Ford 1958) as a discoidal holdfast from Charnwood Forest, Leicestershire, which did not possess an accompanying frond (Ford, 1958). This specimen was originally thought to be the holdfast of *Charnia masoni* Ford 1958. It was only later that a frond was found in direct association with one of these discs, and assigned to *Charniodiscus concentricus* Ford 1963. The Leicestershire frond is clearly rangeomorph in nature, with a 'feathery' appearance, and is seemingly multifoliate (Brasier and Antcliffe, 2009, figs. 12–13). It also lacks a visible central stem.

Material from other global localities was then ascribed to the *Charniodiscus* genus based on its 'frond plus disc' morphology. *Charniodiscus arboreus* Jenkins and Gehling 1978, *C. oppositus* Jenkins and Gehling 1978, and *C. longus* Jenkins and Gehling 1978, were described from Australia (originally as *Arborea* or *Rangea* specimens; Glaessner and Wade, 1966), and these were followed by the Newfoundland specimens *C. procerus*, *C. spinosus* (Laflamme et al., 2004), and *Charniodiscus* sp. Hofmann et al. 2008. The frondose architecture of many Newfoundland forms differs significantly from that of the type *C. concentricus*, with rangeomorph elements not visible in the former, and strongly constrained frond architecture. Our research group does not feel that *C. procerus* and *C. spinosus* belong to the same genus as the type Leicestershire specimen (the former have never been found in Charnwood), and therefore at some point it is likely that revision of the taxon will be necessary. However, due to the taxonomic priority of the Charnwood specimen, it is the non-U.K. material that will require a new genus. Such taxonomic revision is beyond the scope of this current work.

Charniodiscus procerus is considered to be a distinct *Charniodiscus* species, defined by morphometric characteristics (Laflamme et al., 2004). It possesses a large, presumably circular basal holdfast disc, and a long, narrow stem accounting for >50% of the total length of the organism. The single relatively short frond (with respect to the total length) is lanceolate, has <15 primary branches, and is often aligned at an angle to the stem, such that it appears to be bent (e.g. Fig. B1.1 [2, 3, 15]; Laflamme et al., 2004). Although the type species for the genus, *Charniodiscus concentricus*, possesses what appear to be multiple fronds (e.g. Brasier and Antcliffe, 2009, fig. 12), no *Charniodiscus procerus* or *C. spinosus* specimens have been observed with more than one. The *C. procerus* frond has an oval shape, and possesses a straight central positive ridge, with primary branching emanating from this central axis. No secondary branching is observed in any of the E surface specimens.

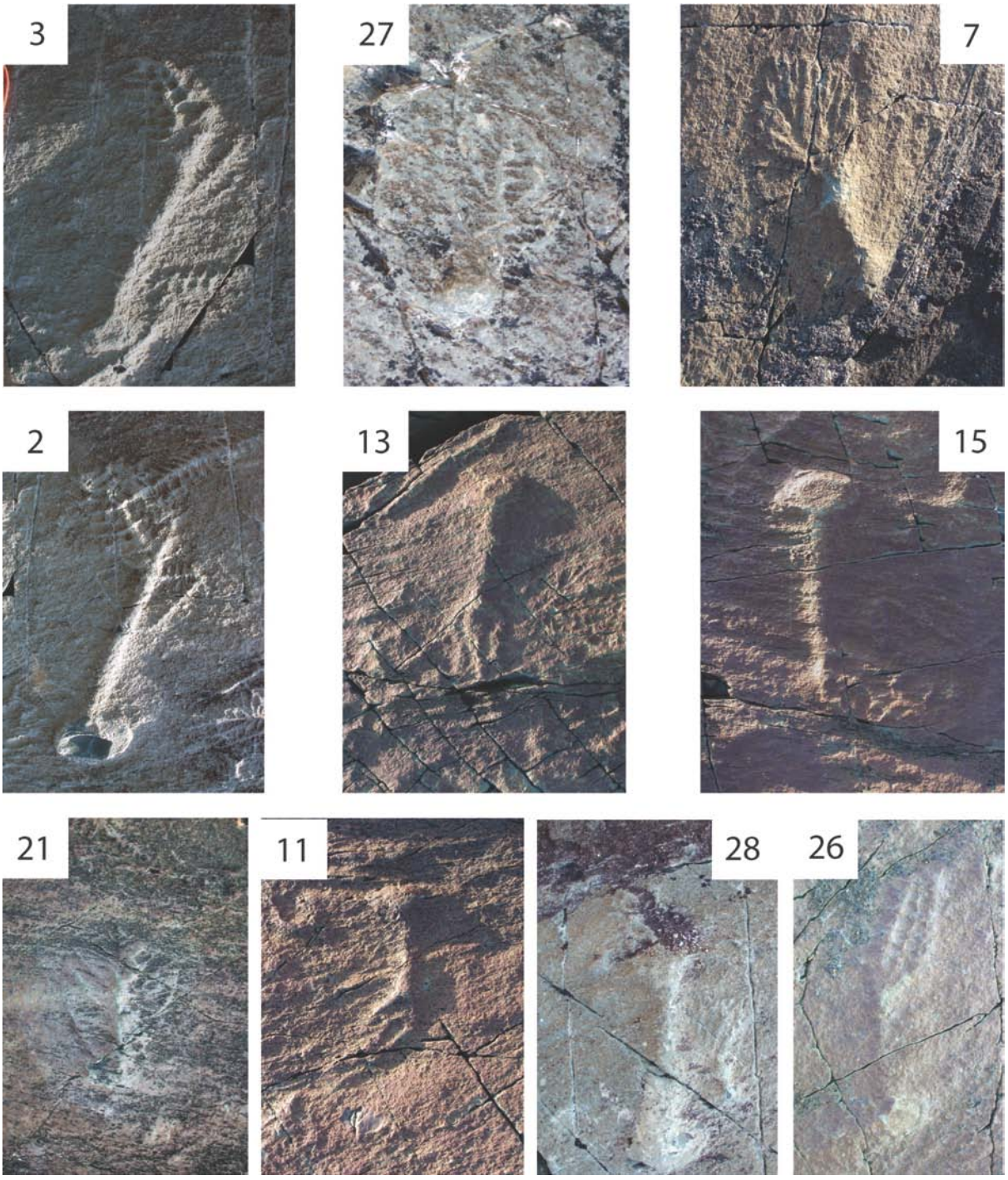

Fig. B1.1. *Charniodiscus procerus* and other specimens from E Surface West, Mistaken Point. The specimens in [7, 27 and 21] are not *C. procerus*, but other rangeomorph organisms with short stems. [7 and 21] are likely to be what has previously been termed a 'spatulate rangiid' (e.g. Narbonne et al., 2005), while [27] is a probable *Beothukis mistakensis* Brasier and Antcliffe 2009.

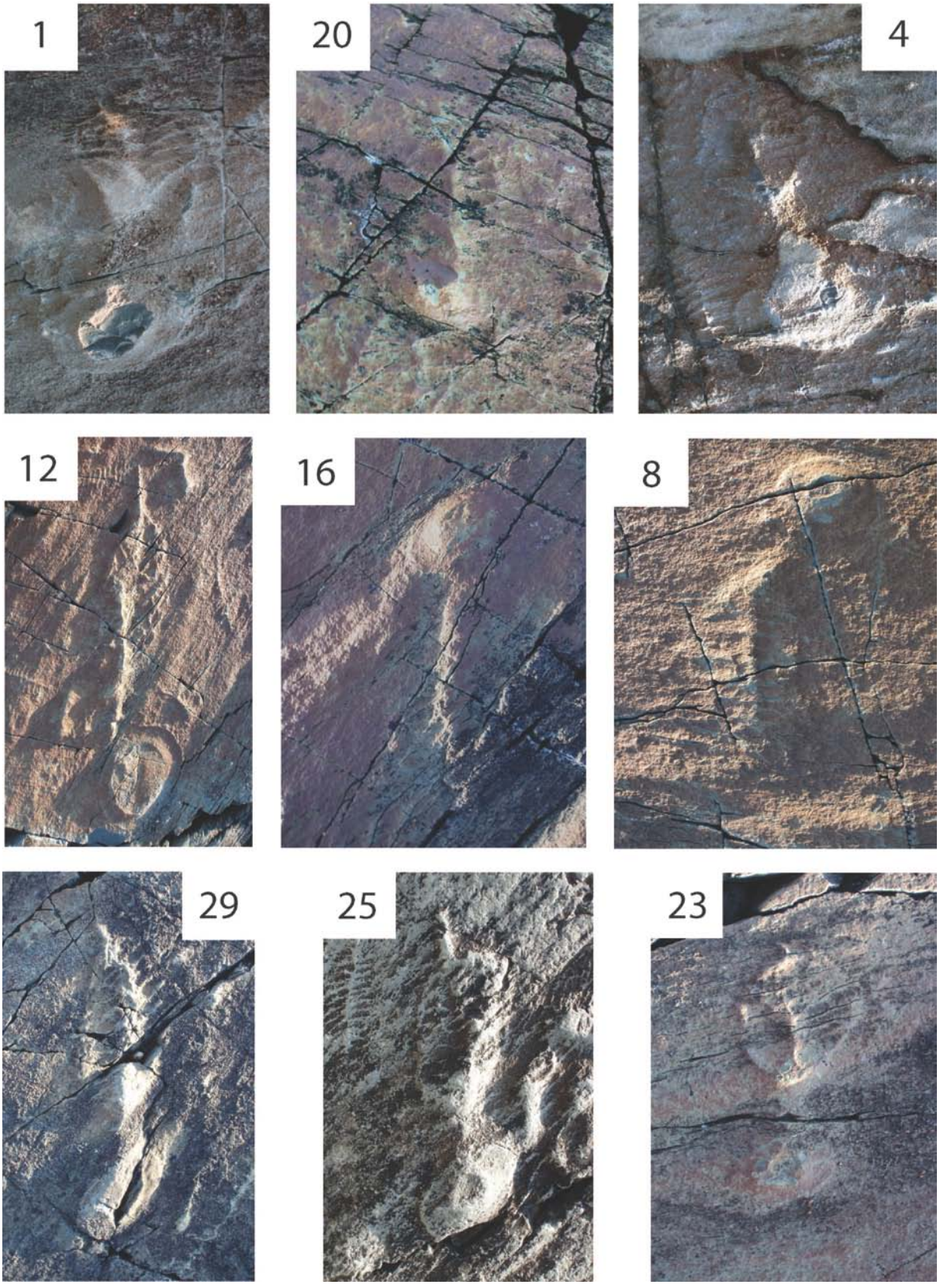

Fig. B1.2. *Charniodiscus spinosus* specimens from E Surface West, Mistaken Point, MP2. Note the characteristic large basal disc, short stem, and broad frond tapering to a 'spinose' tip. All of these specimens are considered to be relatively well-preserved.

Charniodiscus spinosus is diagnosed as having an ovate frond that is aligned with the stem, tapering to a pointed spine, and fewer than 15 primary branches (Laflamme et al., 2004). Those authors note that the holdfast disc of *C. spinosus* is larger than that of *C. procerus* specimens of a similar size, possibly due to the greater surface area of the *C. spinosus* frond experiencing more drag and therefore requiring increased structural support. Although not a defining feature, the majority of the Conception Group *C. spinosus* specimens possess a holdfast disc with one internal concentric ring (Fig. B1.2). All *Charniodiscus* specimens on the E surface are preserved in positive epirelief, by Conception-style or effaced preservation (Narbonne, 2005; Liu et al., 2011).

A large number of fossils on the E Surface do not possess enough well-preserved characteristic features to make a specific identification (Figs. B1.3, B1.9–1.10). However, these specimens are recognisable as *Charniodiscus* or other rangeomorph species, due to the preservation of discs or stems, and/or their general gross morphologies. Such impressions are not limited to regions of the bedding plane that are expected to show poor preservation (e.g. beneath lichen or close to the sea), but are distributed across the bed amongst the well-preserved specimens. This observation suggests that the factors responsible for their low-fidelity preservation are likely to have been original, with gradation in taphonomic quality being a primary feature on the Ediacaran seafloor. This preservational spectrum supports the effaced preservation hypothesis outlined in Chapter 3.

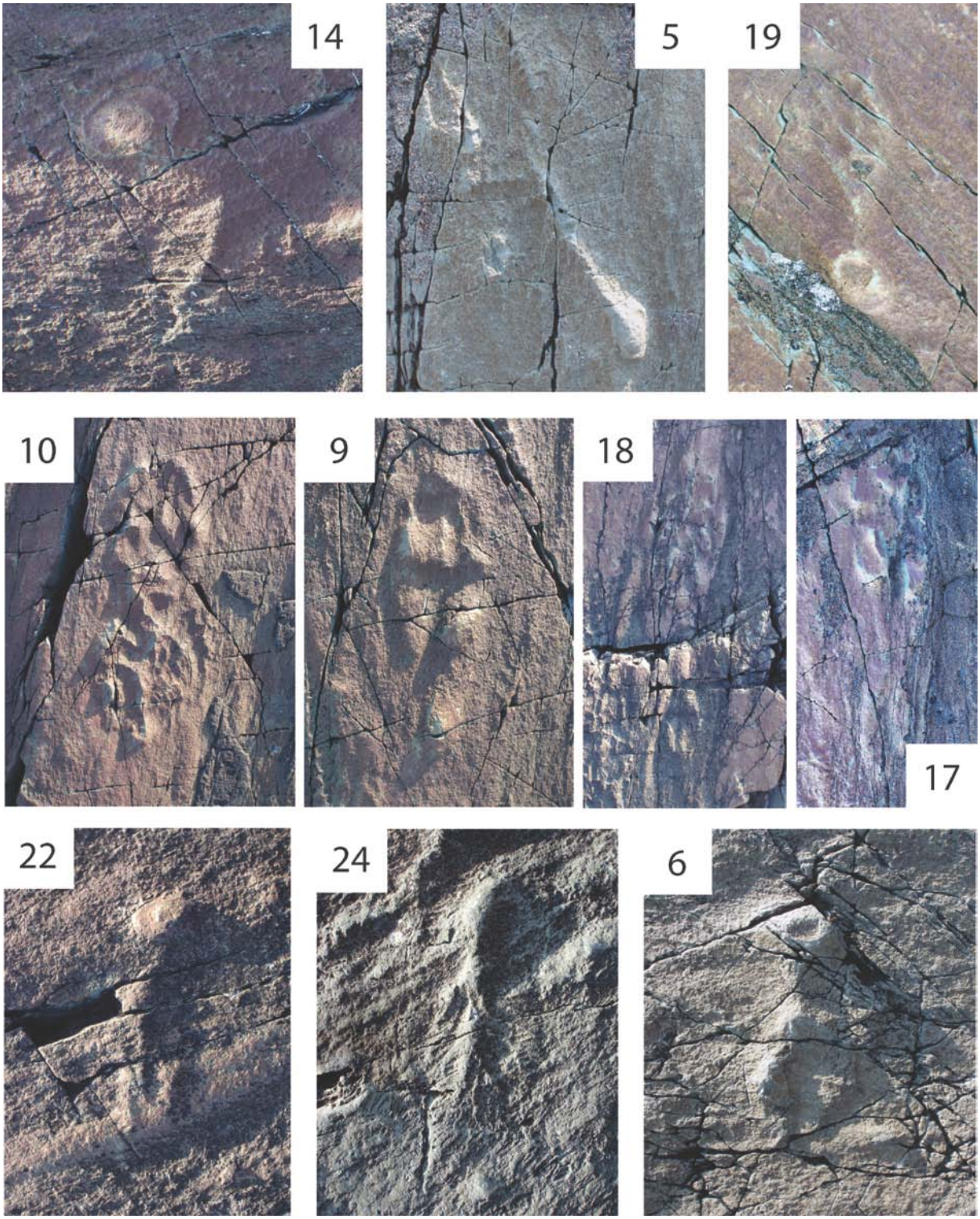

Fig. B1.3. Effaced rangeomorph specimens from E Surface West, Mistaken Point. Note that all specimens exhibit the gross morphological shape of a *Charniodiscus*. Specimen [24] is a rangeomorph organism with well-preserved branching in places, but it is not a *Charniodiscus*, and the splayed nature of the branching is unusual, likely reflecting a degree of effacement. Specimens [6, 9, 10, 17, 18] are the most effaced end-members on the surface, and are suggested to have lain decaying on the seafloor for a longer period of time than any of their neighbours.

The Eastern side of the E Surface

The eastern side of the Mistaken Point E Surface is not visited by tourists, and therefore has undergone little anthropogenic erosion. However, the surface is significantly closer to the ocean than the western outcrop due to the dip of the bedding plane, and therefore its southern end is continuously splashed waves. This coats the bed in salt water, and pummels it with boulders during winter storms, leading to widespread erosion and smoothing of the relief of all fossils in that area. There is also a significant amount of algal cover (black) at the southern end of the bed, obscuring the fossils. The northern end of the bed is relatively sheltered by lower ledges and the morphology of the bay. Subsequently, fossils there are broadly better preserved and the surface appears ‘cleaner’, due to the lack of lichens. This is evident in the following images.

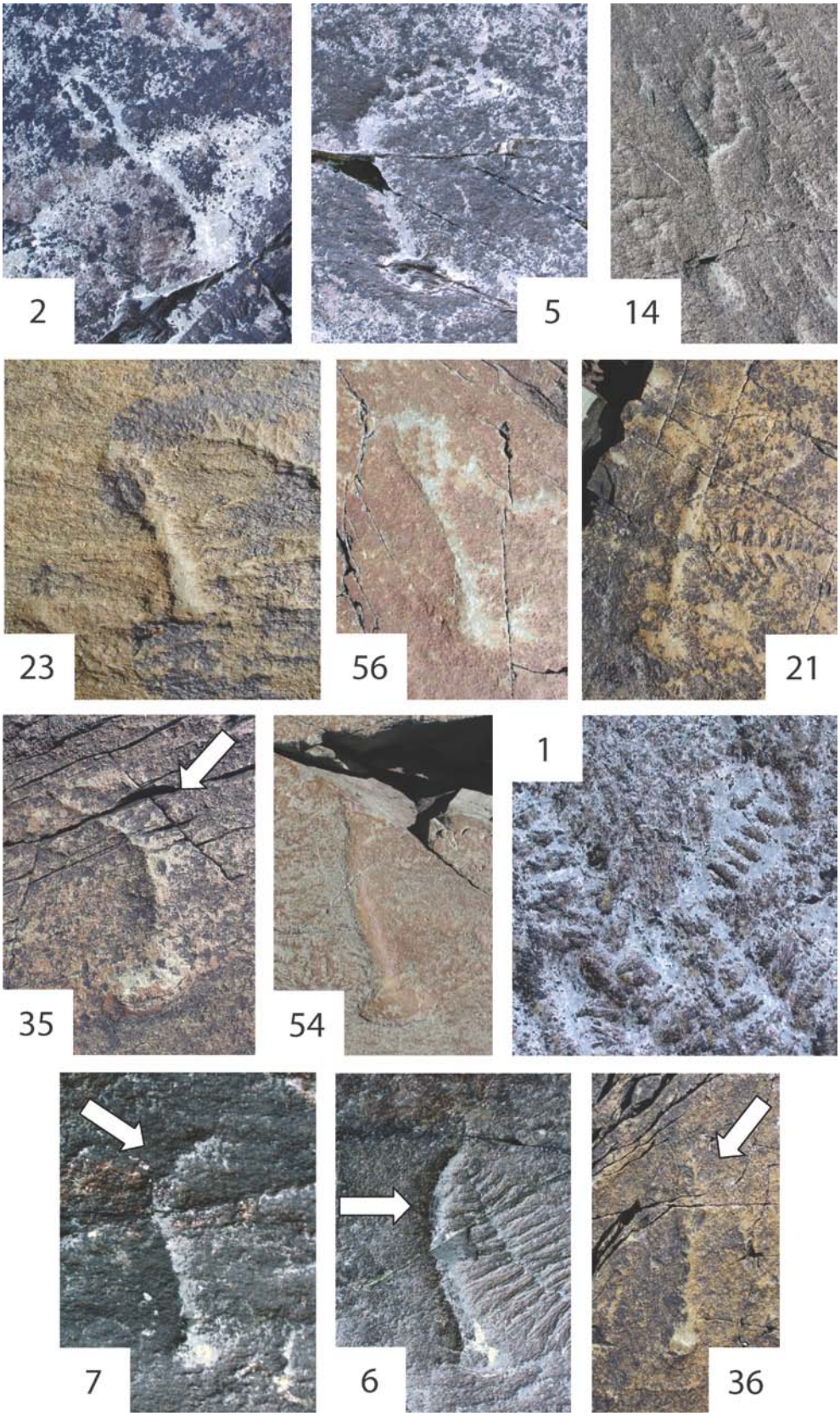

Fig. B1.4. *Charniodiscus procerus*,specimens from the E Surface East, Mistaken Point Formation, Mistaken Point, Newfoundland, Canada. Arrows in selected figures show the location of the effaced frond.

It can be seen that although the *C. procerus* specimens in B1.4 [2, 5, 14, 23, 56, 1, 21] are moderately well preserved and clearly show the characteristic features of the genus, those in the bottom half of the image (B1.4 [35, 6, 7, 36]) are relatively poorly preserved, with the fronds in particular showing substantial effacement (fronds are arrowed). The figure demonstrates the variation in preservation observed on a single bedding plane within one species. The lower individuals are interpreted to have undergone a degree of microbially-induced effacement following death on the seafloor, but they remain identifiable. Such specimens demonstrate the difficulties associated with quantifying the degree of effacement an individual specimen has undergone.

Specimens of *Charniodiscus spinosus* from the E Surface East document a range of preservation quality (Figs. B1.5–1.6). Whilst they all possess the morphological characteristics of a large concentric disc, short stem, and a broad frond with terminal ‘spine’, the completeness of each of these features, and the presence of further finer details, varies widely between specimens.

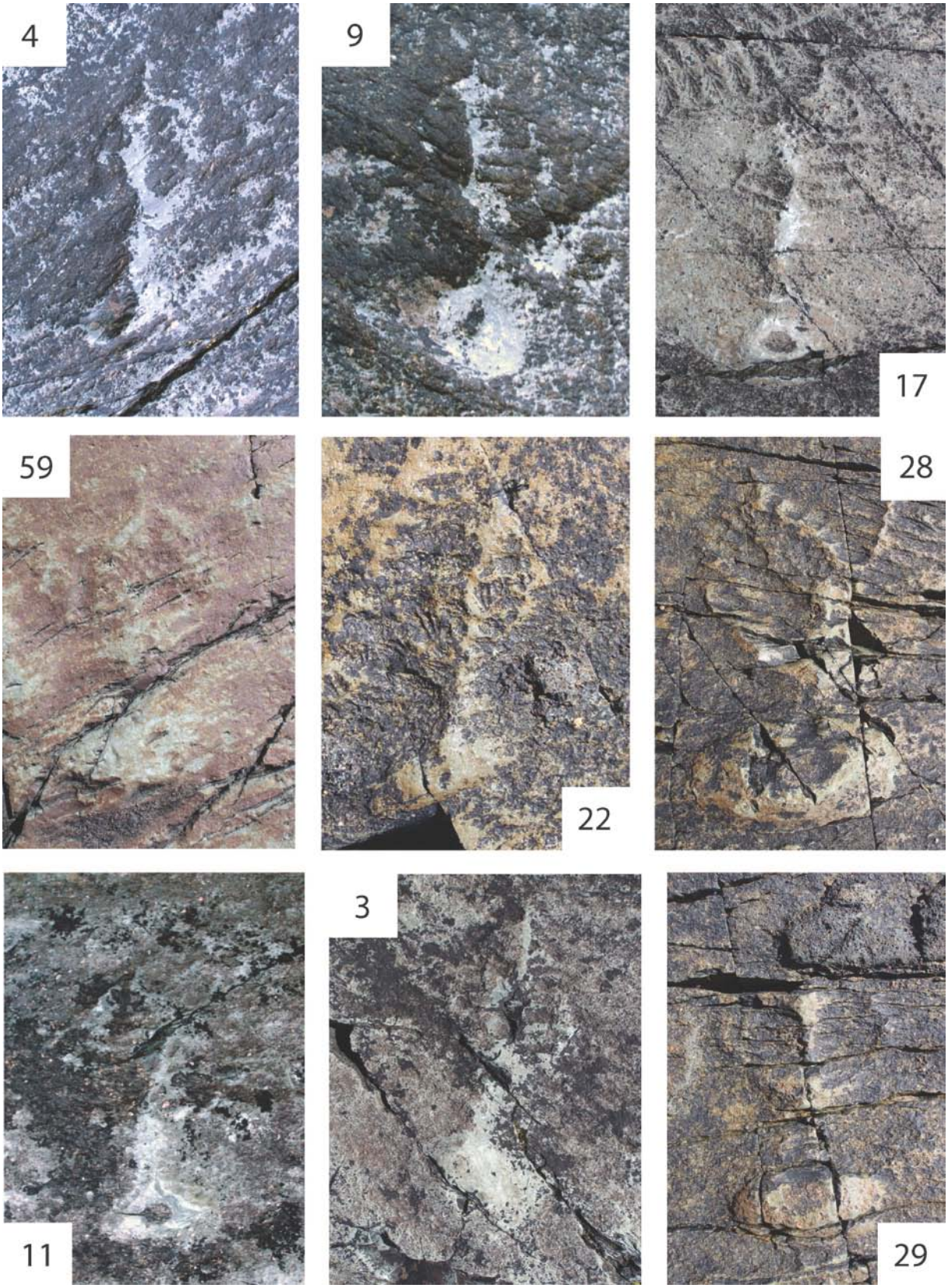

Fig. B1.5. *Charniodiscus spinosus* specimens from E Surface East, Mistaken Point

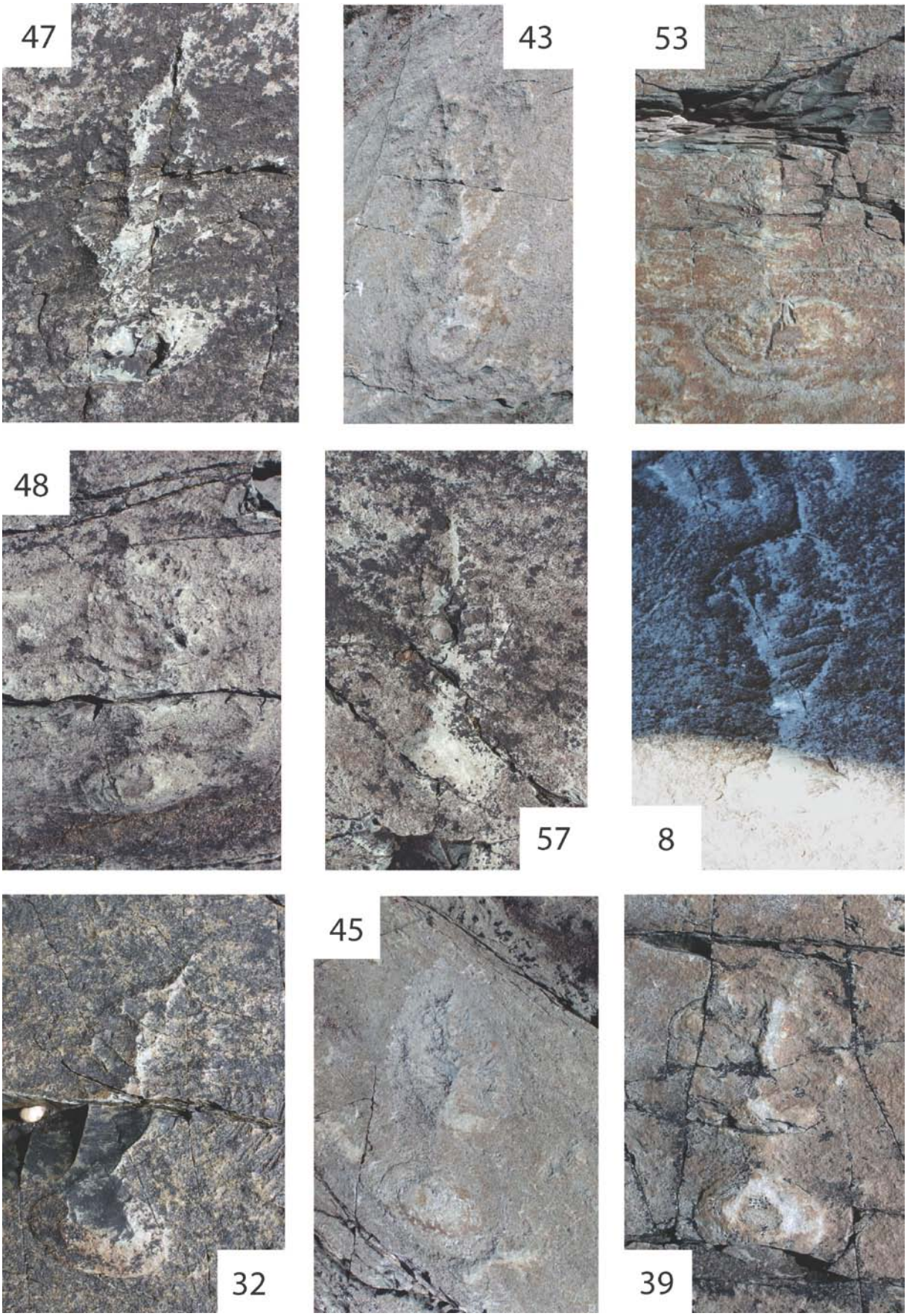

Fig. B1.6. *Charniodiscus spinosus* specimens from E Surface East, Mistaken Point, MP 2.

The specimens in Figure B1.7 are slightly more difficult to interpret due to their angles of branching, and short stem length. Fig. B1.7 [58] is likely to represent a *C. procerus* specimen, while [26] is a *C. spinosus*. The specimen figured in Fig. B1.7 [10] remains unidentifiable, with branching patterns that are not consistent with any known rangeomorph taxon. A similar frond found on bed MP9 (App. D2) suggests this may be a distinct taxonomic variant.

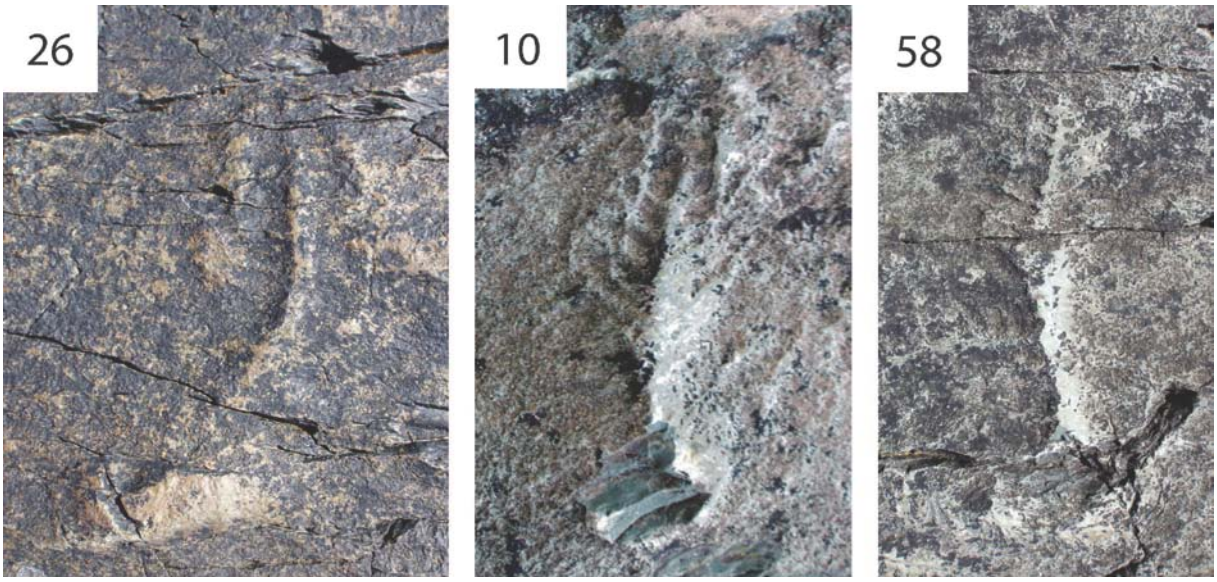

Fig. B1.7. Moderately well-preserved *Charniodiscus* specimens from E Surface East, Mistaken Point Formation, Mistaken Point, Newfoundland, Canada. [26]; *C. spinosus*? [10]; unknown specimen. [58]; *C. procerus*.

The specimens figured in Fig. B1.8 mostly represent uncertain *Charniodiscus* species. In some cases it appears that the branching angle of primary branches is too high to belong to a true *Charniodiscus* (e.g. Fig. B1.8 [18]). However, the majority of these specimens are too strongly eroded and weathered for an accurate identification to be made. Discs and stems are the most resistant parts of the fossil, with the frond being most prone to weathering. It is clear that topographic high points of ridges or lobes do not follow the impression of the disc or stem continuously, and can accentuate certain parts and not record others, producing an irregular, lobate fossil structure (Fig. B1.8 [16, 41]).

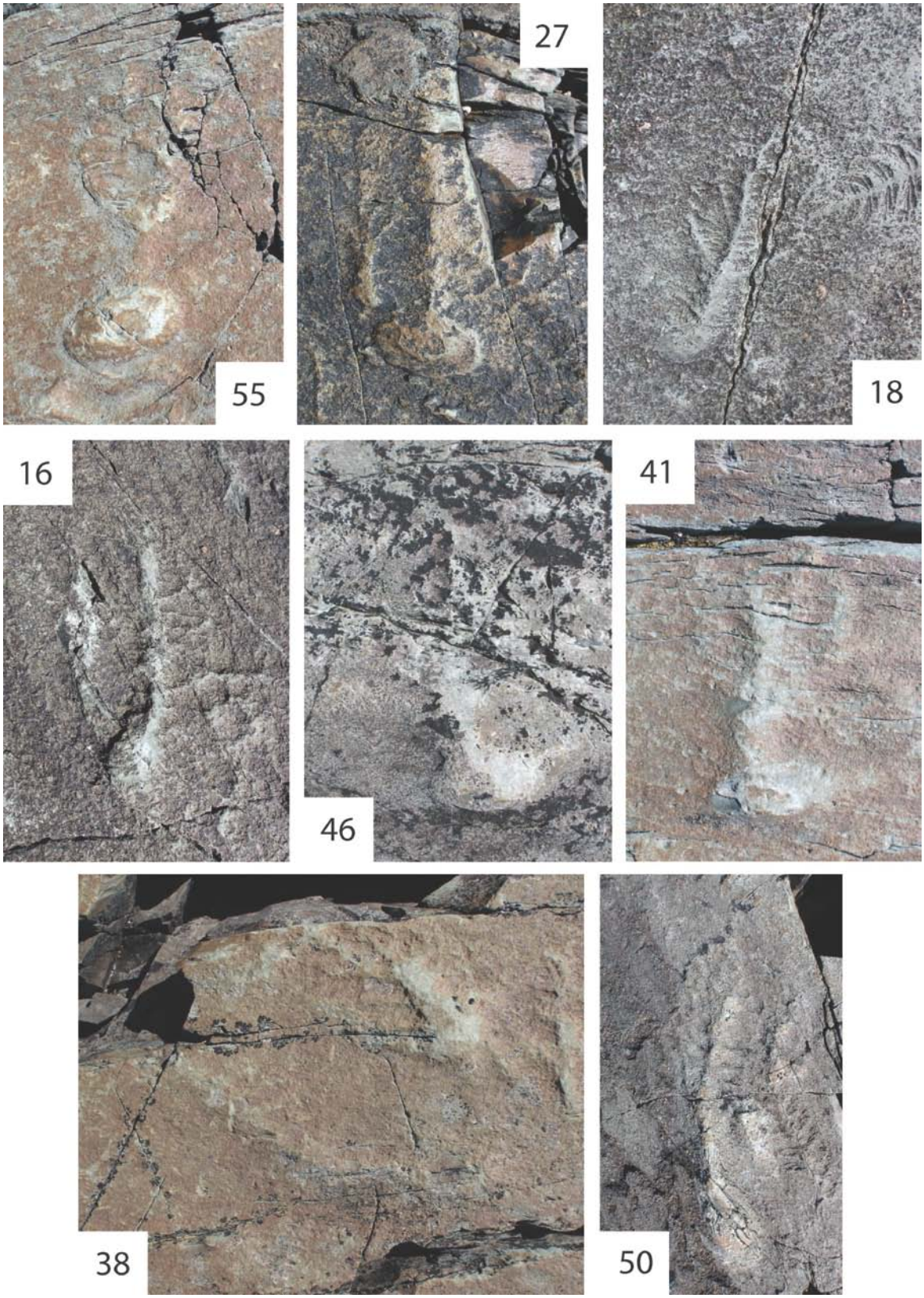

Fig. B1.8. Miscellaneous charniodiscids/rangeomorphs, E Surface East, Mistaken Point. Note that the specimen figured in [50] is identifiable as a *Charniodiscus spinosus*. Due to the limited amount of high-fidelity morphological information preserved in these specimens, it is not possible to identify them all to species level.

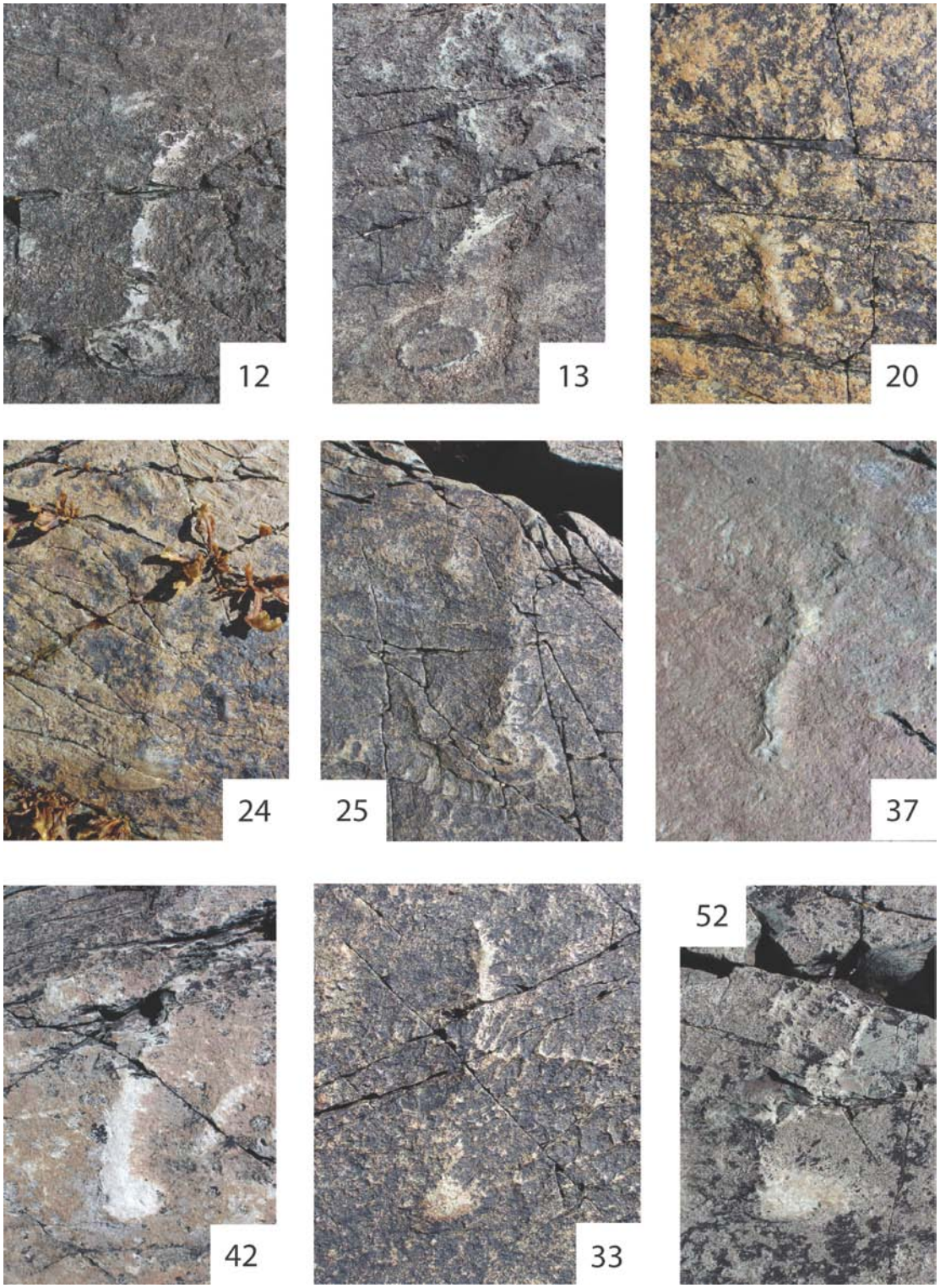

Fig. B1.9. Effaced rangeomorph specimens from E Surface East, Mistaken Point, MP2. Most of these specimens possess high-relief ridges along the central axis of the organism, rather than the lobate lumps and troughs seen in typical ivesheadiomorphs.

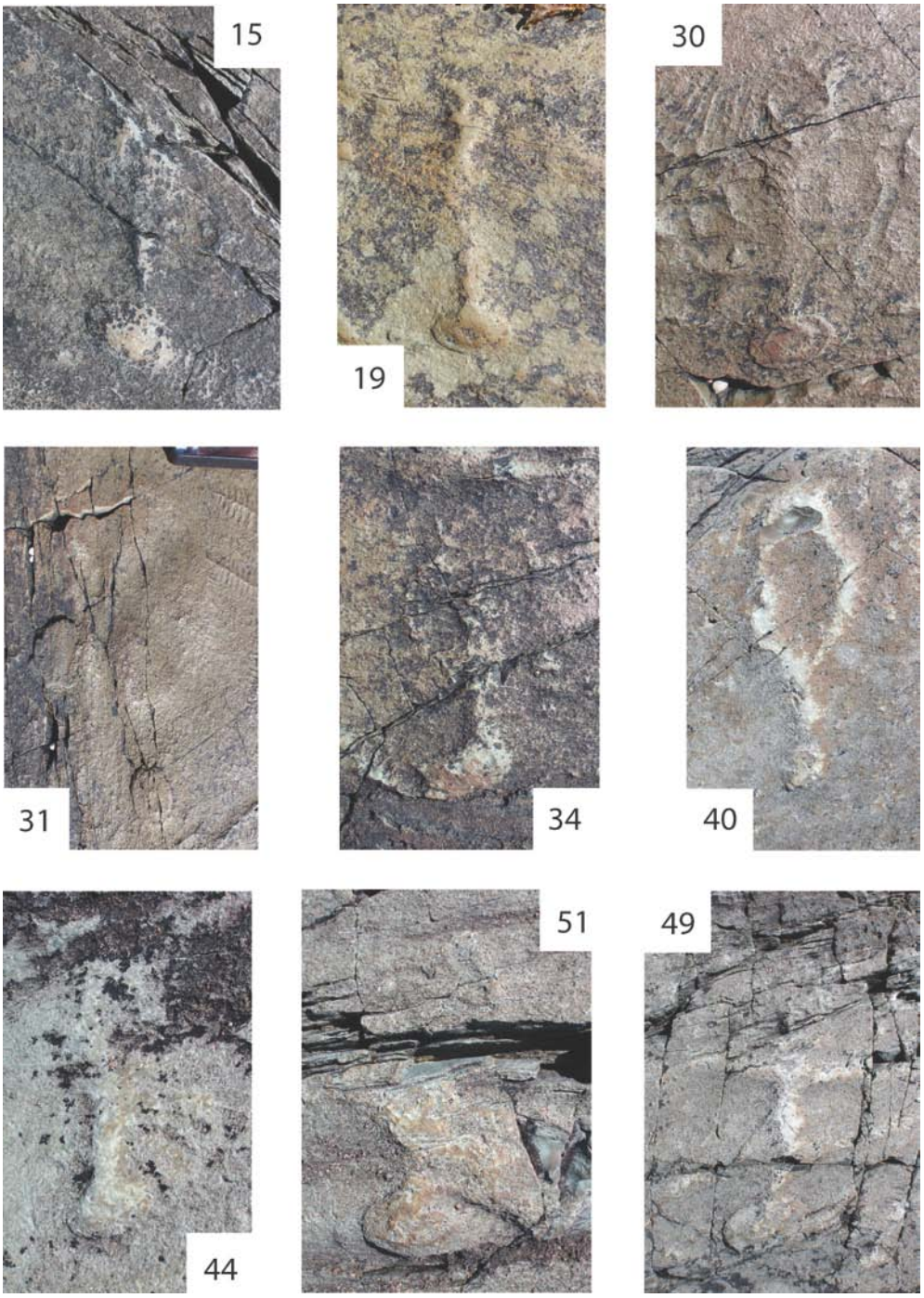

Fig. B1.10. Further effaced rangeomorph specimens from E Surface East, Mistaken Point, MP2.

Effaced forms exhibit a variety of grades of preservation themselves. Some retain discs and stems (e.g. B1.9 [12, 13, 25]), and lose evidence of fronds. Others show the classic lobate irregular structure of ivesheadiomorphs (e.g. B1.10 [31]). There are also a number of specimens that show a mixture of these features, with long broad ridges following the gross

topography of the rangeomorph organism (e.g. B1.10 [40, 19, 49]). These may represent an end-member morphology of effaced preservation.

The *Charniodiscus* fronds in Figures B1.1–B1.10 document the full range of *Charniodiscus* preservational fidelity across a single bedding plane. Although there are noticeable erosional and modern taphonomic artefacts that can be seen to alter preservation quality on the bed, it is shown that these are not responsible for the morphological differences observed throughout the population as a whole.

It is noted that the *Charniodiscus* spectrum presented here is just one of many such spectra envisaged to be preserved on Avalonian bedding planes. All rangeomorph taxa (e.g. *Bradgatia*, *Charnia*, *Hapsidophyllas* etc.) are expected to show similar taphonomic spectra, and therefore a wide range of ivesheadiomorph morphologies, consistent with the effaced preservation hypothesis outlined in Chapter 3 and Liu et al., 2011.

APPENDIX B2

ORIENTATION DATA FOR THE E SURFACE *CHARNIODISCUS* POPULATION

For each *Charniodiscus* specimen photographed from the E Surface (figured in Appendix B1), orientation data was collected to determine whether a relationship existed between the degree of effacement, and fossil orientation on the bedding plane. Datasets are again presented according to which side of the gully the fossils came from (due to a slight offset in bedding plane angle caused by a fault running between the East and West surfaces).

West		**East**	
Specimen Number	Orientation (°)	Specimen Number	Orientation (°)
1	188	1	115
2	191	2	136
3	185	3	144
4	147	4	199
5	225	5	120
6	149	6	138
7	201	7	130
8	145	8	156
9	246	9	113
10	63	10	184
11	163	11	166
12	221	12	160
13	185	13	183
14	-	14	107
15	137	15	125
16	214	16	111
17	70	17	169
18	239	18	170
19	105	19	141
20	118	20	140
21	148	21	112
22	170	22	185
23	164	23	152
24	193	24	167
25	204	25	154
26	192	26	199
27	159	27	147
28	180	28	164

Specimen Number	Orientation (°)	Specimen Number	Orientation (°)
29	200	29	164
		30	173
		31	79
		32	159
		33	193
		34	154
		35	173
		36	228
		37	155
		38	100
		39	157
		40	187
		41	149
		42	188
		43	199
		44	178
		45	129
		46	148
		47	180
		48	167
		49	183
		50	86
		51	165
		52	143
		53	165
		54	145
		55	187
		56	103
		57	145
		58	152
		59	195

The orientation data for the *Charniodiscus* population presented above has been published as Fig. 3.7 in the main text. In that figure, the *Charniodiscus*' were simply distinguished as either effaced or well preserved, regardless of which side of the gully (see pg. xxviii) they resided on. The following figures separate the data further to compare and contrast the orientation data, for individual *Charniodiscus* species, and on either side of the gully. The rose plots reveal interesting patterns, but it must be noted that the sample size for each graph is often relatively small (see 'n' values in the figure captions).

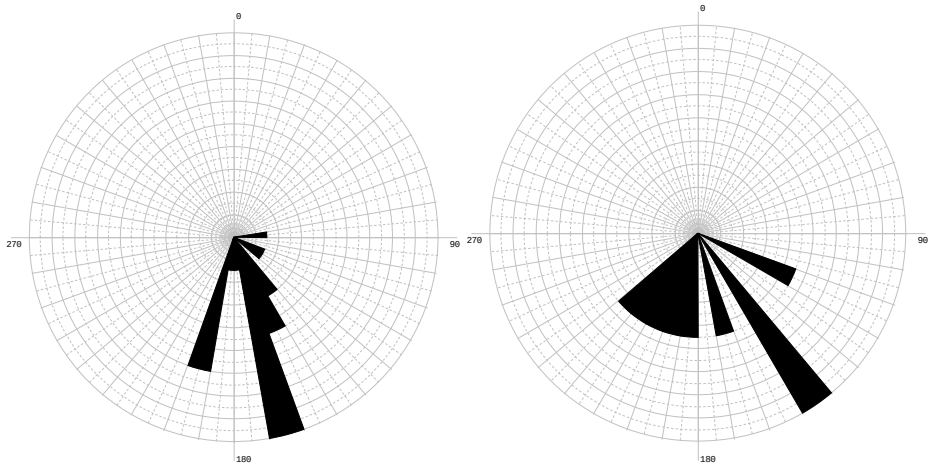

Fig. B2.1. Orientation data for *Charniodiscus spinosus* specimens. **Left**: East E Surface, *C. spinosus*, n = 20. **Right**: West E Surface, *C. spinosus*, n = 9.

When comparing between the three plots (*C. spinosus*, Fig. B2.1; *C. procerus*, Fig. B2.2; effaced specimens, Fig. B2.3), although the general orientation of the fronds is towards the south, there is quite a high degree of variation. On the eastern side of the bed, although *C. spinosus* and effaced alignments are roughly identical, those of *C. procerus* are relatively offset. However, that pattern is not observed on the western side of the gully, where *C. procerus* and *C. spinosus* show broadly consistent orientations, but the effaced specimens show much more variation.

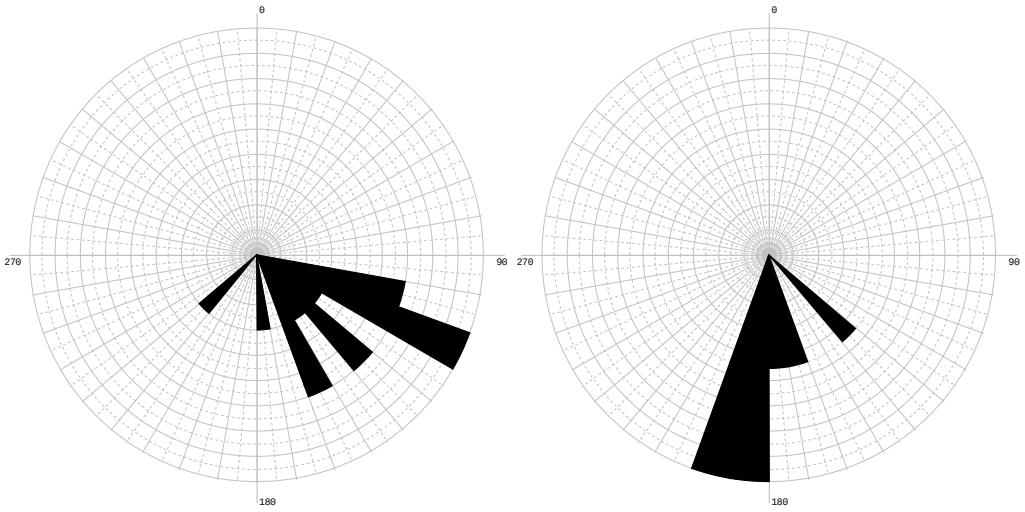

Fig. B2.2. Orientation rose plots for *Charniodiscus procerus* specimens. **Left**: East E surface, *C. procerus*, n = 13. **Right**: West E Surface, *C. procerus*, n = 7.

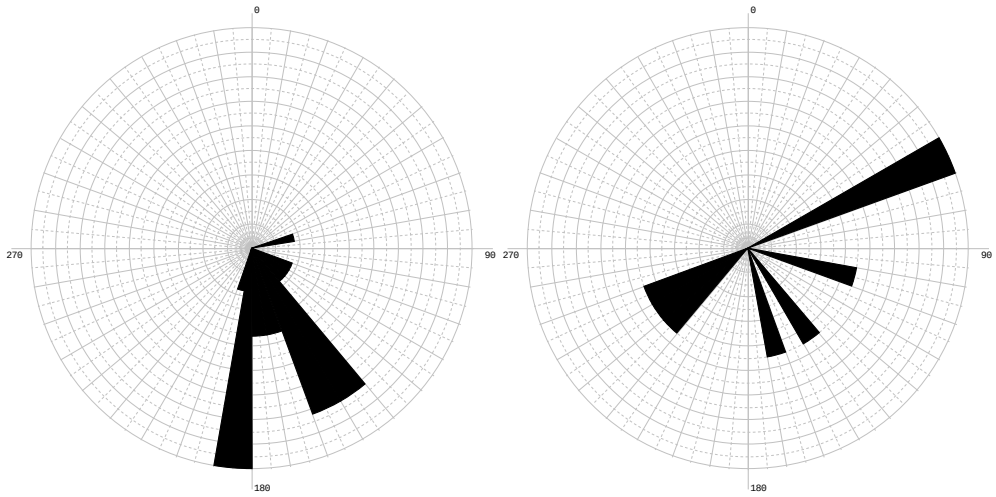

Fig. B2.3. Orientation rose plots for effaced rangeomorphs. **Left**: East E Surface, effaced specimens, n = 22. **Right**: West E Surface, effaced specimens, n = 8.

These differences may be due to a sampling bias caused by the variable sizes of the populations (the two groups with the largest sample size show the clearest alignment). Alternatively, it could be a real pattern. Further analysis of a larger population size on multiple surfaces is required to test this. The fact that the effaced specimens are broadly aligned in the same orientation as the definite *Charniodiscus*' (particularly clear on the eastern surface), supports the assumption that effaced specimens represent decayed *Charniodiscus* specimens, which were felled and aligned by contourite currents some time before the burial of the surface.

Appendix B References

Brasier, M.D. & Antcliffe, J.B., 2009, Evolutionary relationships within the Avalonian Ediacara biota: new insights from laser analysis: *Journal of the Geological Society, London*, **166,** 363-384.

Fedonkin, M.A., Gehling, J.G., Grey, K., Narbonne, G.M., & Vickers-Rich, P., 2007, *The Rise of Animals: Evolution and Diversification of the Kingdom Animalia*: Baltimore, John Hopkins University Press, 326 pp.

Ford, T.D., 1958, Precambrian fossils from Charnwood Forest: *Proceedings of the Yorkshire Geological Society*, **31,** 211-217.

Ford, T.D., 1963, The Pre-cambrian fossils of Charnwood Forest: *Transactions of the Leicester Literary and Philosophical Society*, **57,** 57-62.

Glaessner, M.F. & Wade, M., 1966, The Late Precambrian fossils from Ediacara, South Australia: *Palaeontology*, **9,** 599-628.

Hofmann, H.J., O'Brien, S.J., & King, A.F., 2008, Ediacaran biota on Bonavista Peninsula, Newfoundland, Canada: *Journal of Paleontology*, **82,** 1-36.

Jenkins, R.J.F., and Gehling, J.G., 1978, A review of frond-like fossils of the Ediacara assemblage: *Records of the South Australian Museum*, **17,** 347-359.

Laflamme, M., Narbonne, G.M., & Anderson, M.M., 2004, Morphometric analysis of the Ediacaran frond *Charniodiscus* from the Mistaken Point Formation, Newfoundland: *Journal of Paleontology*, **78,** 827-837.

Liu, A.G., McIlroy, D., Antcliffe, J.B., & Brasier, M.D., 2011, Effaced preservation in the Ediacaran biota of Avalonia and its implications for the early macrofossil record: *Palaeontology*, **54,** 607-630.

Narbonne, G.M., 2005, The Ediacara Biota: Neoproterozoic origin of animals and their ecosystems: *Annual Reviews in Earth and Planetary Sciences*, **33,** 421-442.

Narbonne, G.M., Dalrymple, R.W., Laflamme, M., Gehling, J.G., & Boyce, W.D., 2005, *Life after Snowball: Mistaken Point Biota and the Cambrian of the Avalon*, North American Paleontological Convention Field Trip Guidebook: Halifax, Nova Scotia, 98 pp.

Appendix C
The MP4 Trace Fossil Bed

In order to fully document the new trace fossil assemblage at Mistaken Point (Chapter 6), the bedding plane on which it occurs (MP4, Appendix D2) was mapped, and spatial information was gathered for the whole assemblage. The maps are presented here, along with orientations and dimensions for all of the possible biogenic features preserved on the bedding plane (Appendix C1). All maps were constructed with the assistance of Jack Matthews. Locations of each mapped section figured herein are presented in Figure C1.14. Numbering starts at the southernmost end of the outcrop, and progresses North (Fig. C1.14). Map images are taken directly from my field notebook. The maps are intended to document the broad position and appearance of each possible biogenic feature; they are not intended to be absolutely accurate.

A representative collection of images of the bed and its traces is also included for further reference (Appendix C2).

Appendix C1

Maps of the trail bed

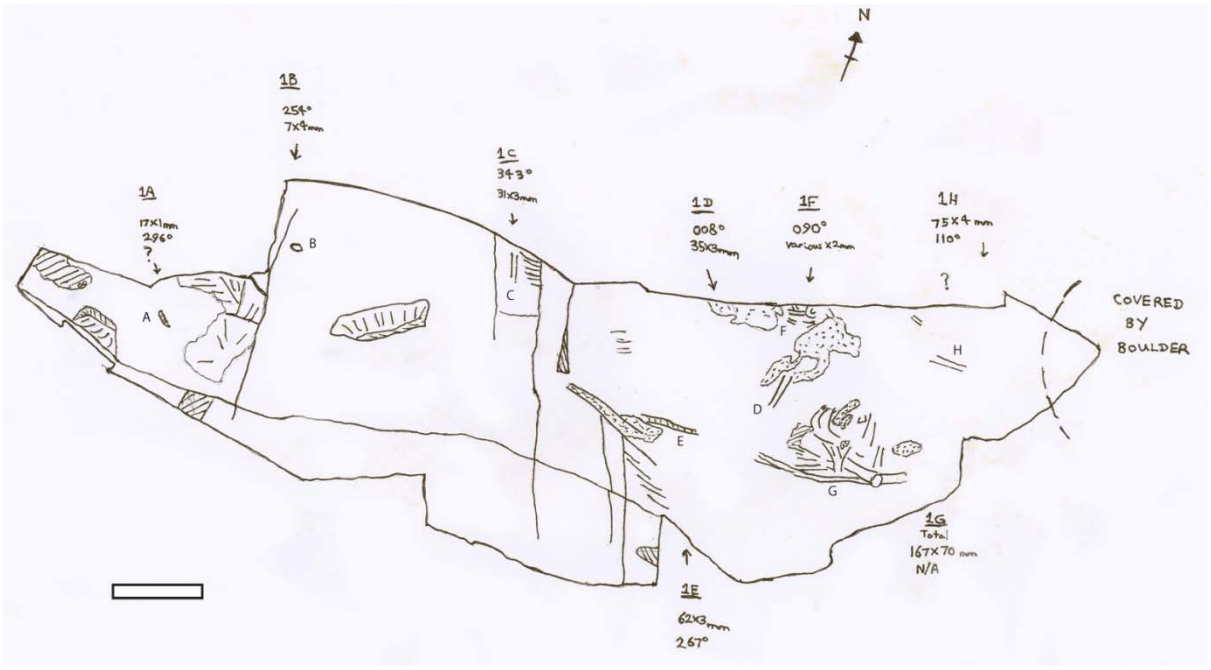

Fig. C1.1. Map of segment 1 of the MP4 surface. For each of these images, stippled patterns indicate regions of tuff cover, hashed diagonal lines represent areas not in the plane of the surface, and solid black regions indicate cracks. A cast of this segment is housed at the Oxford University Museum of Natural History, specimen OUM ÁT.420/p. Scale bar = 0.1 m.

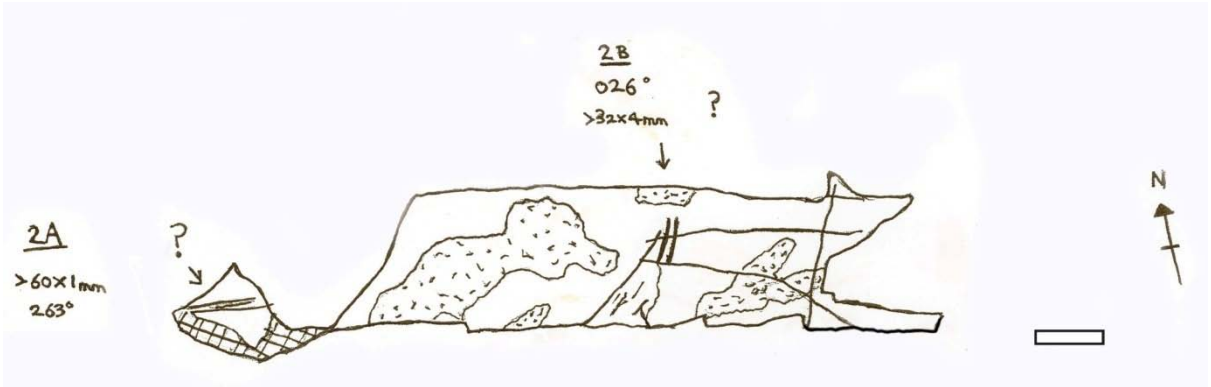

Fig. C1.2. Map of segment 2 of the MP4 surface. Scale bar = 50 mm.

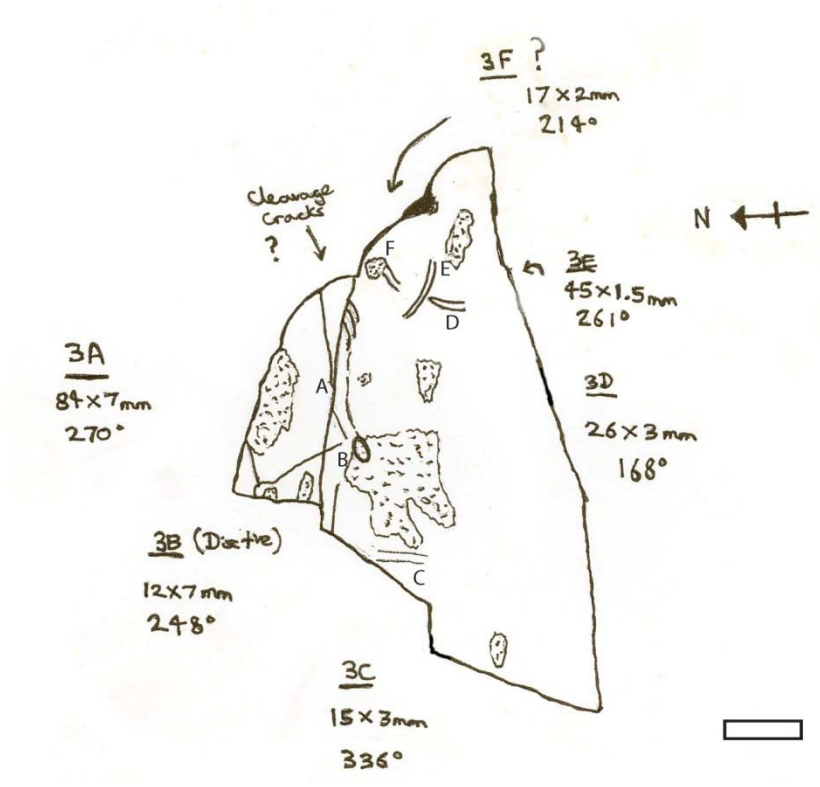

Fig. C1.3. Map of segment 3 of the MP4 surface. Scale bar = 50 mm.

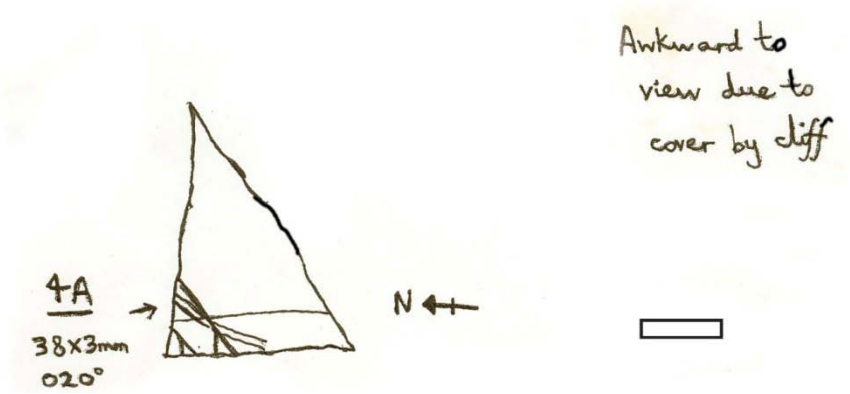

Fig. C1.4. Map of segment 4 of the MP4 surface. Scale bar = 50 mm.

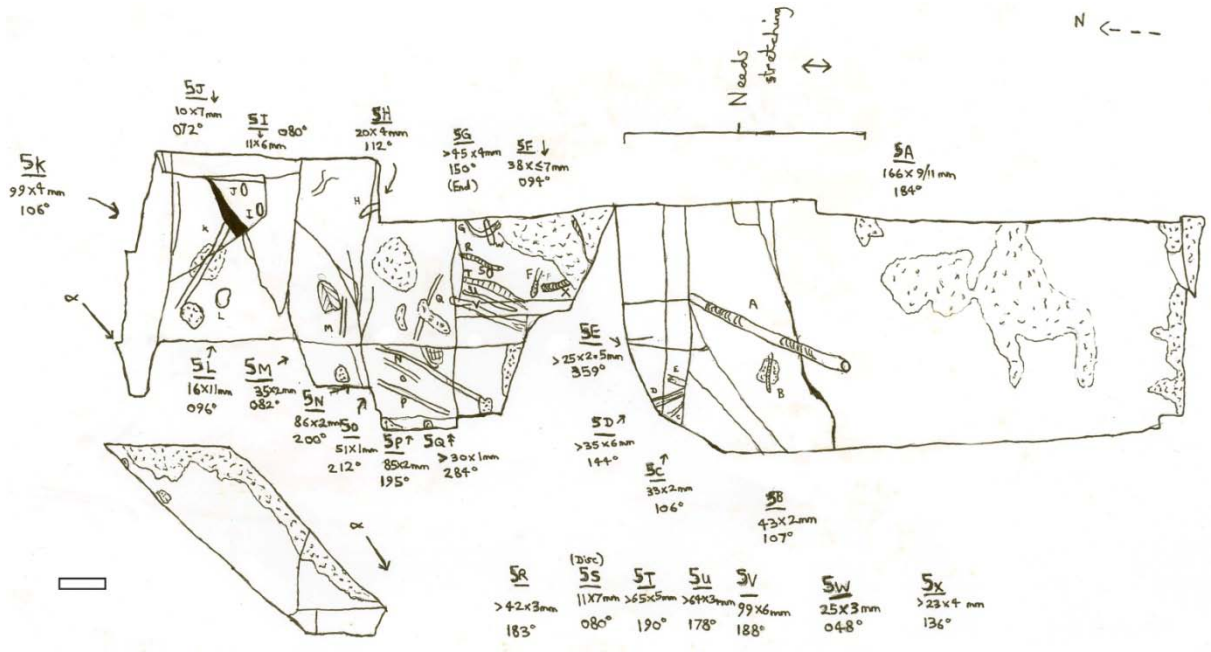

Fig. C1.5. Map of segment 5 of the MP4 surface. Casts of this segment are housed at the Oxford University Museum of Natural History, specimens OUM ÁT.418/p and OUM ÁT.419/p. Scale bar = 50 mm.

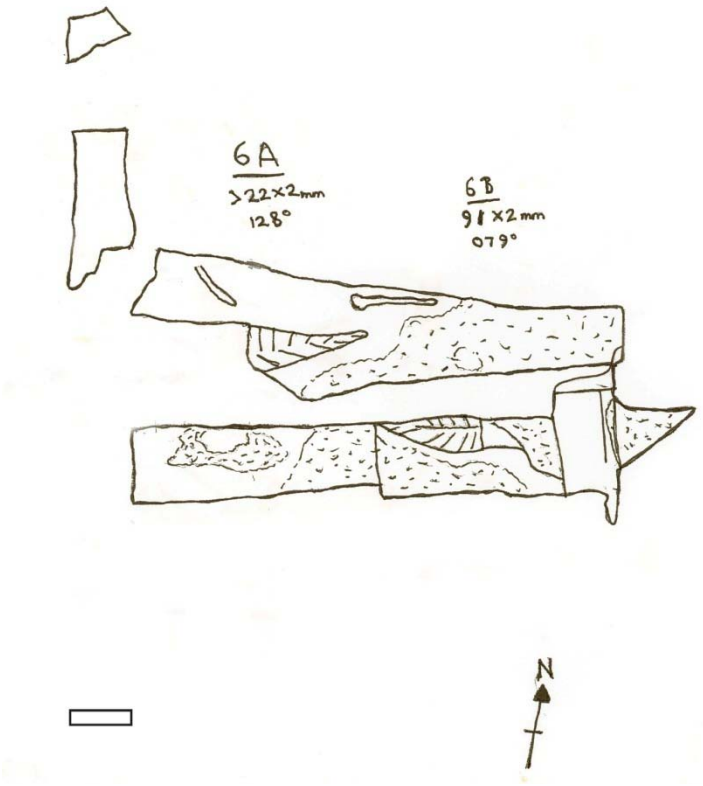

Fig. C1.6. Map of segment 6 of the MP4 surface. Scale bar = 50 mm.

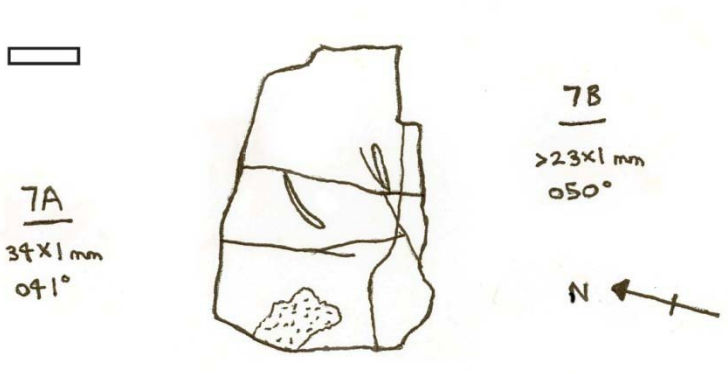

Fig. C1.7. Map of segment 7 of the MP4 surface. Scale bar = 50 mm.

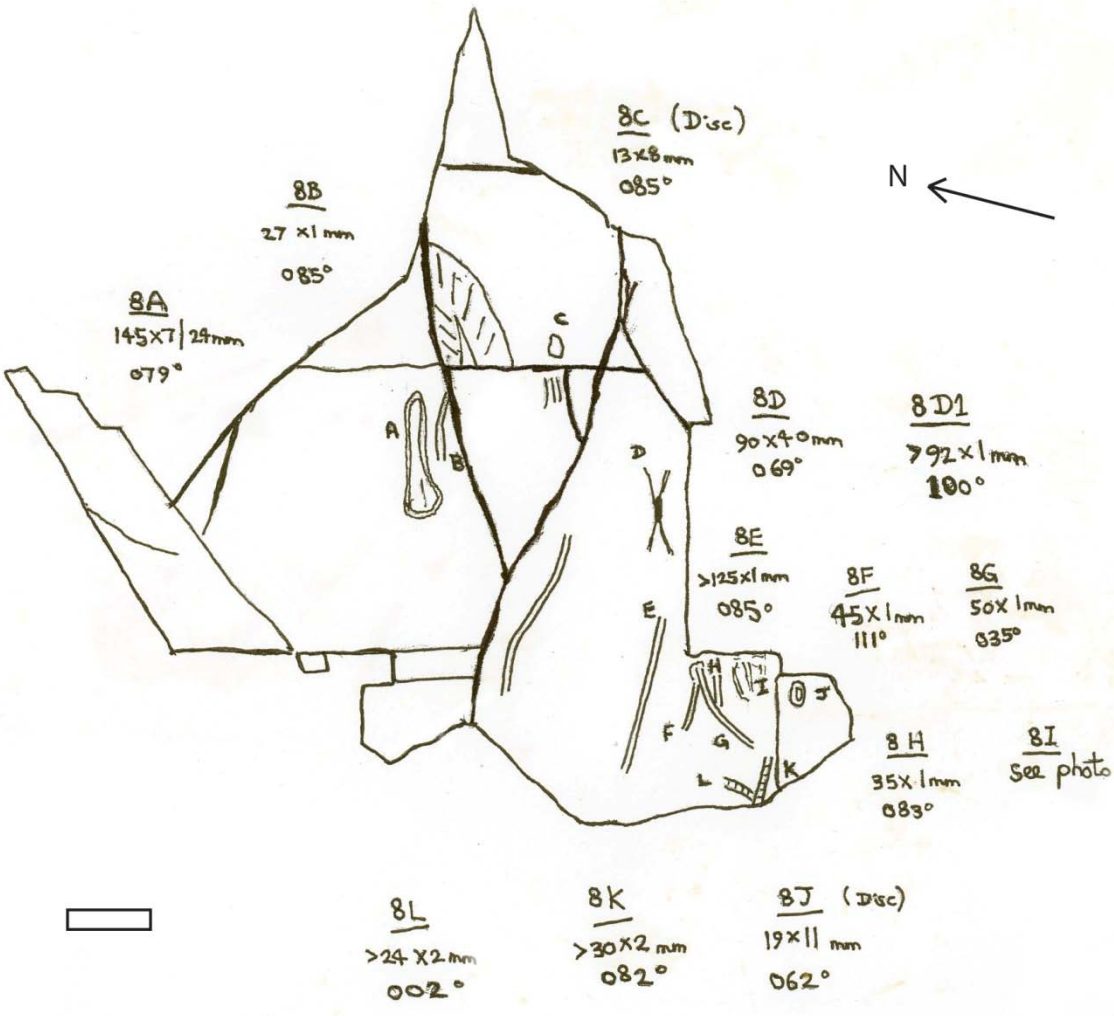

Fig. C1.8. Map of segment 8 of the MP4 surface. Scale bar = 50 mm.

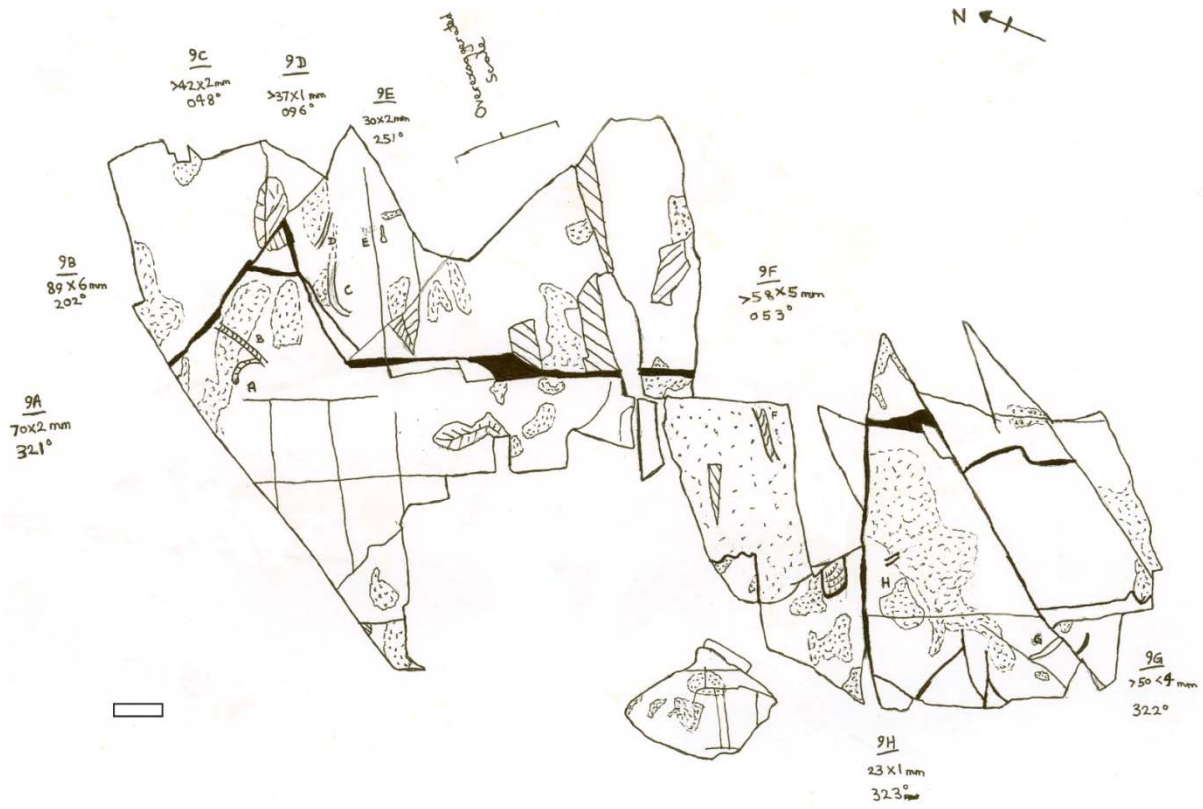

Fig. C1.9. Map of segment 9 of the MP4 surface. A cast of the northern end of this section is housed at the OUMNH, specimen number OUM ÁT.423/p. Scale bar = 50 mm.

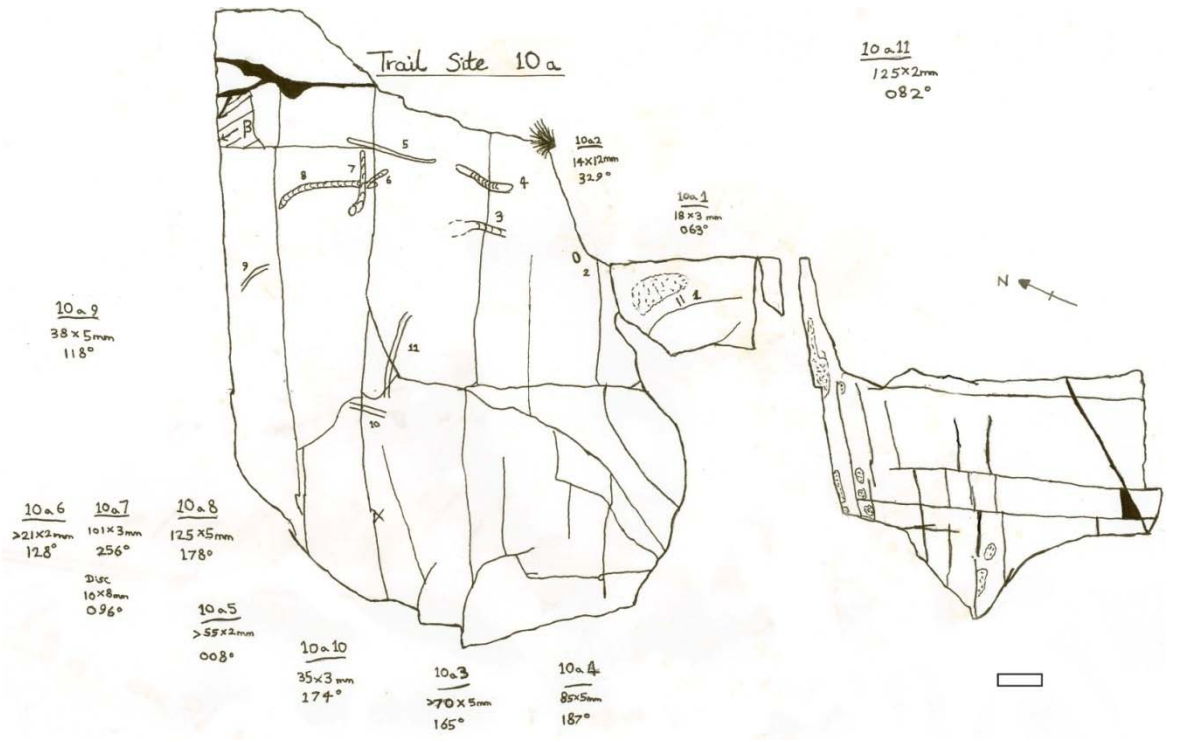

Fig. C1.10. Map of segment 10a of the MP4 surface. A cast of this specimen is housed in the OUMNH, cast number OUM ÁT.421/p. Scale bar = 50 mm.

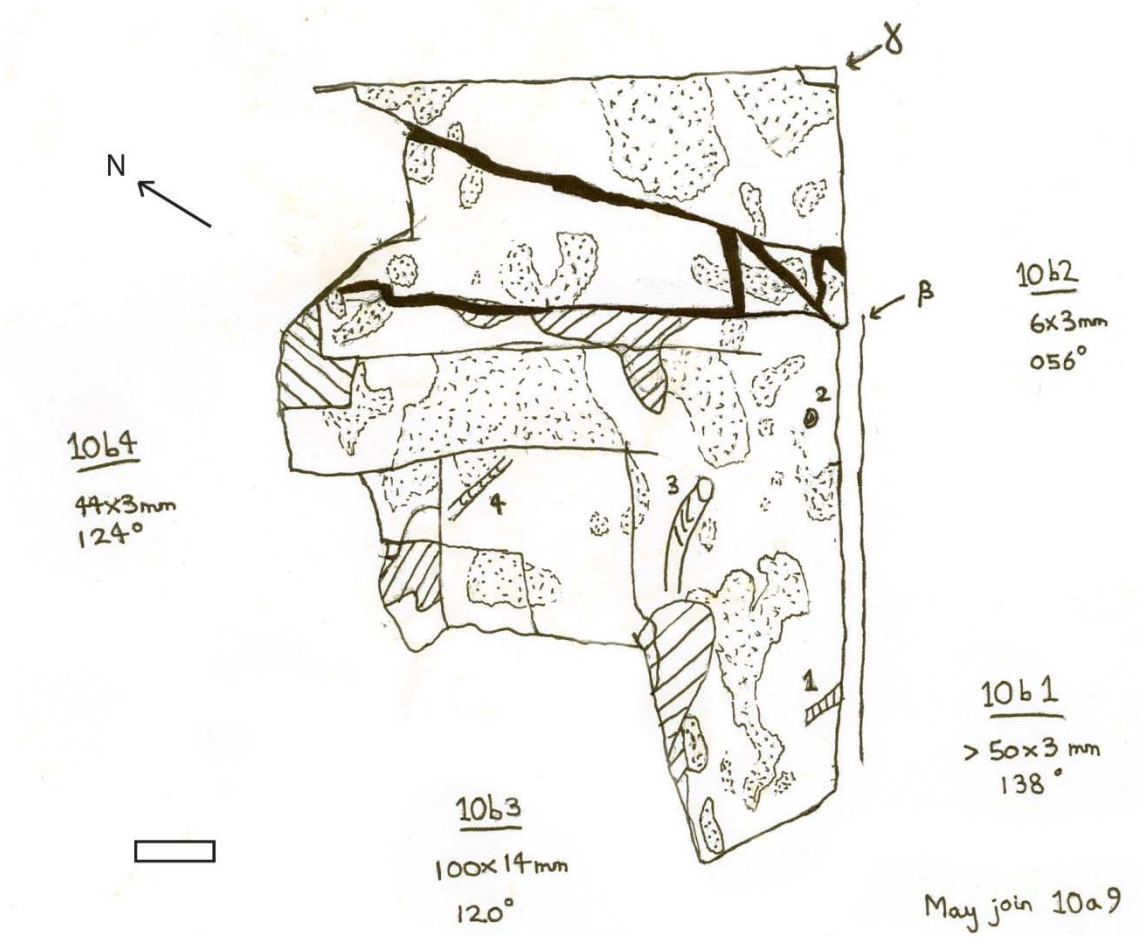

Fig. C1.11. Map of segment 10b of the MP4 surface. Scale bar = 50 mm.

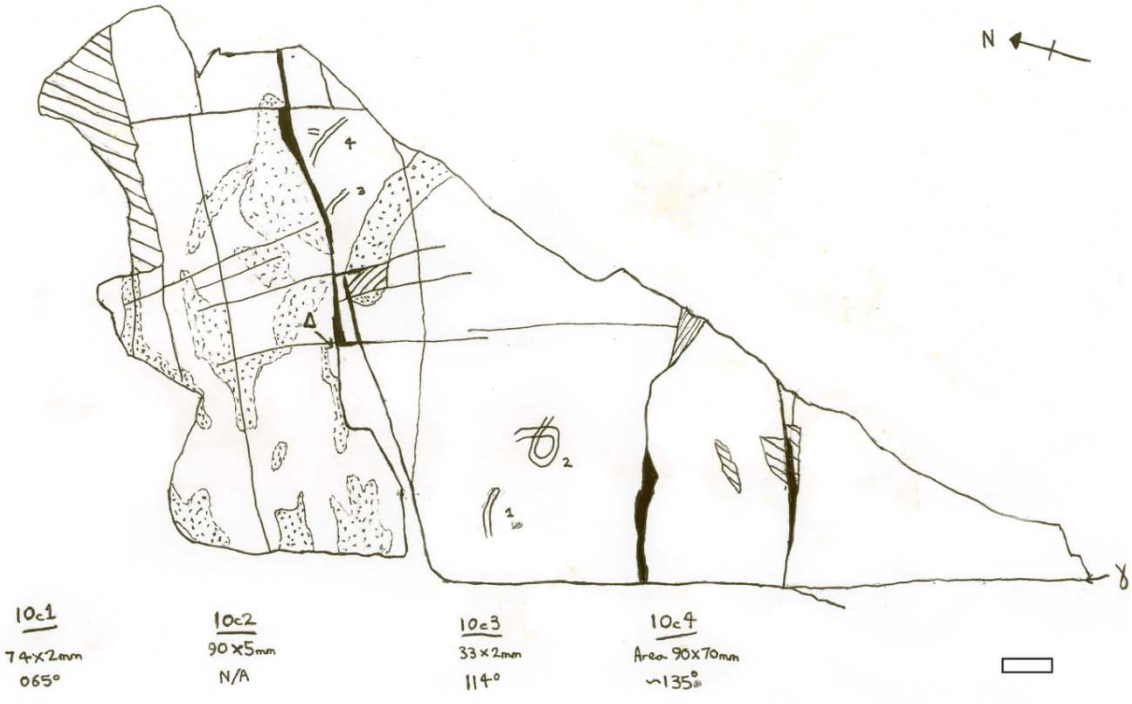

Fig. C1.12. Map of segment 10c of the MP4 surface. Scale bar = 50 mm.

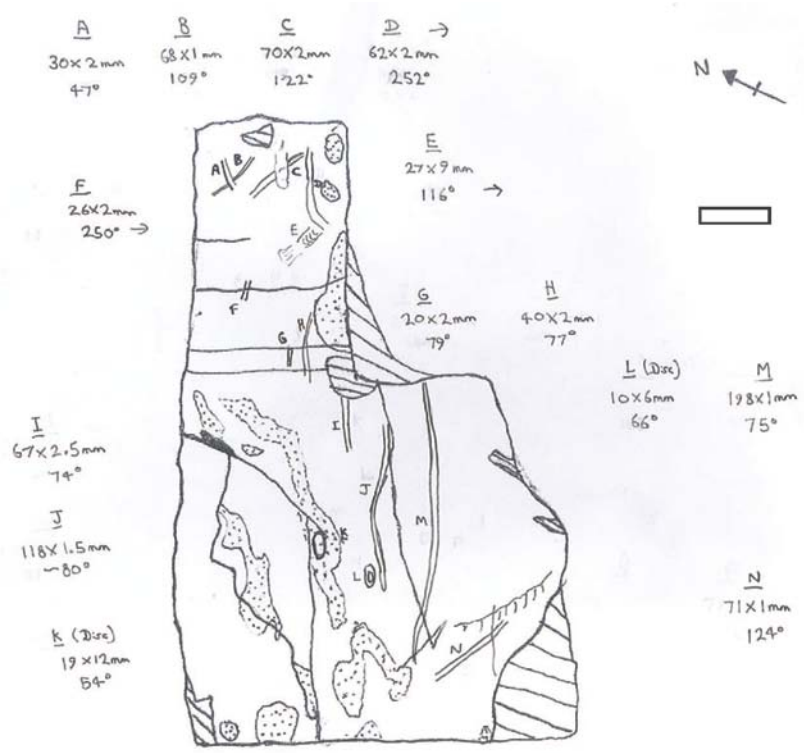

Fig. C1.13. Map of segment 10d of the MP4 surface. Scale bar = 50 mm. OUMNH cast OUM ÁT.422/p.

Fig. C1.14. Image of the MP4 bedding plane, showing the location of each outcropping section of the bed, numbered as per the previous figures. The ledge upon which all small cards rest lies 1.3 m above the basal bed. North is to the left of the image.

Appendix C2

Additional images of the MP4 bed and its fossils

The following images demonstrate some of the features observed on the MP4 bedding plane, including potential fossils, traces, and pseudofossils. They provide a representative sample of the structures as observed in the field. Prior to imaging, the bed was cleaned with a biodegradable detergent to remove lichen and dirt, permitting easier observation of the specimens. References to specimens correspond to the maps in Appendix C1.

Fig. C2.1. Mineral veins cutting through the trace fossil surface. Note that these veins lie at a variety of angles, and seem to continue through the surface on the same trajectory past the occurrence of the actual mineral exposure, exhibiting several surface expressions. None of these expressions, however, can create the negative relief troughs with positive marginal ridges of the candidate traces described in Chapter 6. Black scale box on the card is 10 x 10 mm.

Fig. C2.2. Specimen 9G (arrowed), an unornamented trail from the MP4 bed. Scale block (black) = 10 x 10 mm.

Fig. C2.3. Specimens 9A and 9B, from the MP4 surface. Note the raised marginal levees of sediment, and the different orientations of the specimens. Length of black scale bar at right = 10 mm.

Fig. C2.4. A collection of trails and discoidal impressions (arrowed) from section 5 of the MP4 bed. Black scale box = 10 x 10 mm.

Fig. C2.5. Specimens 5C and 5D from the MP4 trail bed, Mistaken Point, MPER, Newfoundland. These impressions are internally unornamented, but show clear positive relief marginal ridges of sediment. Scale bar (black at base of image) = 10 mm.

APPENDIX D

The content contained within Appendix D of this thesis cannot be made available in ORA.

Appendix E
Experimental Taphonomy Pot Images

This appendix contains images of the taphonomy experiments documented in Chapter 4, exhibiting images of all the pots studied in the marine aquaria.

Microbial decay under controlled conditions

Whilst undertaking the taphonomy experiments outlined in Chapter 4, images of the organic matter decomposing in the experimental tanks were captured every three or four days, until the pots were covered by tuff. The following pages document the images of each pot, with a brief explanation of the information gleaned from each one.

The tanks and pot numbers are explained in Chapter 4 (Fig. 4.1). Image quality varies within individual collages due to the acquisition on the 30th October 2008 of a camera capable of taking underwater shots. This permitted sharper images, and removed the problem of reflections off the water's surface (caused by the ceiling lights in the laboratory). Pots in all images have a diameter at their widest point of 11.5 cm.

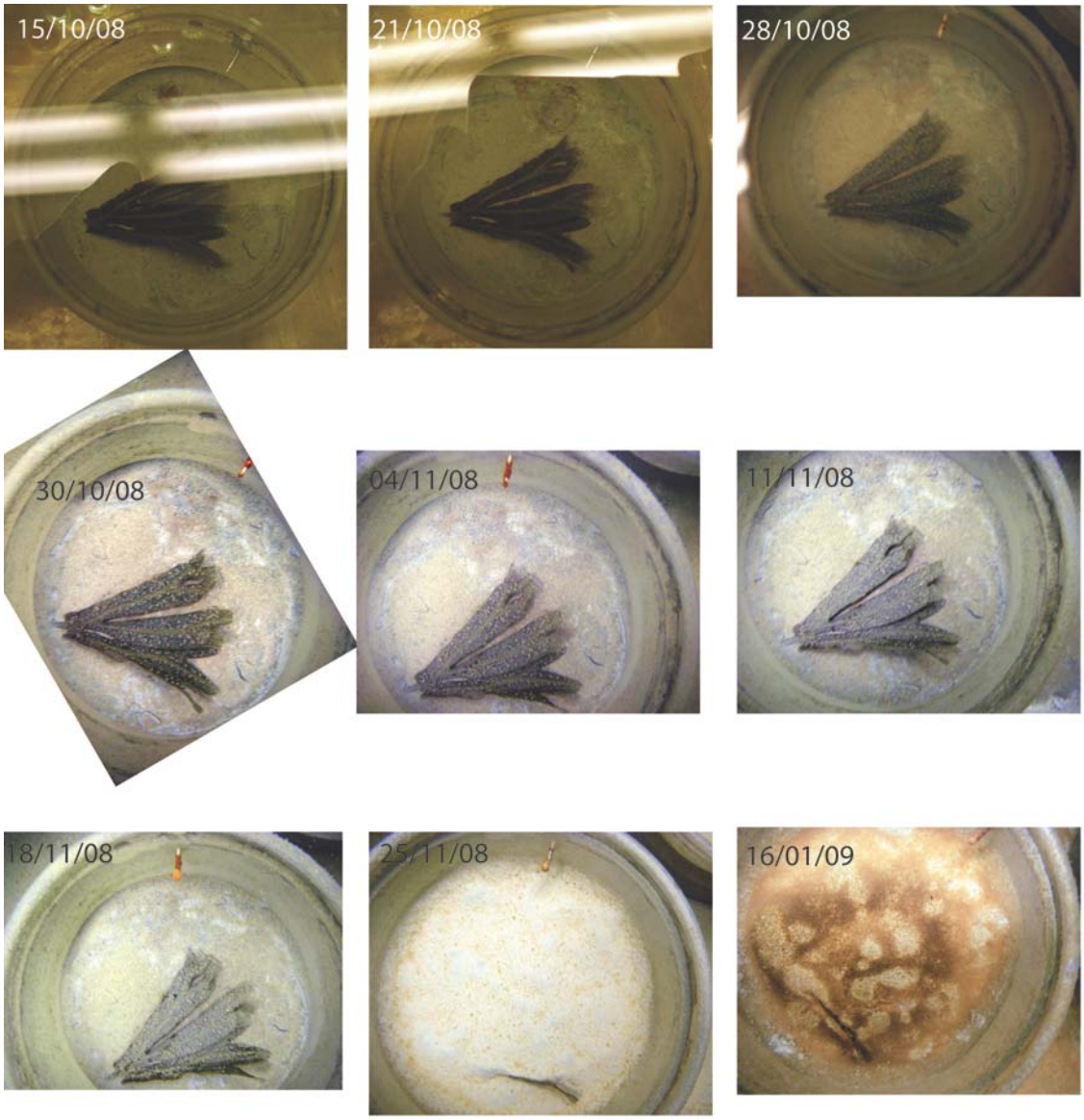

Fig. E1.1. Images of Pot 1A, taken at regular intervals until the pot was smothered with sediment after five weeks. Pot contains an *Aurelia* jellyfish fragment, and a piece of *Fucus* seaweed. In all figures where the pot contains both jellyfish and seaweed specimens, the jellyfish is located on the side of the pot closest to the pin.

Pot 1A demonstrates the rapid degradation of the jellyfish specimen relative to the seaweed (Fig. E1.1). The jellyfish is reduced to a thin organic film by 30/10/08 (i.e. after two weeks). Conversely, the seaweed retains its morphology and structure for at least four weeks, though accumulation of a thin film of sediment on its upper surface is notable throughout the photographed interval.

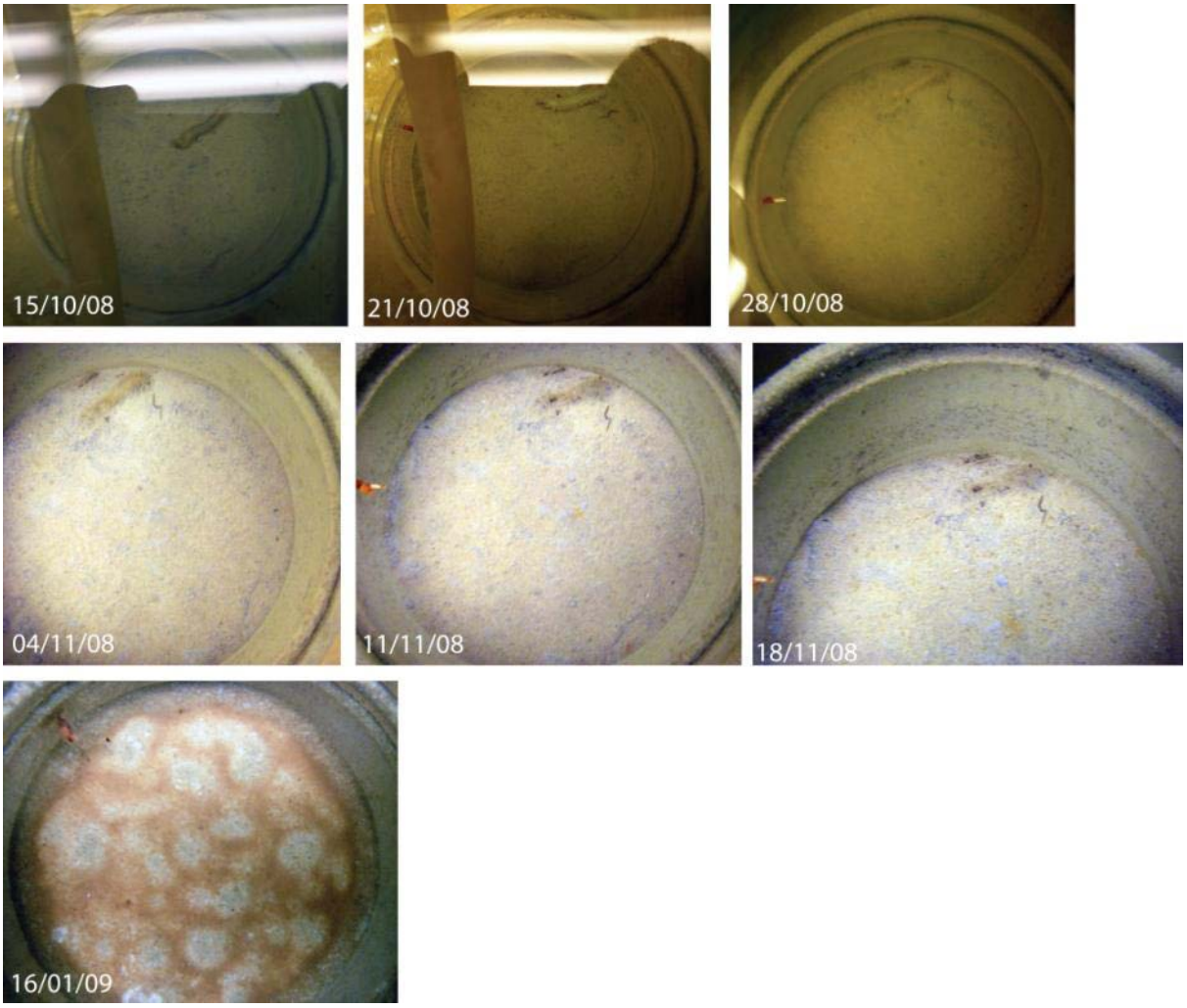

Fig. E1.2. Images of Pot 1B, taken at regular intervals until the pot was smothered with sediment after five weeks. Pot contains one *Nereis* worm.

The nereid worm in Pot 1B degraded rapidly, with the external tissues failing 2–3 weeks after death (Fig. E1.2). Unfortunately, image quality is consistently poor for this pot. An interesting point to note is the mottled appearance of the tuff 6 weeks after deposition (16/01/09; see also Fig. E1.1). This is due to the settling of iron-oxide-rich sediment (red) on the surfaces, into depressions between rounded, higher-relief lobes (white). The lobes form above lumps of insufficiently ground-up tuff, whereas the iron oxide is derived from rusting of the pins. This mottled appearance is therefore wholly abiogenic in origin.

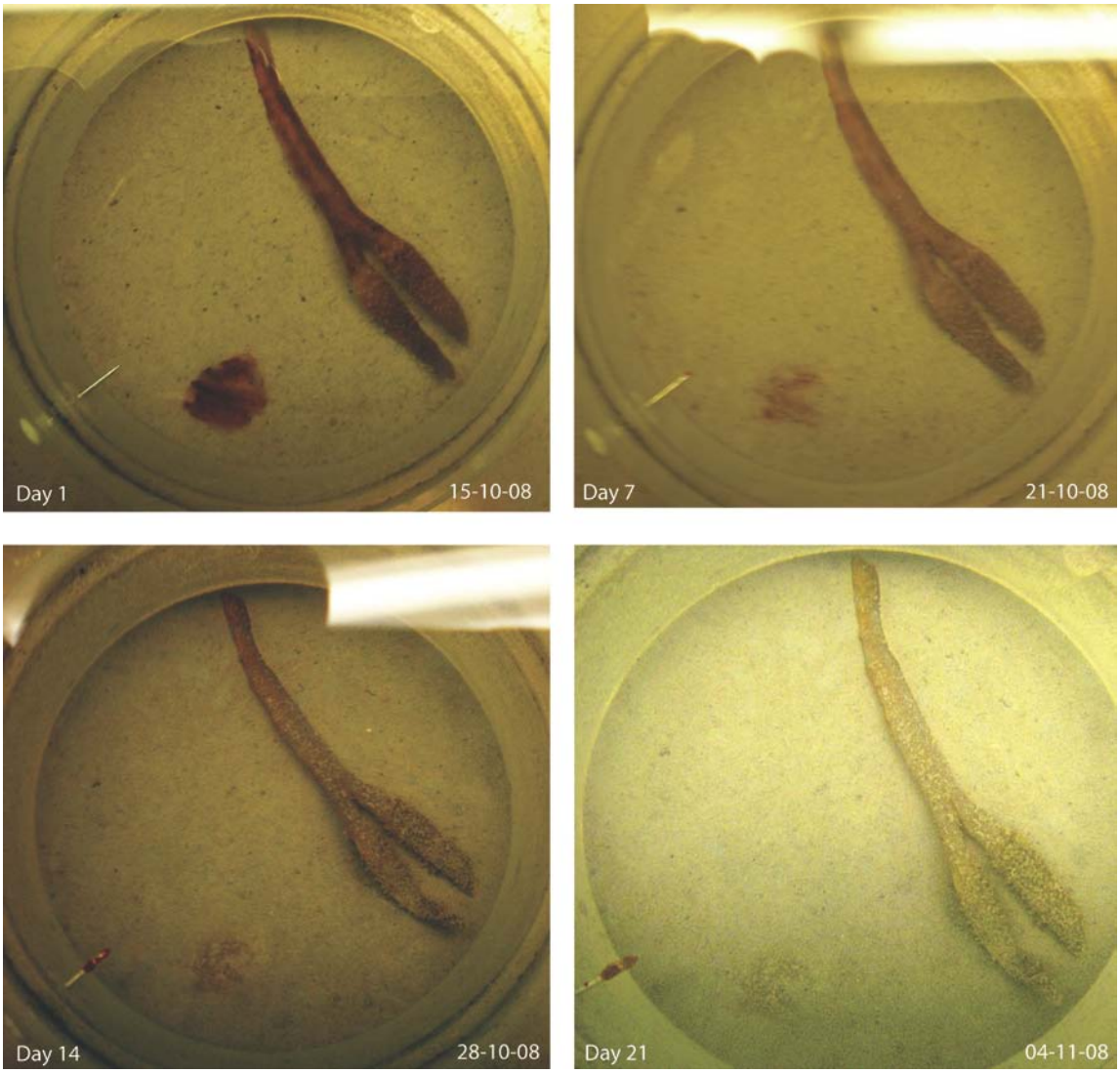

Fig. E1.3. Images of Pot 1C, taken at regular intervals until the pot was smothered with sediment after three weeks. Pot contains *Aurelia* jellyfish fragment, and a piece of *Fucus* seaweed.

Pot 1C again shows rapid degradation of the jellyfish material (Fig. E1.3). The jellyfish material is quickly covered in trapped sediment, and its thinnest regions decay fastest, giving it an irregular, lumpy appearance. Seaweed shows further evidence of trapping and binding of sedimentary particles from the water column, but no gross change in morphology or biological fidelity even after three weeks (though see also Fig. E1.9).

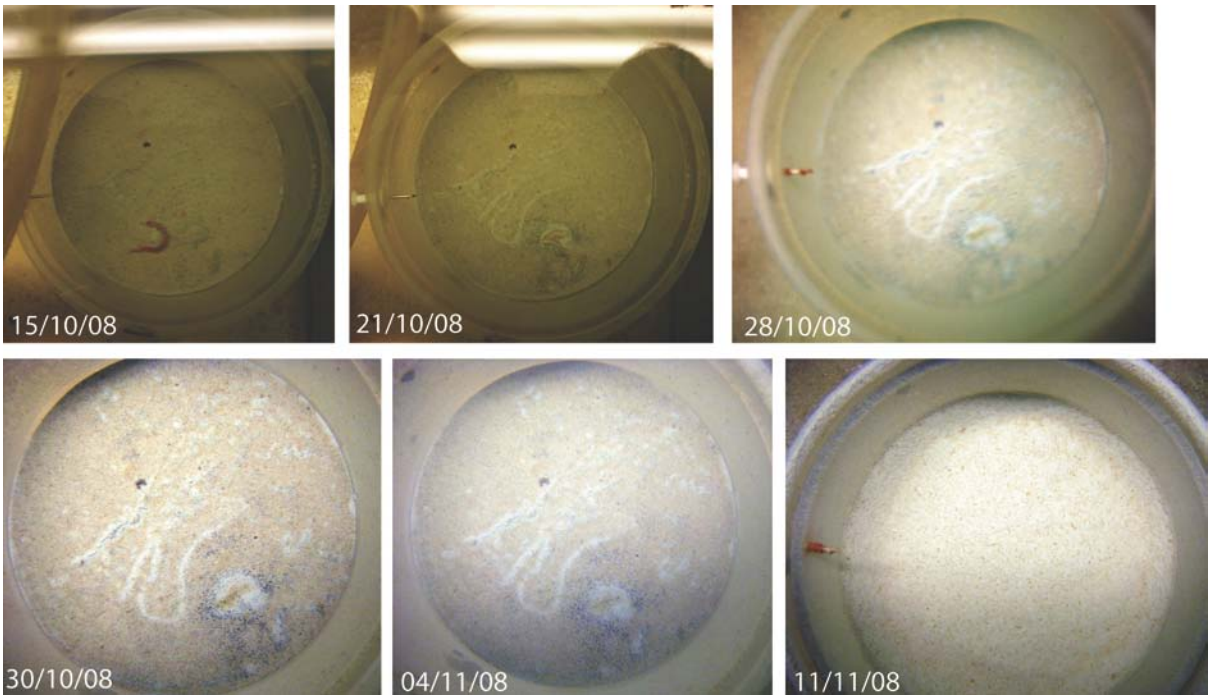

Fig. E1.4. Images of Pot 1D, taken at regular intervals until the pot was smothered with sediment after three weeks. Pot contains one *Nereis* worm.

The worm in Pot 1D decayed quickly, losing fine morphological features such as bristles after one week, and comprising little more than a smudge on the sediment surface after three weeks (Fig. E1.4). What appears to be a reaction or leachate 'halo' surrounding this particular specimen, is actually disturbance of the microbial mat upon which the specimen was deposited. As is evident from the first two images, the organism moved (leaving a clear trail) within the first few hours of the experiment, despite being thought to be dead, and this motion was recorded by the mat on the surface (see also McIlroy et al., 2009).

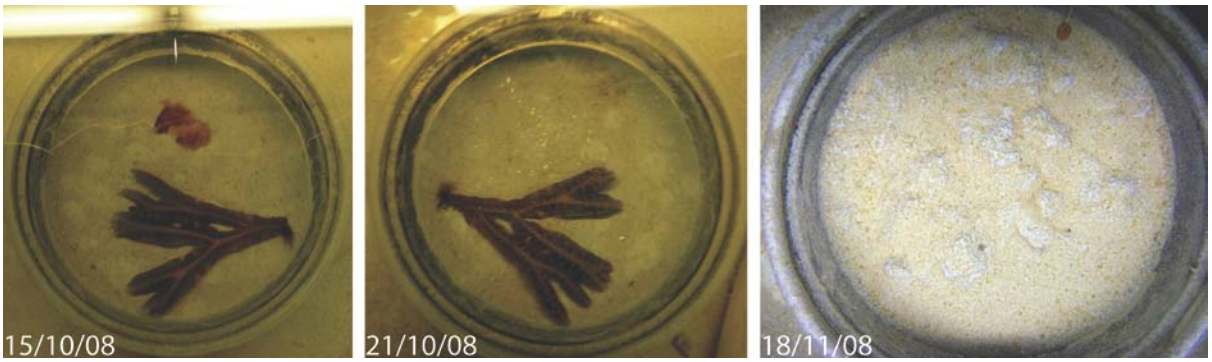

Fig. E1.5. Images of Pot 1E, taken at regular intervals until the pot was smothered with sediment after one week. Pot contains *Aurelia* jellyfish fragment, and a piece of *Fucus* seaweed.

Pots smothered by tuff after just one week still exhibited a significant degree of decay of organic matter, particularly in the metazoan specimens (Figs. E1.5–1.6). The speed at which some of the organic material can be removed is remarkable (for example, the jellyfish in Fig. E1.5 is almost completely effaced after just one week).

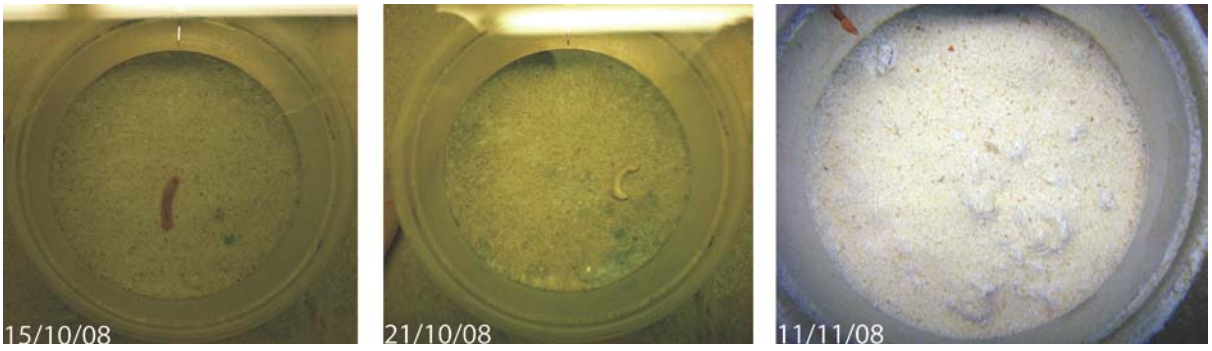

Fig. E1.6. Images of Pot 1F, taken at regular intervals until the pot was smothered with sediment after one week. Pot contains one *Nereis* worm.

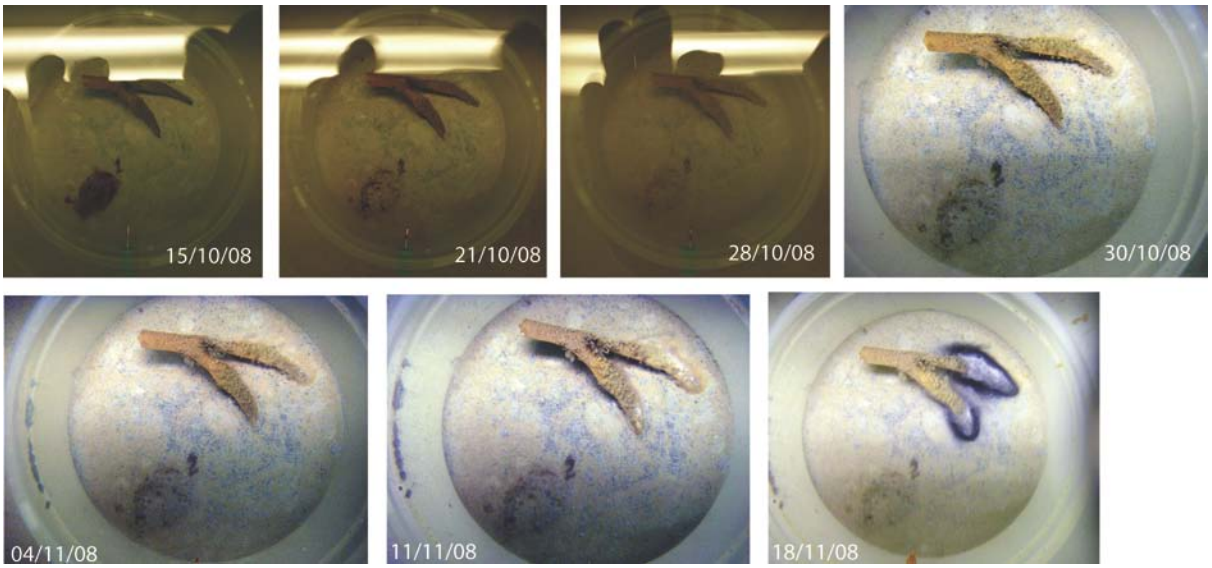

Fig. E1.7. Images of Pot 2A, taken at regular intervals until the pot was smothered with sediment after five weeks. Pot contains *Aurelia* jellyfish fragment, and a piece of *Fucus* seaweed.

Pot 2A clearly shows the gradual decay and effacement of jellyfish material (Fig. E1.7). Within one week, sediment has settled upon the jellyfish specimen, giving it an irregular, lobate appearance, which remains for a further three weeks. By the fifth week of the experiment, the jellyfish material is almost completely decayed, and only an organic film remains.

The seaweed in this pot also shows evidence of substantial microbial (this time fungal) decay, which takes effect after 5 weeks (18/11/08). A clear ‘halo’ of leached fluids and microbial growth surrounds the decaying regions of the seaweed, seen as a black stain on the sediment surface.

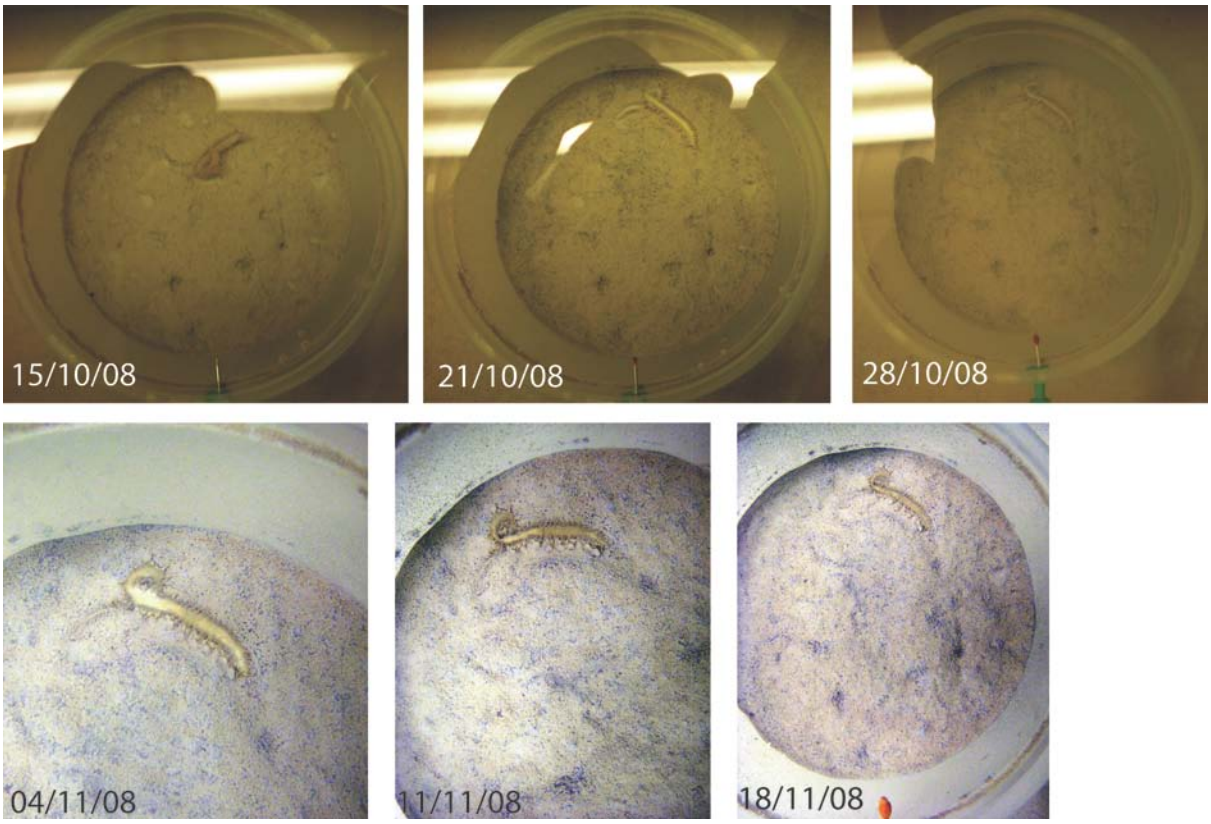

Fig. E1.8. Images of Pot 2B, taken at regular intervals until the pot was smothered with sediment after five weeks. Pot contains one *Nereis* worm.

The *Nereis* worm in Pot 2B did undergo some microbial decay and effacement over the course of the five weeks prior to burial (see the spheres of microbial growth on either side of the specimen, Fig. E1.8, 04/11/08), but when compared to that in Pot 1B, decay is seen to have been nowhere near as rapid. Since all other variables remain unchanged, this is highly likely to result from the far shorter period of time that the pots in Tank 2 spent acclimatising prior to the addition of organic material (five days compared to two months in Tank 1). This implies that microbial growth in Tank 1 was significantly faster than in Tank 2 because there was a larger, more mature population of micro-organisms present within the sediment of pots in Tank 1 from the very start of the decay process.

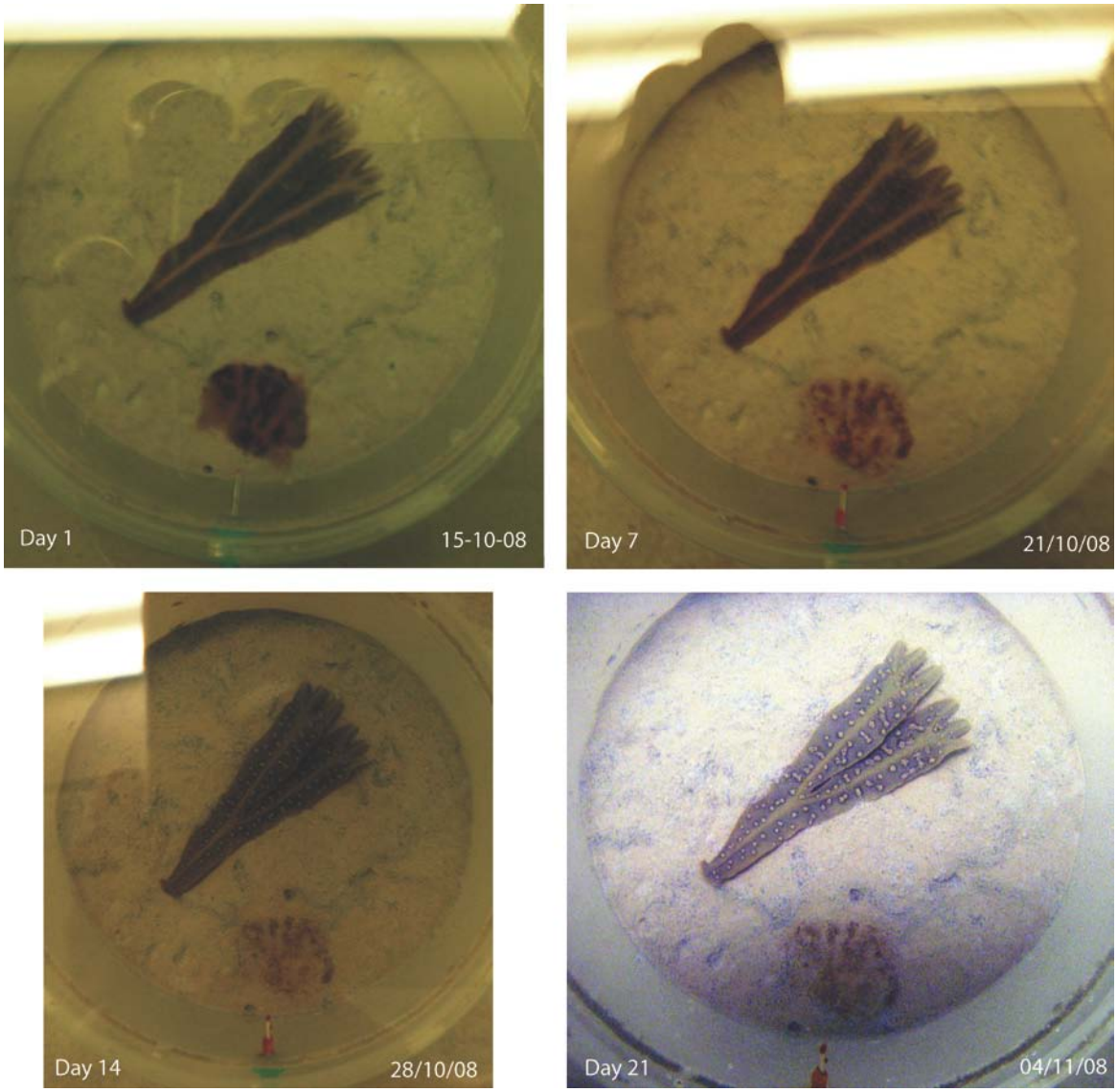

Fig. E1.9. Images of Pot 2C, taken at regular intervals until the pot was smothered with sediment after three weeks. Pot contains *Aurelia* jellyfish fragment, and a piece of *Fucus* seaweed.

Pot 2C (Fig. E1.9) shows decay of jellyfish and seaweed material, and again sees decay progressing at a slower rate than in the comparable pot in Tank 1 (Fig. E1.3). The seaweed morphology is still pristine here after three weeks (in Tank 1 it exhibited substantial microbial growth by this stage; Fig. E1.3), while the jellyfish is also clearly visible (whereas after two weeks in Tank 1 it had been all but removed; Figs. E1.1, E1.3). Again note the lobate irregular appearance of the effaced jellyfish material.

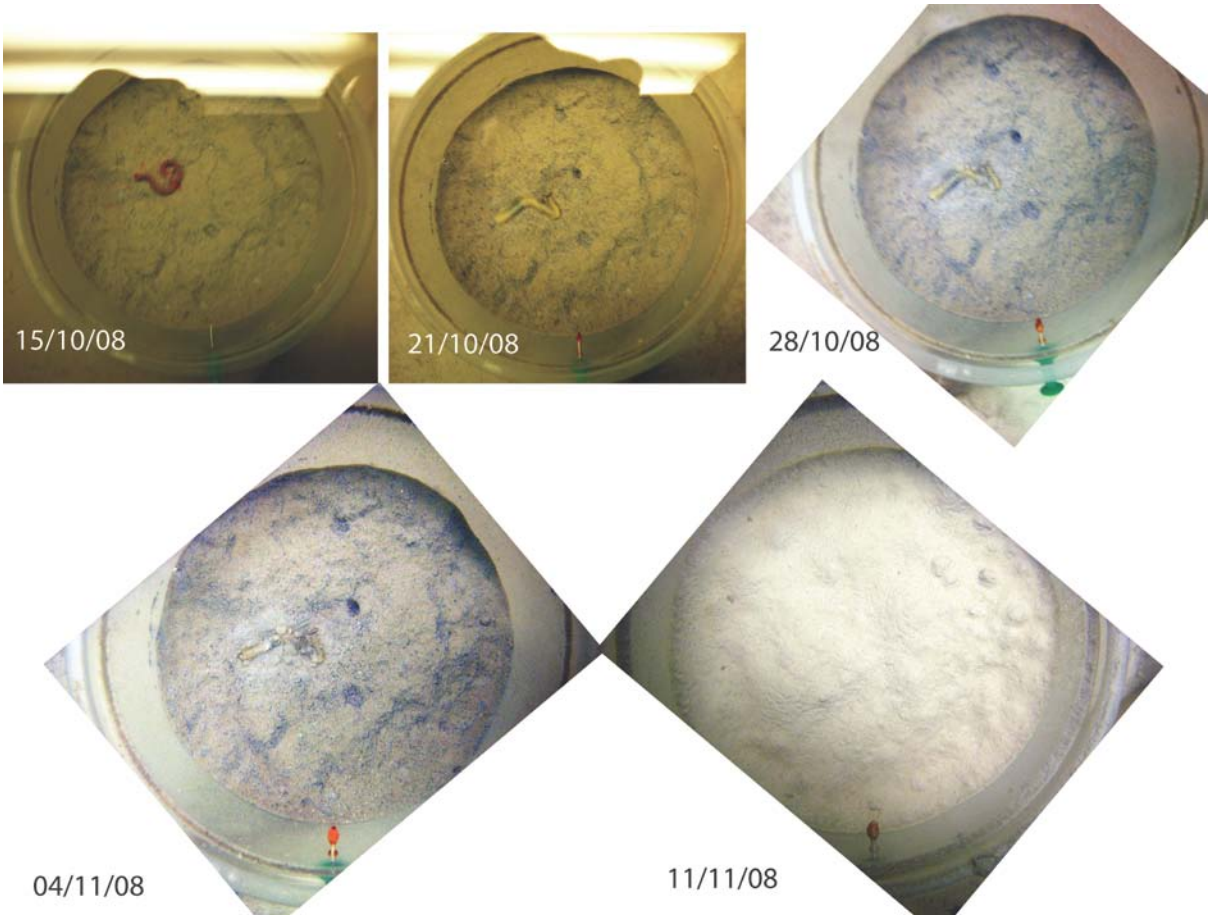

Fig. E1.10. Images of Pot 2D. Photographs were taken at regular intervals until the pot was smothered with sediment after three weeks. Pot contains one *Nereis* worm.

In Pot 2D, the *Nereis* specimen does undergo notable degradation, particularly with the body exterior breaking apart after two weeks. However, as opposed to similar settings in Tank 1, the effect of microbial degradation is significantly reduced in Tank 2, with autolysis likely to be the initial primary breakdown mechanism rather than microbial activity (due to the previously mentioned variation in settling times between the two tanks). When the full range of pots are assessed, decay is seen to occur consistently faster in Tank 1, where microbial mats had been allowed time to develop upon the substrate prior to beginning the experiment. The maturity of the benthic microbial community is also likely to have influenced decay rates in Avalonian ecosystems.

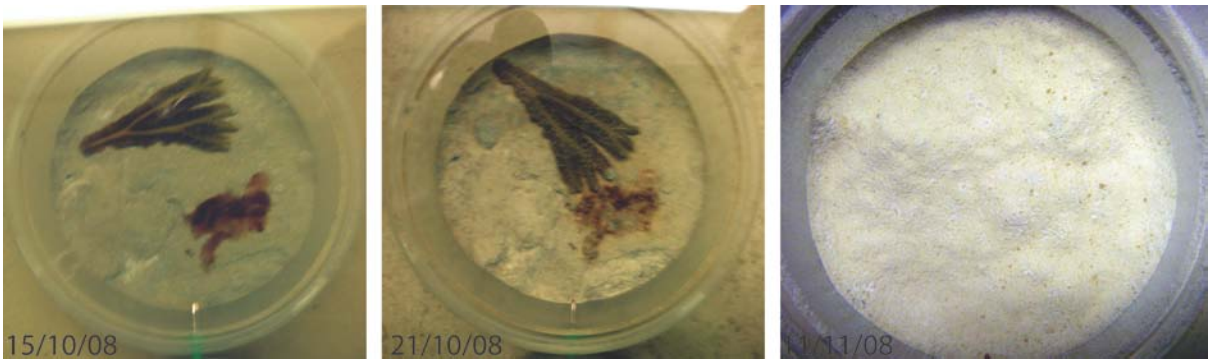

Fig. E1.11. Images of Pot 2E, taken at regular intervals until the pot was smothered with sediment after one week. Pot contains *Aurelia* jellyfish fragment, and a piece of *Fucus* seaweed.

When compared with pots smothered after just one week in Tank 1 (Figs. E1.5–1.6), it is clear that although decay has also occurred in Tank 2 in similar pots (Figs. E1.11–1.12), it again has not progressed as rapidly. Organic matter still retains its shape, even in metazoan tissues, and a considerable degree of topography remains (this had been almost entirely removed in comparable Tank 1 microcosms.

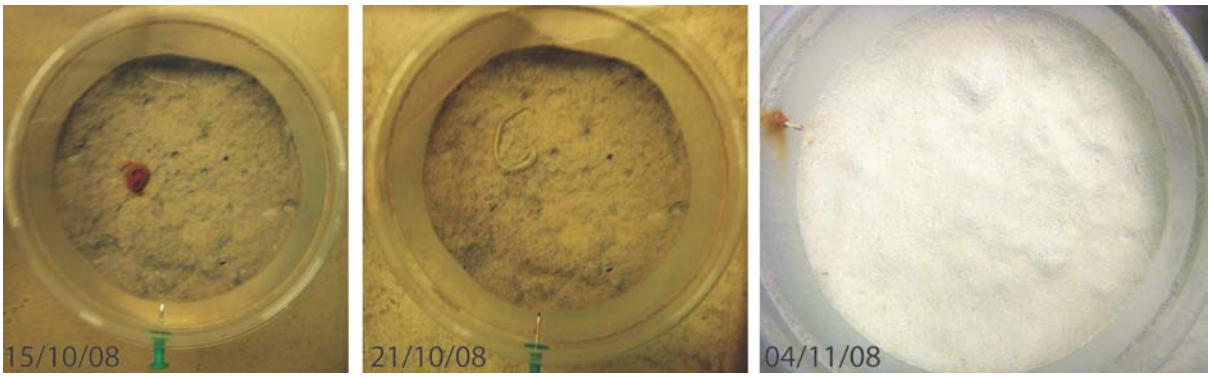

Fig. E1.12. Images of Pot 2F, taken at regular intervals until the pot was smothered with sediment after one week. Pot contains one *Nereis* worm.

Fig. E1.13. Images of Pot 2I, taken at regular intervals. This pot was not covered by 'tuff' at any point during the experiment. Pot contains *Aurelia* jellyfish fragment, and a piece of *Fucus* seaweed.The final (lowermost) image is of the pot in November 2010, after it had been dried out.

Jellyfish tissues in Pot 2I decayed away after about two weeks, faster than in other pots in this tank. Seaweed began to decay noticeably after six weeks (Fig. E1.13). By the time the pots were removed from the system a year later, all organic matter on the surface had decayed away and been removed, with no imprint or remnant of the organisms remaining on the sediment surface (Fig. E1.13, lowermost image). This implies that on the deep seafloor, if decay is allowed to run to completion, all traces of soft-bodied organisms will be removed. There is no reason to believe that this would not have also been the case in the Ediacaran Period.

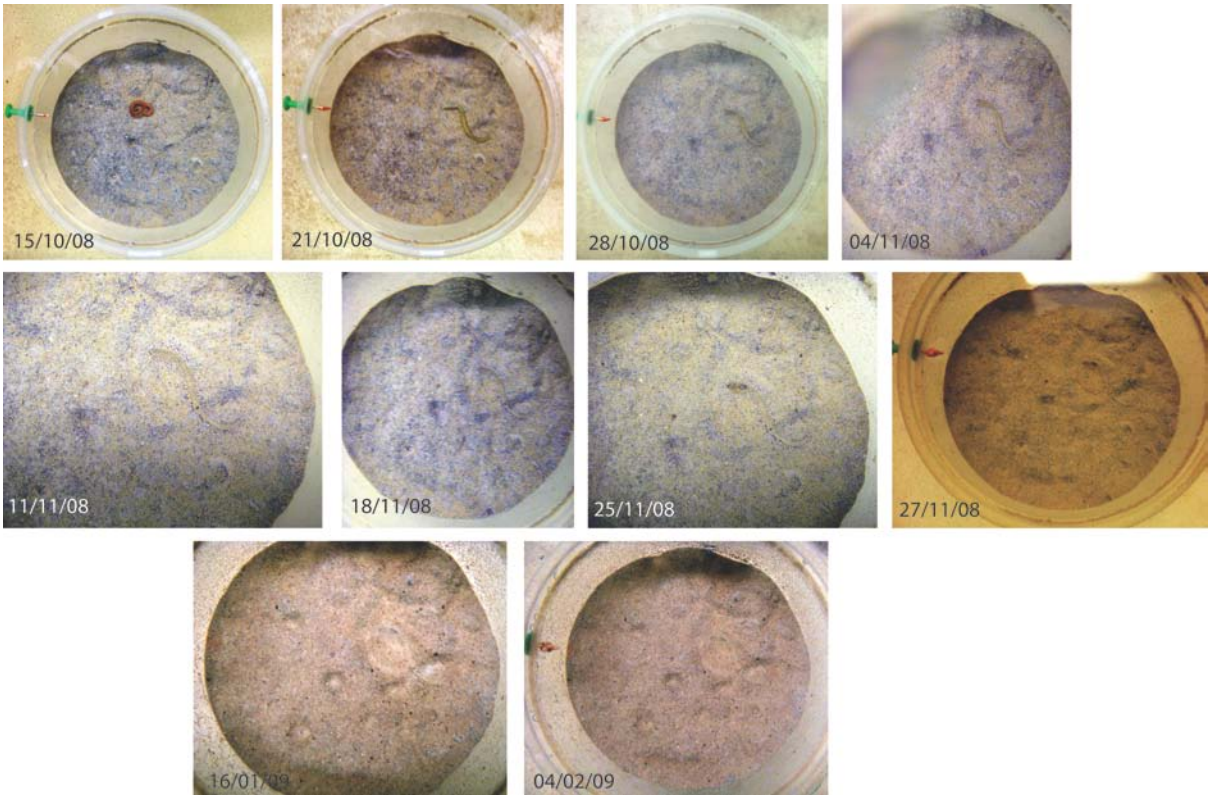

Fig. E1.14. Images of Pot 2J, taken at regular intervals. Pot contains one *Nereis* worm. This pot was not smothered with sediment.

In Pot 2J, worm tissue is still visible, and recognisable as worm tissue, even after six weeks. Compare this to similar pots in Tank 1, where organisms had lost their fidelity within three weeks.

In summary, microbial decay and autolysis can effectively decay organic material from metazoan and algal sources, over periods of weeks to months. Metazoan material is broken down faster than that of seaweed, and decay rates for all materials are strongly influenced by the maturity of the microbial population on the seafloor prior to decay. A more mature microbial population can decay organic matter 2 to 3 times faster than on a surface with little to no prior microbial community. Metazoan tissues can be effaced to produce irregularly positioned lobes and troughs. Effaced metazoan cnidarian material can remain on surfaces

already populated by microbial communities, in a preservable form, for at least 5 weeks.

Seaweed remains can persist for far longer.

Fig. E1.15. The experimental tanks fully coated with foam to keep out light, therefore preventing photosynthetic micro-organisms from partaking in the degradation of the organic matter. Tank 1 is on the left.

Fig. E1.16. The filamentous and pustulose growth of microbial organisms on the surface of a decaying anemone, 18 days after death. Note the globular growth at bottom right, the ‘mesh’ fabric of filamentous growth in the lower centre of the image, and the threads of filamentous growth extending both on to the surrounding sediment, and into the organism’s interior.

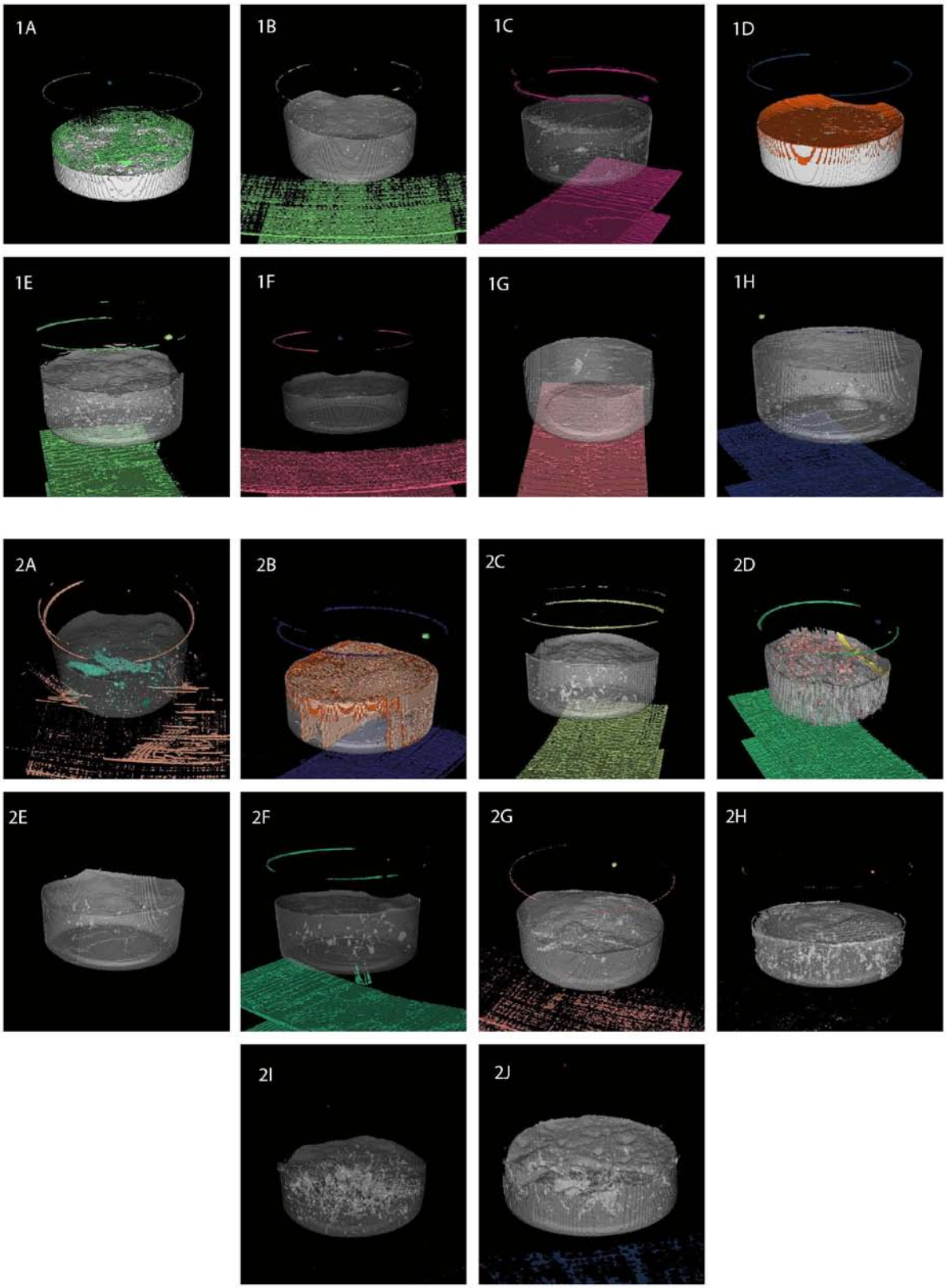

Fig. E1.17. CT renderings of all pots. Labels are consistent with the pot label used in the original experiments. All pots have a diameter of 11.5 cm at their widest point. Colourful rectangles beneath the pots are the mats upon which they were placed into the scanner. The degree of transparency, smoothing and differentiation of material varies in each pot.

Appendix F

Data for Palaeoecological Reanalysis

Appendix F1

Reanalysis of the Clapham et al. 2003 dataset

The data presented in Chapter 5 is compiled here into one simple table. The values are either taken directly from the Clapham et al. (2003) paper, or recalculated to remove tapho-taxa, namely the ivesheadiomorphs, and lobate discs. The original Clapham et al. data can be found in figs. 2, 5 and 9, and tables 1–3 of Clapham et al., 2003, or within the original text of that publication.

Surface	SH	G	E	D	LMP	BC	PC
Clapham et al. 2003 data							
Area studied (m^2)	47.0	7.05	104.75	63.4	14.0	0.71	16.7
Number of fossils	370	162	4188	1488	304	106	239
Species richness	6	6	10–12	8	11	4	3
Fossil density (ind./m^2)	7.9	23.0	39.7*	23.5	21.7	149.3	14.3
Areal Coverage (%)	3.4	6.2	12.4	11.2	7.2	6.3	10.7
Shannon diversity	0.46	1.54	1.52	0.7	1.31	0.67	0.87
Shannon evenness	0.26	0.86	0.61	0.33	0.55	0.48	0.80
Revised data							
Revised species richness	5	5	10	7	10	3	2
Revised fossil density	7.3	21.6	37.7	23.5	21.7	147.7	14.0
Revised areal coverage (%)	1.2	4.2	6.6	10.7	7.2	5.6	2.5
% loss of ‘census’ population	7.9	5.8	5.6	-	-	1.1	2.5
% of necromass within biomass	63.9	32.4	46.4	4.7	-	10.6	76.4

Table G1.1. Data upon which the arguments in Chapter 5 are based. * Average value, since fossil density values range from 31.9 to 56.5 ind./m^2 depending on which outcrop of the E Surface (East, West or Watern Cove) is studied. All revised data presented to 1 decimal place.

APPENDIX F2

CALCULATION OF THE SHANNON DIVERSITY INDEX

The Shannon diversity index has a maximum possible value in a community, which is dependent on the species richness S (the proof for this is widely available):

$$H'_{max} = \ln S$$

It is therefore possible to calculate H'_{max} for a range of theoretical populations by varying the value of S. This produces the values presented in the following table. The colours of the cells correspond to the 'typical' (green) and 'extreme' (yellow) values for Shannon diversity index cited in Clapham et al., 2003, consistent with those colours used in Figs. 5.4–5.6.

S (species richness)	H'_{max} (ln S)
1	0
2	0.693
3	1.099
4	1.386
5	1.609
6	1.792
7	1.946
8	2.079
9	2.197
10	2.303
11	2.398
12	2.485
13	2.565
14	2.639
15	2.708
20	2.996
25	3.219
30	3.401
50	3.912
100	4.605
200	5.298

Table F2.1. Values of H'_{max} for a range of species richness values. This H'_{max} value is only obtained if the assemblage also exhibits maximum evenness.

The values demonstrate that it is not possible to obtain a H'_{max} value of >2.5, regardless of how evenly distributed the population of the community is, unless the population contains more than 12 species (i.e. S > 12). All values are given to three decimal places.

Since none of the Mistaken Point bedding plane assemblages studied by Clapham et al. (2003) contained more than 12 species in the original study, it is argued that the range of values for Shannon diversity index exhibited by modern communities is of no use for comparison with these fossil communities. The Shannon diversity index is therefore demonstrated to be incapable of determining whether a Mistaken Point fossil community shares similar diversity to modern epibenthic animal ecosystems.